Westfälische
Wilhelms-Universität
Münster

Analytische Chemie

Development of a new small-sized plasma optical emission detector for gas chromatography

Inaugural-Dissertation

zur Erlangung des Doktorgrades

der Naturwissenschaften im Fachbereich Chemie und Pharmazie

der Mathematisch-Naturwissenschaftlichen Fakultät

der Westfälischen Wilhelms-Universität Münster

vorgelegt von

Rasmus Janzen

aus Wolfenbüttel

-2013-

Dekan:	Prof. Dr. Bart Jan Ravoo
Erster Gutachter:	Prof. Dr. Uwe Karst
Zweiter Gutachter:	Prof. Dr. Jan Andersson
Tag der mündlichen Prüfung:	03 . 07 . 2013
Tag der Promotion:	03 . 07 . 2013

Contents

1. Introduction, Aims and Objectives

1.1. Introduction

The great number of articles dealing with speciation analysis of mercury and tin compounds in environmental samples shows the high relevance and importance of this topic [1–7]. The interest in this topic can be explained by the high toxicity of the organic species in comparison to their inorganic species as discussed in detail in literature [8, 9]. The origin of these toxic compounds in the environment is often of anthropogenic nature because of their application in industrial processes, pesticides or antifouling paints [8–11]. Beside man made products, alkylated species are also generated in natural processes like e.g. methylmercury formation by biomethylation [12–14]. This highly toxic species accumulates in animal tissue and by bioaccumulation and biomagnification enters our food chain, leading to public health concern about fish consumption. Tributyltin (TBT) mainly enters the environment via its use as a pesticide and antifouling agent. In the aquatic environment it de-

posits in sediments and degrades only very slow to dibutyltin (DBT) and monobutyltin (MBT) [11, 15–18]. Today TBT is classified as an endocrine disruptor, first recognized by its hormone like effects on mollusks [19, 20] leading to the so called "imposex". Due to this, different regulations have been established to restrict application of these compounds [21, 22] and to monitor its presence in the environment down to the ppt level.

Though Gonzalvez *et. al.* and Vieira *et. al.* have reviewed non-chromatographic techniques for speciation analysis of organometallic compounds [23, 24], usually hyphenated techniques combining highly selective separation techniques with a sensitive detection technique are applied [25]. In this context, chromatographic as well as electrophoretic techniques have been used as separation technique. Due to its excellent separation efficiency, the availability of a wide range of sensitive detectors and marginal solvent requirement, gas chromatography (GC) is often applied to investigate organometallic species of mercury and tin [3, 5, 26–32]. To provide volatility required for separation, species are usually alkylated in a derivatization step during sample pretreatment. Such derivatization step comes with benefits as well as disadvantages. On the one hand an additional preparation step increases the risk of analyte loss, sample contamination or species transformation [33–37]. On the other hand derivatized species are more stable and their separation from sample matrix is simplified [38]. Element selective detection is either accomplished by atomic emission spectrometry (AES) or mass spectrometry (MS). A commonly applied detector in

this context is the inductively-coupled-plasma (ICP) mass-spectrometer (MS). The advantages of mass spectrometry in comparison to atomic emission are its higher detection sensitivity and the possibility to make use of the application of isotope dilution (ID). Hereby, errors resulting from sample loss are eliminated and application of species specific ID (SSID) allows identification of species transformations [13, 39, 40]. Unfortunately, ICP-MS is very cost-intensive due to high instrument purchase and operation costs. However, species transformation during sample preparation and strategies for its suppression are well described, so that application of SSID is not stringently required and operation of more cost efficient detectors, which do not offer the application of ID, becomes suitable [31, 34, 40–42].

Microwave-induced-plasma (MIP) atomic-emission-detection (AED) also provides element selective signals. Due to its high excitation efficiency, it also provides sensitive detection [43]. Moreover, it offers excellent compatibility with low gas flows commonly used in GC and can be connected to GC columns avoiding dead volumes causing quality-deteriorating signal broadening. Applications for mercury and tin speciation analysis using MIP-AED are manifold in literature [3, 44–51]. The lower costs in acquisition of the commercial available MIP-AED system from *JAS* compared to ICP-MS systems and its low gas consumption with resulting low costs in application characterize this detection system. Due to the highly resolving Czerny-Turner monochromator with high spectral resolution used in this commercially available system, a wide wavelength range from 171-837 nm is covered for analytical applications. Thus,

many elements are detectable. In turn, high resolution limits the simultaneously observable spectral range of this instrument to a predefined 40 nm window [52]. Hence, multi element capability is limited to elements with emission lines in the corresponding spectral region.

1.2. Aims and Objectives

The goal of this work was the development of an easy to use, element selective detector for gas chromatography. Controlling and maintenance of the plasma based detection system should be simplified by a straightforward setup and a system adapted software solution, providing controlling, monitoring as well as data acquisition and data evaluation. Instrumental parameters like gas flows should be optimized to assure high sensitivity and selectivity for detection of mercury and tin species. Physical and chemical characterization is requested, concerning parameters like plasma temperature, electron number density, selectivity as well as limits of detection and the linearity in the working range. Subsequently the developed and optimized system should be validated by analysis of different certified reference materials and comparison with established methods. Participation in an interlaboratory study is desired to prove the required robustness for applicability in routine analysis.

2. Theoretical Background

2.1. Microwave Induced Plasma

2.1.1. Plasma Characteristics

Gaseous material consisting totally or partly of separate ions and electrons is defined as a plasma [53]. According to this, a plasma appears electrically neutral to the environment, but still interacts with electromagnetic fields. This behavior is essential for the generation of artificial plasmas, as the energy required for continuous generation of new charged particles may be coupled in by application of high frequency electromagnetic fields. Certainly, the most important plasma source in analytical spectrometry is the inductively coupled plasma (ICP) sustained in argon, which is excited at frequencies of 27.12 MHz or 40.68 MHz. Higher frequencies are used in microwave plasmas (MWP), either 0.915 GHz or even 2.45 GHz. These plasmas are commonly operated with helium as its high ionization energy allows spectral excitation and sensitive detection of nonmetals [54]. Due to the high frequency applied in MWPs, heavy particles like ions are not able to follow the oscillation of the electromagnetic field. In contrast, electrons are accel-

erated very efficiently and gain high amounts of energy in a very short period of time [55, 56]. This process, that occurs in the whole MWP discharge, results in inelastic collisions of electrons with heavier particles. The transferred energy causes ionization of neutrals and thus is essential to sustain the plasma as illustrated in equation 2.1 [55, 57].

$$e^- + He \longrightarrow He^+ + 2e^- \tag{2.1}$$

Moreover, fast electrons can be involved in excitation processes of analyte atoms as illustrated in equation 2.2. The superscripts * is referring to excited species. A symbolize the analyte atoms.

$$\begin{aligned} e^- + A &\longrightarrow A^* + e^- \\ e^- + A^+ &\longrightarrow A^{+*} + e^- \end{aligned} \tag{2.2}$$

Due to the fact that kinetic energies of electrons within the plasma follow a *Maxwellian* distribution, beside high energy electrons a majority of electrons with low energies is populated in the plasma. Even these electrons and ions with low energies can participate in the excitation process according to equation 2.3 [57, 58].

$$\begin{aligned} He^+ + A &\longrightarrow He + A^{+*} \\ e^- + He + A^+ &\longrightarrow He + A^* \end{aligned} \tag{2.3}$$

Nevertheless, the most often postulated excitation mechanism in MWP is proposed to be the Penning ionization followed by radiative ion-electron recombination or ion excitation as described in equation 2.4 [56, 57]. The superscript m is referring to metastable species.

$$\begin{aligned} He^m + A &\longrightarrow He + A^+ + e^- \\ A^+ + e^- &\longrightarrow A^* + h\nu \\ A^+ + He^m &\longrightarrow A^{+*} + He \end{aligned} \tag{2.4}$$

As kinetics of heavy and light particles in MWP are different, no total thermal equilibrium is reached. Accordingly, theories that require equilibrium state cannot be used for description of these plasma sources. To describe fundamentals in terms of temperature and population density in the plasma, it is necessary to define local thermal equilibria (LTE). Therefore, mathematical terms can be used to describe each species in the plasma. The resulting different temperatures like T_{gas}, T_{rot}, T_{exc} or T_{ion} are expressions for different processes occurring in the plasma.

Gas Temperature: The gas temperature (T_{gas}) represents the translatory kinetic of heavy particles like atoms, ions and molecules in the plasma. Its theoretical description is based on the *Maxwell-Boltzmann* distribution [59]. Three different methods for its measurement have been described: Evaluation of the Doppler broadening of emission-lines [60], pressure changes due to the temperature in the isolated system [61] and *Rayleigh* scattering of laser radiation [62]. T_{gas} is commonly associated with the ability of desolvation, volatilization and at-

omization of introduced compounds. Therefore, the relatively low gas temperature of low and moderate power MWPs is reflecting their limited matrix tolerance [56, 63].

Electron Temperature: The theoretical description of the electron temperature (T_e) is also based on the *Maxwell-Boltzmann* distribution as it is depending on the velocity of free electrons. Its determination is mainly achieved by two methods. The first one is the *Langmuir* probe which is based on monitoring the electrical current between two wires, introduced into the plasma [64]. The second one is laser based *Thomson* scattering. It is applied more often for T_e determination as it provides noninvasive data collection [65].

Rotational Temperature: Rotational excitation states are described via the rotational temperature (T_{rot}). Due to the fact that low energies are required to change rotational states of molecules, a rapid exchange with kinetic energy of molecular species can occur [66]. Therefore, T_{rot} is usually slightly higher compared to T_{gas} and is often used for estimting T_{gas}. For its calculation, line intensities of molecular emission bands of N_2 or OH can be measured and evaluated based on their *Boltzmann* energy distribution (compare 2.5), describing the population distribution on different energy states. [63, 67].

Excitation Temperature: Like T_{rot}, the excitation temperature (T_{exc}) is based on the *Boltzmann* distribution. The most efficient and commonly applied approach for calculation of T_{exc} is a Boltzmann plot

for the atomic energy levels of the support gas or an introduced element. This method has often been used for diagnostic evaluation of MWPs [63, 68–74]. Its theoretical background is described in literature [75].

Ionization Temperature: The determination of the ionization temperature (T_{ion}) is based on the investigation of emission line intensities of two adjacent ionization levels. Adequate results require sufficiently intense atomic and ionic lines. Therefore, Fallgater *et al.* proposed the use of Sr and Ca as thermometric species [76]. From the measured level population of the thermometric species in both ionization states, the prevailed temperature responsible for the level distribution is calculated by using the *Saha* equation.

As a result of the temperature differences between electrons and heavy atom, the general temperature trend in MWPs can be summarized as follows [75]:

$$T_e \gg T_{ion} \approx T_{exc} > T_{rot} \approx T_{gas}$$

Nevertheless, even LTEs just approximate plasma processes. The degree of deviation from the LTE can be evaluated by comparison of the theoretical and experimental electron number density (n_e) in the plasma [55]. Data for n_e can be obtained by precise evaluation of the broadening of spectral lines e.g. of hydrogen or the plasma gas [67–69, 72, 74]. Details have been described by Starn *et al.* [77].

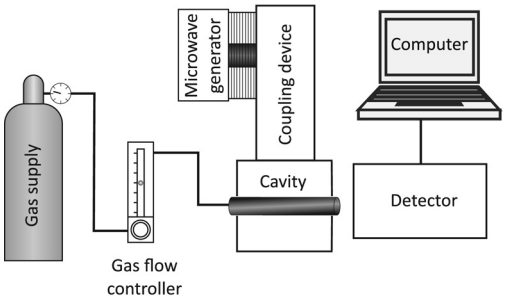

Figure 2.1.: *Components required for a microwave induced plasma (MIP) detection system.*

2.1.2. Instrumentation

According to the method of power transmission to the plasma gas, MWPs can be divided into two groups. In capacitively coupled microwave plasmas (CMPs) a flame-like plasma is formed at the tip of an electrode [78]. The second type are microwave induced plasmas (MIPs), in which the energy required for sustaining the plasma is transferred via a standing microwave formed in a suitable resonator. In this case the energy is either coupled in by a magnetic or an electrical field component of the electromagnetic wave [56]. While CMPs can operate over a wide frequency range, MIPs are limited to one working frequency due to the fixed dimensions of the resonator. Figure 2.1 illustrates the components required for the generation of a microwave induced plasma.

Microwave Generator: For microwave generation different components are available. Low power ($<$ 100 W) microwave generation is often achieved by application of klystrons [75]. Quite more popular is the application of magnetrons as the operation is simple, efficient and, due to the domestic utilization, also cost efficient [79].

Coupling device: Microwave power transfer from the generator to the excitation source is accomplished by suitable transportation and coupling devices. For this purpose, different types of waveguides and connectors are available. The most common ones are coaxial cables and rectangular waveguides [80]. Coaxial cables consist of two coaxially arranged metallic cylinders. During its transport the microwave is reflected between these two cylinders. The related electric current is just located in the metallic skin (Skin Effect) of the inner cylinder surface and the skin depth decreases with higher frequencies. Thus, high attenuation is resulting for the transport of microwaves in coaxial cables. Accordingly coaxial cables are not efficient to transport microwave power over long distances [75].
For the operation of high power MWPs, where transmission efficiency is more relevant, application of rectangular waveguides is reasonable. The smallest suitable waveguide size is half of the wavelength. Accordingly, the dimensions of these devices are limited. The consequence of growing miniaturization efforts, forces the application of coaxial cables for energy transfer [56, 75].

Cavity: The resonator cavity is the most important component in a MIP system as it provides the formation of a standing wave and focuses microwave energy into the plasma. Since the first application of an MIP in 1952 [81], many different cavities have been developed and tested for their analytical applicability. Certainly, the most often used cavity was developed by Beenakker. It allows the operation of a He plasma in a quartz discharge tube under atmospheric pressure [57, 82, 83]. By this development, the technical setup was quite simplified compared to former plasma sources, which required reduced pressure to sustain He plasmas.

Almost parallel to the work of Beenakker, Moisan *et al.* described an integrated surface wave plasma launcher (Surfatron) [84, 85]. The system is also able to sustain He plasmas under atmospheric pressure. The system shows several advantages over the Beenakker system.
On the one hand, operation under atmospheric or reduced pressure is possible, so that operation with different plasma characteristics is possible. On the other hand, tuning and operation are easier than for the Beenakker cavity [85–88]. Therefore, the surfatron has been often used in various applications [75, 88–91].
During the 1990th further cavities have been developed to overcome the problem of low solvent tolerance of conventional applied cavities [92–95]. In 1991 Jin *et al.* described a microwave plasma torch (MPT) sustaining a flame like plasma with a central channel for sample introduction. With this setup an efficient vaporization, atomization and excitation was assured [96]. Matusiewicz described a "microwave plasma cav-

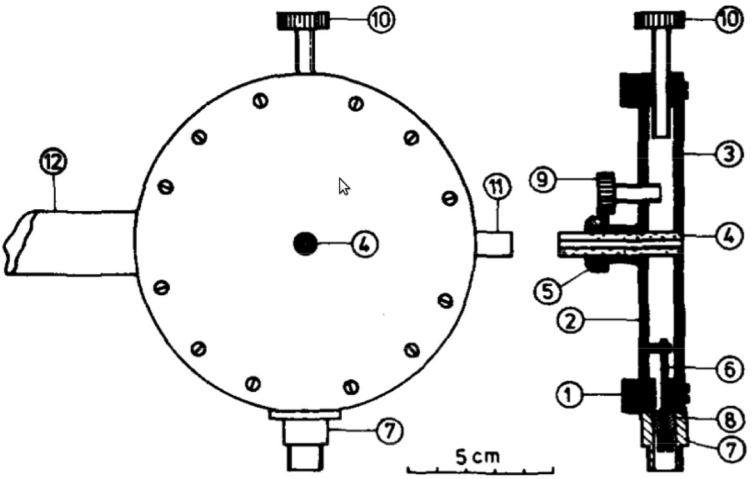

Figure 2.2.: *The Beenakker Cavity: (1) Cavity Wall (made of copper; inner diameter 93.0 mm), (2) fixed bottom, (3) removable lid, (4) discharge tube made of silica, (5) discharge tube holder, (6) coupling loop, (7) connector for coupling loop, (8) seal, (9) screw for tuning, (10) screw for tuning, (11) hole for viewing or air cooling, (12) fixture [82]*

ity/magnetron" (MPCM) which allows high microwave power and efficient coupling between cavity and magnetron. Thus, even wet aerosol introduction was possible [97]. These and other cavities for the generation of MIPs have been described in reviews [80, 98, 99].

Plasma Gas: MWPs are usually sensitive to the applied gas flow. Therefore, usage of precise gas flow controllers is essential to provide high performance characteristics [71, 83, 100, 101]. In this context, various plasma gases are applicable, including noble gases as well as molecular gases like nitrogen or carbon dioxide [97, 102]. The resulting discharges differ in behavior, dimensions and characteristics. This topic will be shortly discussed in the following section.

Helium: MIPs sustained in pure helium generally form a single filament [86, 97, 103]. Radial dimensions are commonly limited by the inner diameter of the discharge tube, while axial dimensions are limited by the cavity walls [103]. The plasma dimensions are driven by two effects. On the one hand the high ionization energy of helium leads to relative low electron densities with a low skin effect resulting in a diffuse plasma discharge and good sample penetration [68]. On the other hand, the high thermal conductivity of helium is beneficial for a homogeneous plasma heating and energy transfer to the sample, which improves desolvation and vaporization [56]. In turn, high dissipation of the microwave energy is resulting in higher forward power requirements for a stable plasma discharge [86, 104]. For a comparable power level, a lower gas temperatures compared to Ar plasmas is observed [68, 69].

Nevertheless, resulting from the high ionization energy, high excitation temperatures are provided leading to the ability to even excite non-metals [56, 68, 75, 80].

Argon: In contrast to helium discharges, argon is forming thin plasma filaments. The quantity of filaments is depending on the applied gas flow and microwave power [86, 88]. The main reason for this different behavior is the lower ionization energy, resulting in high electron density and thus a high skin effect, reducing the plasma diameter [68, 69]. The argon plasma filament tends to extend beyond the cavity walls which could lead to microwave leakage [97,103]. As already mentioned, the gas temperatures is slightly higher compared to helium plasmas sustained under similar conditions. Resulting from the lower ionization energy of argon, lower excitation temperatures are observed [68, 69].

Nitrogen: The diameter of a nitrogen plasma is similar to that of a helium plasmas as it fills the whole discharge tube, owing to the low electron density. Oppositional is the behavior at high microwave energy and gas flow as the plasma expands outside the discharge tube [102]. The main disadvantage compared to noble gases is the higher spectral background, worsening the sensitivity of nitrogen plasmas [97].

2.2. Detection

Since the introduction of MWP sources, different detection methods have been tested to gain element selective signals. Doubtless, optical

emission spectrometry (OES) is most often used, but also mass spectrometry [105–109], atom fluorescence spectrometry (AFS) [110, 111] and atomic absorption spectrometry (AAS) [112,113] have been applied. As the developed system is based on OES detection, the theoretical background of this technique will be further discussed.

2.2.1. MIP-Optical Emission Spectrometry

OES is based on the detection of radiation from an excitation source. MIPs provide high excitation power resulting from high energetic species in the plasma (see page 13), so that these sources have been early used for excitation purpose [54, 81, 82, 114]. Qualitative information about sample composition is generally obtained via the element specific emission lines. Emission originates from electronic relaxations from high to low energetic states so that for one element many emission wavelength are obtained. As energetic levels of atoms and ions of one element differ, it is necessary to distinguish between atomic (I) and ionic (II) emission lines. The relative intensities are depending on the population density of electrons in the upper and lower states. This population is expressed by the *Boltzmann* distribution law shown in equation 2.5 [115].

$$\frac{N_1}{N_0} = \frac{g_1}{g_0} \cdot e^{\left(\frac{-\Delta E}{kT}\right)} \tag{2.5}$$

With N_x as number of atoms in the corresponding state x and g_x representing the number of degenerated energy levels. ΔE expresses the energy difference between the states 1 and 0. T is the temperature in Kelvin and k represents the Boltzmann constant.

At constant plasma conditions, line intensity of an emission line is only depending on the concentration of the element in the plasma, so that quantitative information are accessible. In consequence for sensitive element detection appropriate wavelengths need to be selected. In this context excitation characteristics of the plasma are relevant, so that wavelength tables of spectra from ICP do not provide intensity information usefull for MIPs [116, 117].

Spectral Background: In MIPs some spectral regions are usually interfered by band spectra from excited molecular species (mainly OH, C- and N-species) [56, 100]. Band spectra usually show an intensive head degrading in intensity either to shorter or longer wavelengths, depending on the nature of vibrations in the molecule. Evaluation of element lines interfered by these molecular bands generally call for background correction to avoid quantification errors.
Commonly a separate background signal is measured and subtracted from the analyte signal to eliminate interfering background radiation. Due to differences in the background signals from different spectral regions, it is essential to collect the background adjacent to the used detection wavelength. Depending on signal stability, a sequential or simultaneous background correction can be applied.
In sequential correction, background and element signal are collected at the same wavelength but at different times. Thus, in transient chromatographic data, identification and accurate measurement of background emission is difficult. In contrast, the simultaneous approach is more suitable as the background and analyte emission are collected at

the same time but on different wavelengths. Therefore, adjacent spectral regions must provide an interference-free wavelength range to collect background radiation. Quimby *et al.* reported higher selectivities using simultaneous correction [83]. The used background correction methods will be further discussed in chapter 3.1.2.

Detectors: Radiation from the plasma is usually focused on the detection device by lenses or mirrors. For the required wavelength selection and subsequent detection, different systems are available.
The simplest option is application of interference filters as just a small wavelength range around the transmission maximum can pass the filter while wavelengths outside the bandpass are eliminated by destructive interferences and spectral blocking coatings on the filter surface. Therefore, detection may be accomplished by usage of photo-diodes or photo-multiplier-tubes (PMT). As interference filters only offer low spectral resolution, the amount of unspecific radiation arriving at the detector is relative high. For the required background correction an oscillating interference filter was proposed by Cammann *et al.* [118] and has been applied successfully for detection of halides and organomercury compounds [45, 118, 119]. This technique will be further discussed in chapter 3.1.2. Detection of more than one element is possible by application of a splitted fiber optics in combination with appropriate filters. The driving force for the development of systems using interference filters was simplicity of the optical design [45, 118].
As costs for interference filters have not been decreased over the last decades, but costs for spectrometers due to miniaturization declined,

today spectrometers are normally used. Further more, spectrometers provide higher flexibility in combination with better spectral resolution. Sequential/scanning spectrometers focus the dispersed light on the exit slit of the monochromator. Detection is mostly accomplished by a photomultiplier tube (PMT) as they cover a wide wavelength range with high sensitivity [56]. For transient signal collection, rapid scanning systems are required to enable a background correction near the observed detection line, and provide the high sampling frequency necessary for this purpose. Using these systems, for multielement detection a small wavelength region has to be selected to provide the required data rate [52, 120]. Multichannel spectrometers are usually working with charged coupled device- (CCD) or photodiode array detectors. Depending on detector dimensions and required resolution, wavelength ranges of several hundred nanometers are covered, allowing for extended multielement capabilities. Background correction can be achieved simultaneously so that detection limits are reduced by reduction of noise originating from the sample introduction [56, 121]. Resulting from the commercial availability of a MIP-OES detection system for GC from *JAS*, this technique has been applied for many analytical problems [19, 43, 44, 122–124] which have been discussed during the last decades by many reviews [79, 125–127].

2.3. Gas Chromatography Plasma Hyphenation

Due to the high separation efficiency of gas chromatography it is often applied for speciation analysis of organometallic compounds. Like in other chromatographic techniques, the separation is based on the interaction of the analytes with the stationary phase. Nowadays capillary columns with inner diameters from 0.10 to 0.53 mm are commonly applied. As a result of the small inner diameter of capillaries, sample capacity is limited but separation efficiency is enhanced. To avoid sample overload with resulting peak broadening, often split injection is applied. In this technique the gas flow is splitted in a known ratio within the injector, and the smaller part is guided onto the GC column.
The mobile phase, mainly helium, hydrogen or nitrogen, is responsible for sample transport, as its inertness prohibit chemical interaction [115]. As common GC Detectors like the flame ionization detector (FID), the thermal conductivity detector (TCD) and the electron capture detector (ECD) provide no element selective signals, plasma based detectors are often used for this purpose. The required interface between separation column and plasma source has to assure 100% analyte transfer by maintaining eluting analytes in gaseous form. Moreover, condensation of high-boiling analytes on cold parts has to be avoided because of the resulting chromatographic peak broadening [128]. Such problems can be avoided by two approaches. On the one hand, a heated transferline

can be used to guide the GC effluent to the plasma and avoid cold spots. On the other hand, analyte transfer can be achieved by using an aerosol carrier, generated by an usual solvent nebulizer [129].

2.3.1. Gas Chromatography - Microwave Induced Plasma Hyphenation

Tolerance of MIP sources against solvent or aerosol introduction have been reported to be relatively low [95]. Therefore, these plasma sources are generally directly hyphenated to GC via a transferline. The technical setup is very simple, as the heated transferline can transport the column effluent directly towards the plasma by placing its end a few millimeters away from the plasma. Moreover, carrier gas and plasma gas are commonly helium so that no plasma disturbance is expected [95, 130]. To make sure that the solvent introduced by GC injection does not causes problems, GC-MIP systems are usually equipped with solvent venting systems [92, 95]. The complexity of these systems differ. The simplest device is a heat resistant three way valve [83]. A more complex solvent venting system which is reversing the plasma flow direction in the discharge tube has been described by Quimby and Sullivan [94]. This setup is also used in the commercial available MIP atomic emission detector (AED) provided by *JAS* [93]. Apart from improved plasma

stability, a further advantage of the applied solvent venting is the reduction of carbon depositions in the MIP discharge tube which may lead to peak tailing, and plasma instability as consequence from reflecting microwaves power [131].

2.3.2. Gas Chromatography - Inductively Coupled Plasma Hyphenation

Direct Hyphenation: For direct hyphenation of GC with ICP-MS, different setups have been proposed [132–137]. While in the early days, unheated interfaces were used for the detection of volatile species [133], nowadays totally heated interfaces are prefered especially for higher boiling point compounds [129]. Efficient sample transfer is assured either by coupling the interface to the injector tube of the ICP torch or by replacing the injector tube with the transferline. As the GC effluent flow is to low to punch the hot plasma by formation of the central channel through the plasma, an additional argon makeup gas flow is added to support analyte transport to the plasma [138]. In later works this gas flow is preheated by Ni-Cr wires or guiding the gas supply line through the GC oven [132, 135, 136, 139]. In addition, passing this gas flow through the complete transferline assures a homogeneous heat distribution and thus a constant temperature in the transferline [132]. A typical direct GC-ICP coupling setup is shown in figure 2.3. For tuning of the MS and the sampling position, addition of xenon to the makeup gas flow is proposed [139–141]. The added xenon allows to compensate drift-

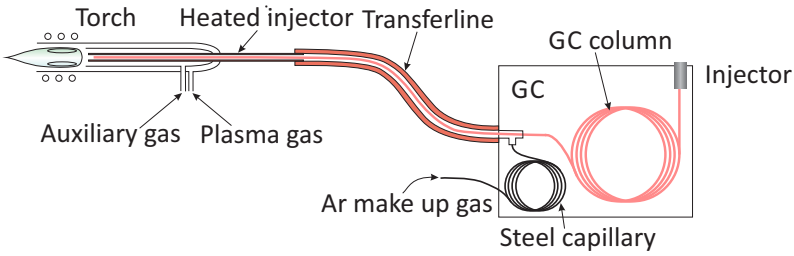

Figure 2.3.: *Direct GC-ICP hyphenation via completely heated transfer line.*

effects caused by the plasma . However, optimum sampling position, plasma parameters and MS lens settings are depending on the element of interest and the observed mass range, Xe tuning is not suitable for optimum sensitivities [142, 143]. The main advantage of this hyphenation approach operated under dry plasma conditions are reduced polyatomic interferences due to the absence of an additional solvent load to the plasma.

As the ICP is very tolerant against solvent, normally no solvent venting systems are applied. However, since the introduction of organic solvents may lead to carbon deposition on the sampler cone, addition of oxygen to the makeup gas may be beneficial.

Aerosol Carriers: Operating the ICP under wet plasma conditions by using an aerosol carrier, shows some advantages over direct hyphenation for GC-ICP hyphenation. Changing the system between standard mode

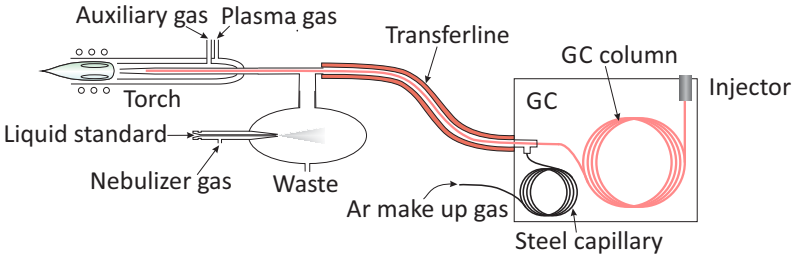

Figure 2.4.: *GC-ICP hyphenation via spray chamber to generate an aerosol carrier according to Krupp* et al. *[144].*

and hyphenated mode by dis- and reassembling the sample introduction system can be omitted by hyphenation of the GC via the spray chamber. While the setups proposed by Peters *et al.* and Prohaska *et al.* are either injecting aerosol or gas chromatographic effluent [145, 146], in the setups of Feldmann *et al.* and Krupp *et al.* - shown in figure 2.4 - GC effluent and aerosol are mixed before injection [144, 147]. Using the latter approach, nebulization of element standards allows the generation of continuous signals. Thus, not only tuning of the instrument is simplified but also drift compensation by using internal standards is allowed. Resulting from wet plasma continuous, no oxygen addition is required since oxygen is generated from the water continuously introduced [144].

3. Technical setup

The basic technical set up of MIPs has already been introduced on page 16. Different set ups and parameters have been tested during the development process to provide optimum performance characteristics of the new detection system. The different approaches will be discussed in the following chapter.

3.1. Detection

3.1.1. Detection Wavelength

As already mentioned, high selective and sensitive spectrochemical detection of elements with plasma excitation sources requires the selection of optimum detection wavelength. Therefore, literature known emission wavelengths for mercury, tin and carbon (table 3.1) have been evaluated for sensitivity and possible interferences. Due to the fact that line intensities are depending on excitation characteristics of the used plasma, all wavelengths listed in table 3.1 have been evaluated with respect to line intensity and interferences from spectral background. This

Table 3.1.: *Literature known emission wavelengths applicable for detection of mercury, tin and carbon.*

Element	Wavelength [148]	Rel. Intensity
Hg	253.65 nm (I)	1000
Sn	235.49 nm (I)	700
	242.95 nm (I)	700
	270.65 nm (I)	500
	284.00 nm (I)	1000
	303.41 nm (I)	600
C	193.09 nm (I)	1000
	247.86 nm (I)	400

background radiation can usually be attributed to atomic and molecular emissions generated from components eroded from the discharge tube or impurities in the plasma gas. Depending on the emission wavelength, analyte detection can be influenced by such interfering radiation, so that background correction is necessary.

3.1.2. Spectral Background

In figure 3.1 the emission spectrum of our setup, typical for a microwave induced He plasma, is shown. Obviously main background emissions are resulting from excitation of diatomic nitrogen or oxygen compounds. Therefore, the most affected spectral range between 306 and 360 nm is not applicable for optical emission spectrometry. Certainly, one reason

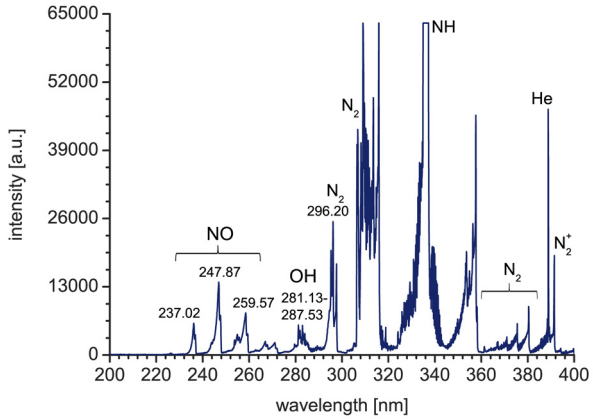

Figure 3.1.: *Emission spectrum of a microwave induced helium plasma (He flow: 200 mL/min; MW power: 65 W). The spectrum was sampled with an integration time of 5 ms and a spectral resolution of 0.2 nm (FWHM).*

for the high presence of nitrogen in the plasma is its type of construction (discussed in chapter 3.2) which allows nitrogen diffusion into the plasma. Obviously element detection between 235 and 260 nm is interfered by different NO-bands. Due to differences in elemental emission wavelengths of target compounds and molecular emissions bands, elimination of NO interferences should be possible by a simple background correction method. As already mentioned in the theoretical section, si-

multaneous background correction offers some advantageous over the successive approach. Therefore a simultaneous method was used to ensure a proper correction.

3.1.3. Interference Filter

A simple and fast background correction method, using a narrow bandpass interference filters for wavelength separation was described by Cammann *et al.* [118]. Plasma radiation is first collimated, to provide the best filter efficiency. The transmitted radiation is subsequently focused on the detector. As illustrated in figure 3.2, the detection is accomplished by a simple photo diode. Filters have to be chosen by selecting their transmission maximum fitting to the analyte element emission line. Tilting of the interference filter leads to a shift of the filter's transmission maximum to shorter wavelengths. Therefore, spectral background collection can be achieved by tilting the interference filter, providing high selectivity with low technical effort. To provide a high data acquisition rate a fast oscillation between tilted and perpendicular positions is necessary. A subtraction of both signals results in a background corrected element signal. As multielement capability requires usage of a splitted fiber optics with different filter systems and dedicated photo diodes, the technical setup will become more complex. Additionally the light intensity, available for the different detectors is limited through the beam divider. Therefore, the sensitivity is reduced in multielement detection and thus multielement capability of this approach is rather limited.

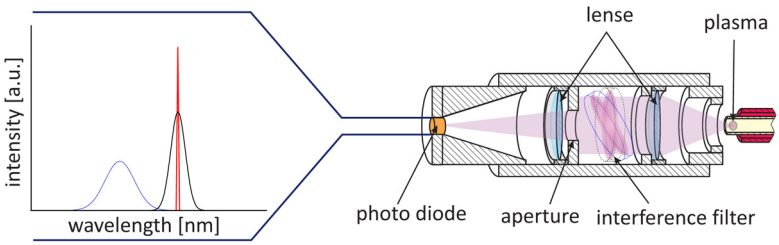

Figure 3.2.: *Scheme of background correction with narrow bandpass interference filter technique. An element emission line is represented by the red signal. The black and the blue curves represent the transmission of the filter at detection and background positions, respectively.*

Analytical performance of this approach for the hyphenated GC-MIP-AES system was investigated by measuring a solution of dimethylmercury (∼460 ng/mL in hexane) as model species. In this context chromatographic baseline stability and sensitivity have been evaluated. All relevant instrumental parameters are listed in table 3.2. A chromatogram recorded with the interference filter based background correction method is shown in figure 3.3. It is obvious that plasma quenching as consequence of solvent load is leading to strong negative peaks during the solvent peak. Moreover the baseline drift, resulting from solvent residues in the plasma, is not eliminated by the interference filter technique. Nonetheless a high sensitivity with an absolute detection limit (calculated as 3-times the signal-to-noise ratio) of 16 pg for mercury has been achieved within this work.

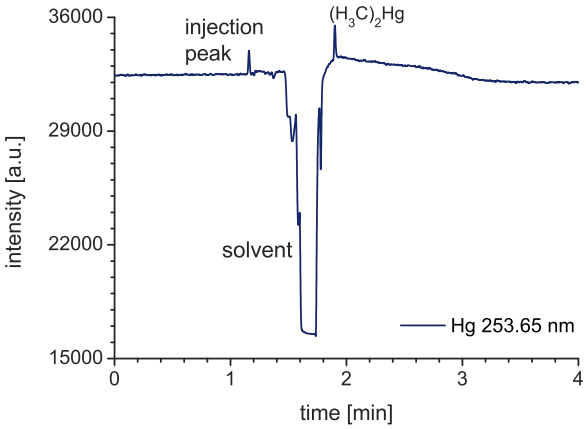

Figure 3.3.: *Chromatogram of dimethylmercury collected with an interference filter based detection and background correction.*

As the interference filter only transmits a small wavelength window, no further information about plasma characteristics or plasma performance are accessible. Moreover it prohibits spectral information about possible atomic or molecular interferences. Hence, method development and troubleshooting is difficult. Due to the fact that all sensitive emission wavelengths of mercury and tin are more or less interfered by molecular emissions (compare figure 3.1) a more flexible system consists of a small CCD spectrometer (ca. 1800 euros) was evaluated for detection purpose.

Table 3.2.: *Instrumental parameters for evaluation of the optical system used for detection.*

GC		**Setting**
Injection	Vol.	1 µL
	Mode	Split 8:1
	Start Temp.	200 °C (0.2 min)
	Ramp	12 °C/s
	End Temp.	280 °C
Column	Type	HP-1
		(30 m; 0.25 mm; 0.25 µm)
	He Flow	2.2 mL/min
Oven	Start Temp.	50 °C (1 min)
	Ramp	15 °C/min
	Hold	80 °C (0 min)
	Ramp	60 °C/min
	Hold	250 °C (1 min)
Transferline	Temp.	280 °C
Plasma		
	Cavity	Rectangular Resonator
	Power	35 W
	Gasflow	150 mL/min
Optics		
	Filter	253.6 nm (FWHM 1.5 nm)
	Spectrometer	190-410 nm (FWHM 0.2 nm)

3.1.4. Spectrometer

The used CCD spectrometer is providing a higher spectral resolution of 0.2 nm (full width at half maximum (FWHM)) compared to the interference filter (1.5 nm FWHM). Moreover, it offers multielement capabilities in the spectral range between 190 and 410 nm. Thus, simultaneous background correction can be applied by defining appropriate background wavelengths and polynomial fitting of this background below the analyte signal. Background intensities at the position of the emission peak can then be calculated and subtracted from the analyte peak's intensity to obtain a background corrected signal. By this approach, continuous spectral background can be effectively deduced. Even structured interfering background emissions e.g. from NO or OH molecules may be effectively removed, if wavelengths of band head and observed emission line are sufficiently different.

Detection of Mercury: The spectral background adjacent to the mercury emission line at 253.65 nm is shown in figure 3.4. As depicted, the background NO band emission can be well calculated and subtracted by a fitted 2^{nd} order polynomial function. The resulting chromatogram is shown in figure 3.5. It was collected by injection of dimethylmercury (DMM) ($\sim$460 ng/mL in hexane) under instrumental parameters as listed in table 3.2. It is obvious that the CCD spectrometer is providing better sensitivity compared to the interference filter. Additionally, baseline drift resulting from plasma quenching by solvent or carbon residues are efficiently eliminated. By this, an absolute detection limit of

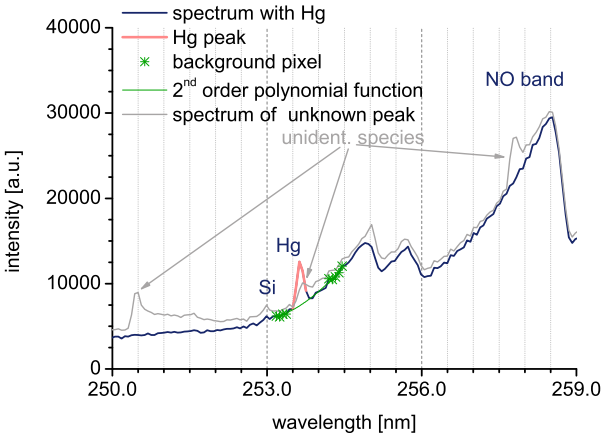

Figure 3.4.: *Optical emission of the helium MIP in the spectral range adjacent to the mercury emission line at 253.65 nm. The polynomial function illustrates the calculated spectral background. In light grey a spectrum collected at an unidentified chromatographic peak is shown. This carbon containing species is interfering with the mercury emission line.*

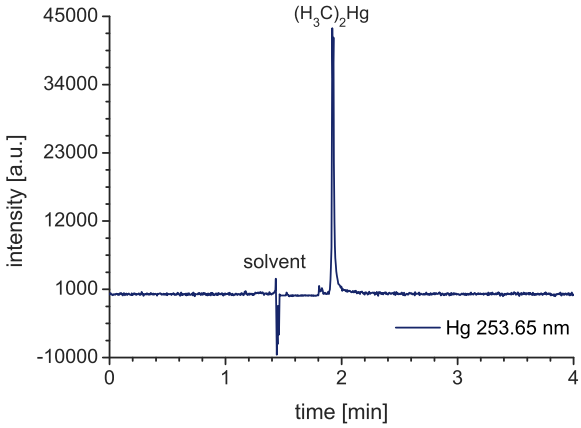

Figure 3.5.: *Chromatogram of dimethylmercury. Detection and background correction has been accomplished by a CCD spectrometer.*

1.4 pg for mercury was obtained. Certainly one reason for this improvement compared to the interference filter technique is the higher spectral resolution, as less collected background emission leads to a better differentiation of blank signal and analyte signal. Additionally elemental emission intensities on different CCD pixels of the spectrometer can be statistically weighted. This mathematical step increases the statistical significance of the emission intensities in the center of the emission line by multiplication with normalized weighting factors (0.031, 0.237, 0.440, 0.260, 0.302). The result is a decreased statistical significance of emissions at the borders of the line, which are strongly influenced by

spectral background and noise. In contrast the intensities and thus the significance in the center of the emission line is increased, resulting in higher sensitivity.
Limits of a background correction with fixed background positions becomes obvious from figure 3.4 (Spectrum in light grey). It shows the spectrum collected at the chromatographic peak maximum of an unidentified carbon containing species. With an emission maximum of 253.7 nm this interfering emission is located very close to the mercury emission line and therefore,effectively corrected by background subtraction is not possible. The influence of this interference on mercury is low in terms of calculated selectivities (compare chapter 5.3.1). Fortunately identification is easy by additional emission bands arising in the spectrum specific for this interference.

Detection of Tin: In contrast to mercury with only one emission line between 200 and 400 nm, tin provides numerous detection wavelengths with usable sensitivity, available in this range as listed in table 3.1. As already mentioned by other authors using MIP-OES, for detection of tin, addition of hydrogen to the plasma gas is required. Added hydrogen is binding free oxygen as hydroxides and forces formation of volatile hydride species, thus preventing oxide formation and increasing tin emission intensity [46, 100, 149]. Hence, for selection of background wavelengths 0.5% hydrogen were added to the plasma gas flow of 200 mL/min. The resulting spectrum is shown in figure 3.6. It is obvious that emission intensities of all oxygen containing species have been decreased compared to the spectrum of the pure helium plasma

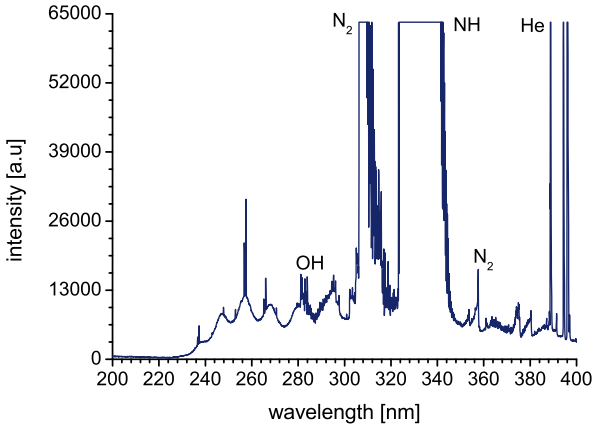

Figure 3.6.: *Spectrum of the helium MIP (helium flow: 200 mL/min; MW power: 65 W) with 0.5% hydrogen as dopant. The spectrum was collected with an integration time of 40 ms and a spectral resolution of 0.2 nm (FWHM).*

(figure 3.1). The apparent increase in background intensities from figure 3.1 to figure 3.6 is a result of different integration times used for spectra recording.

To generate tin signals, tetraethyltin (TTET) dissolved in methanol (MeOH) with a final concentration of 100 µg/mL, was injected via the GC. GC conditions are listed in table 3.3. Figure 3.7-3.9 illustrates the observed tin emission lines resulting from 100 ng Sn (absolute) in the spectral range suitable for the spectrometer. The background around 235.49 nm and 242.95 nm can be well interpolated by a 2nd order poly-

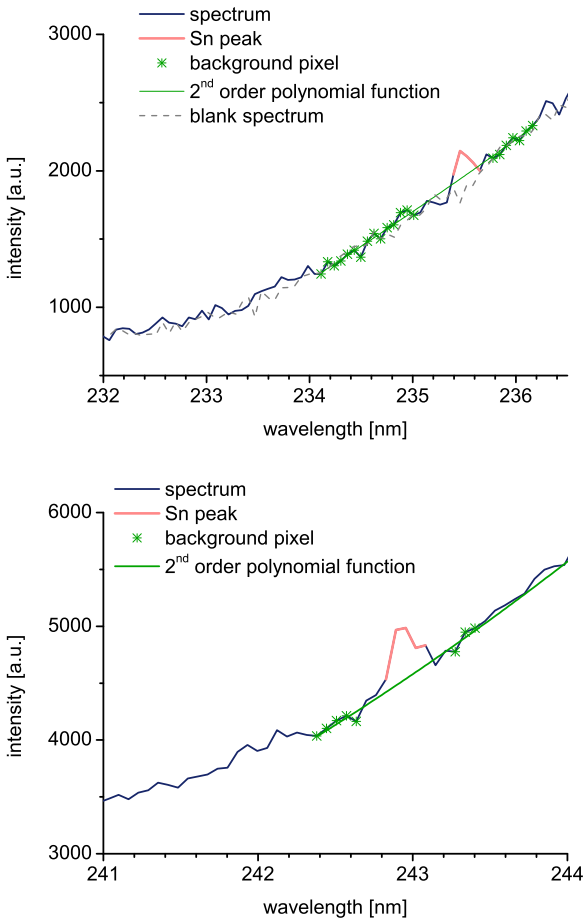

Figure 3.7.: *Optical helium MIP emission in the spectral range adjacent to the tin emission lines at 235.49 nm and 242.95 nm.*

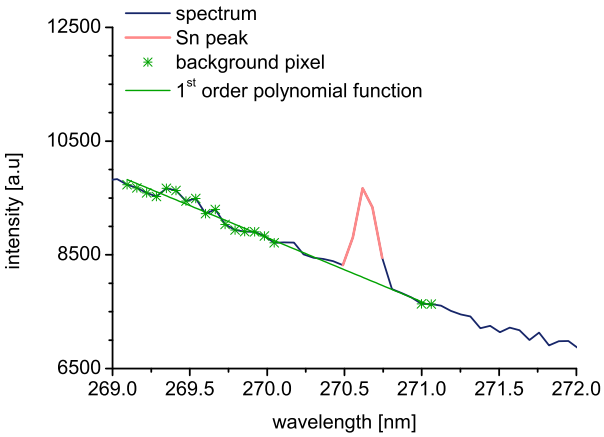

Figure 3.8.: *Optical helium MIP emission in the spectral range adjacent to the tin emission line at 270.65 nm.*

nomial function as visualized in figure 3.7. For the spectral background around 270.65 nm, a linear fitting is more suitable (R^2: 1st order polynomial 0.989; 2nd order polynomial 0.976). Tin emissions at 284.00 nm and at 303.41 nm are interfered by OH emission bands as shown in figure 3.9. A robust background correction is assured by usage of a 1st order polynomial function for background calculation as shown in the corresponding spectra.

Resulting chromatograms are depicted in figure 3.10. It can be seen that peak intensities increase from 235.49 nm to 284.00 nm. Intensity for tin at 303.41 nm is little lower compared to 284.00 nm. Peaks resulting from plasma quenching during the solvent peak are observed on

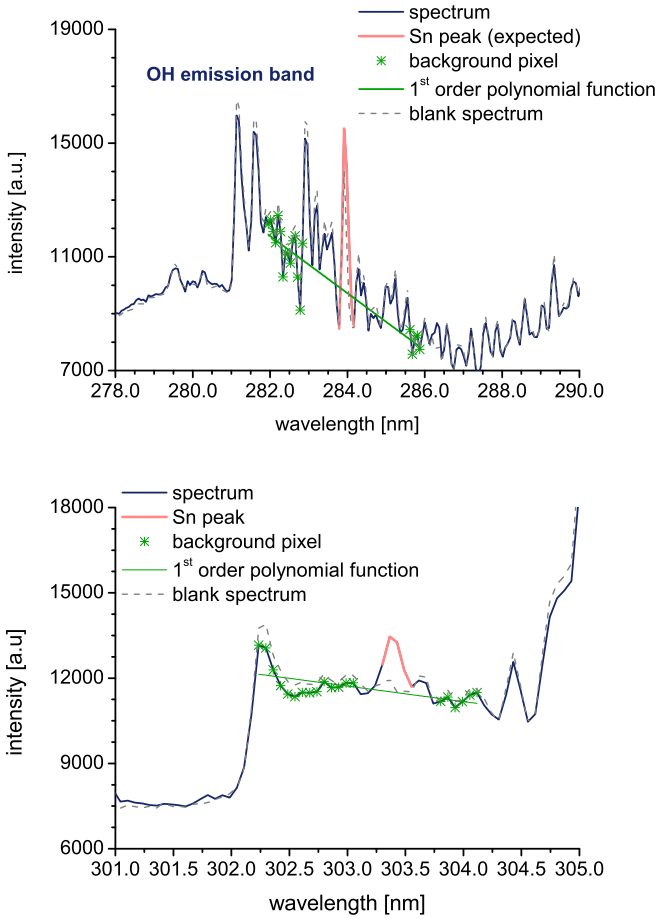

Figure 3.9.: *Spectral range around tin emission lines at 284.00 nm and 303.41 nm.*

Table 3.3.: *GC conditions used for injection of TTET (100 µg/mL in MeOH).*

GC		**Setting**
Injection	Vol.	1 µL
	Mode	Split 10:1
	Start Temp.	200 °C (1 min)
	Ramp	12 °C/s
	End Temp.	240 °C
Column	Type	HP-1
		(30 m; 0.32 mm; 3.00 µm)
	Gas	Helium
	Flow	4 mL/min
Oven	Isothermal	150 °C
Transferline	Temp.	250 °C

all emission lines. Its degree will be discussed in chapter 5.3.1. Signal-to-noise ratios have been used to evaluate performance of the different tin detection wavelength. Results are listed in table 3.4. Though detection wavelength at 284.00 nm and 303.41 nm are partly interfered by molecular emissions of OH molecules, best signal-to-noise ratios are observed. The reasons for this are the high intensity of these emission lines and low fluctuation of the interfering OH bands, leading to a low-noise background signal.

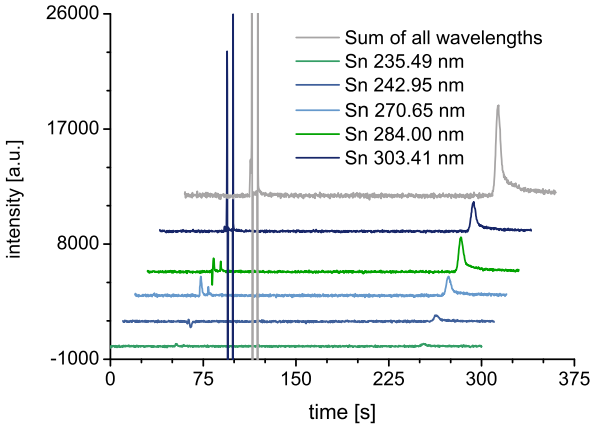

Figure 3.10.: *Element chromatograms of tetraethyl tin collected at different detection wavelength.*

To improve certainty and sensitivity, summation of different detection wavelength for one element is proposed in literature [150]. The idea of this approach is that random noise will be eliminated and the element signal will increase. Thus, summation was applied for the chromatograms shown in figure 3.10. It is obvious that intensity of the TTET peak increases by summation. The actually resulting signal-to-noise ratio is just slightly higher compared to that from tin emission at 284.00 nm. Using summation, spectral background for every element emission line need to be evaluated carefully to avoid analysis errors, as interferences are also summed up.

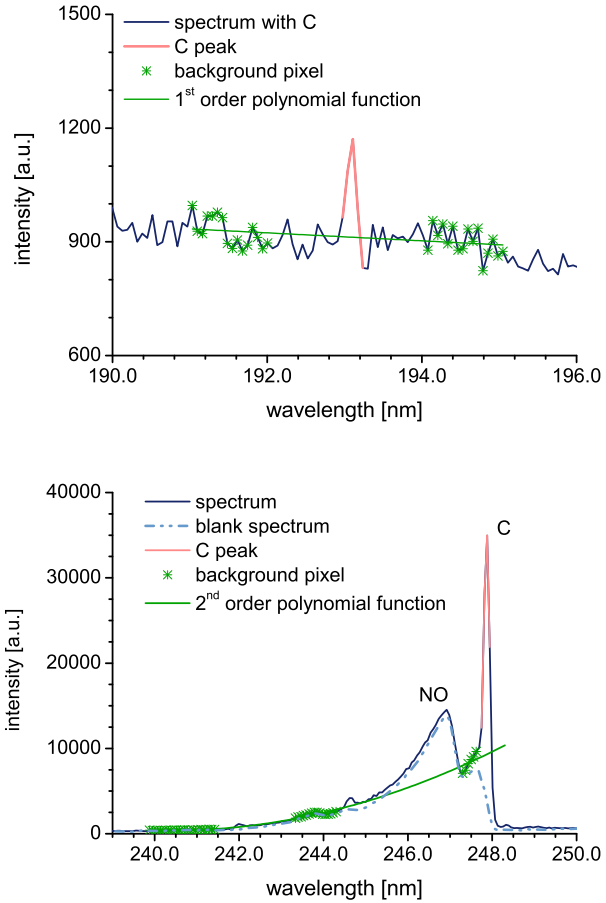

Figure 3.11.: *Spectral background of appropriate carbon detection wavelength.*

Table 3.4.: *Comparison of signal-to-noise ratios for different tin emission wavelengths.*

Wavelength	S/N	Rel. Intensity
235.49 nm	2.290	0.087
242.95 nm	5.737	0.219
270.65 nm	11.004	0.420
284.00 nm	26.205	1.000
303.41 nm	23.186	0.885
sum signal	32.923	1.256

Detection of Carbon: To provide further information about alkylation of organometallic species or possible coelution of carbon containing components, two detection wavelength for carbon were evaluated. Figure 3.11 shows the spectral range around carbon emission lines listed in table 3.1. As C emission at 193.09 nm is not interfered by atomic or molecular emissions a 1^{st} order polynomial function is used to eliminate plasma background radiation. Unfortunately line intensity is very low. One possible reason is that the CCD in the spectrometer is not efficient for detection of this short wavelength. Even further carbon excitation in the MIP may be inefficient or the emitted radiation in the vacuum UV range absorbed by air in the optical system. Nevertheless, a carbon signal resulting from injection of 200 ng of TTET into the plasma can be observed as shown in figure 3.12.

In contrast to line intensity published in literature, in the used MIP carbon emission provide higher intensity at 247.48 nm compared to 193.09 nm. In figure 3.11 a blank spectrum is compared with a spectrum collected at a carbon containing (4 ng abs.) chromatographic peak. Challenging for detection at 247.9 nm is the interference of a NO band with the band head located at the same wavelength. To eliminate fluctuation of the NO background, interpolation of the NO emission band with a 2^{nd} order polynomial function has been tried. By this approach, low carbon emissions are not detected as long as emission intensities are of lower quantity than the NO emission band used for background calculation. Nontheless this approach was found to be suitable as shown in figure 3.12.

3.2. Cavities

As already described in chapter 2.1.2, the cavity of the plasma excitation source provides formation of a stationary wave and focuses microwave power in the discharge tube to sustain a stable plasma discharge. Two types of microwave induced plasma sources were tested for detection of the target compounds.

3.2.1. Setup

Rectangular Resonator: The first plasma source used is based on the "Automated Speciation Analyser" (ASA) MIP developed by Rosenkranz *et al.* [66, 119]. As shown in figure 3.13 microwaves are generated in

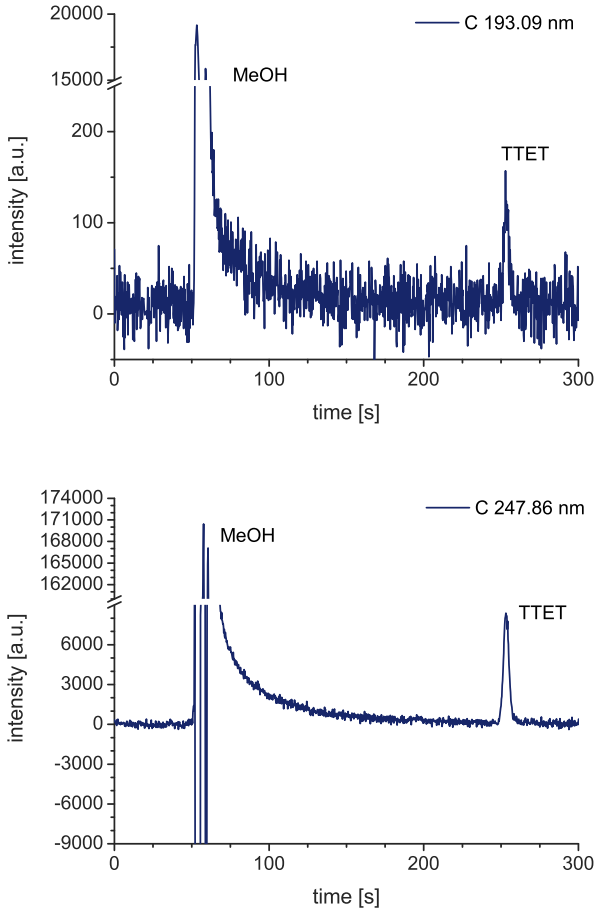

Figure 3.12.: *Carbon chromatograms gained by injection of TTET (100 µg/mL in MeOH) (4 ng carbon (abs)).*

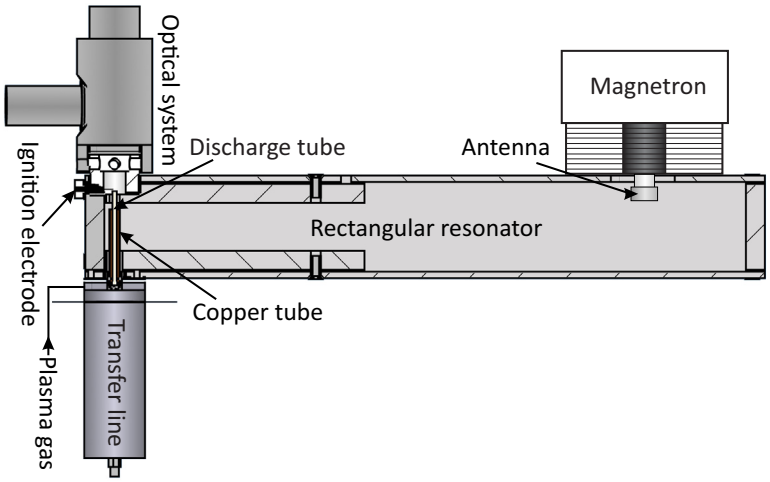

Figure 3.13.: *The ASA microwave-induced plasma source, consisting of a rectangular resonator.*

a common magnetron and coupled into a rectangular resonator, also working as waveguide. The plasma is sustained in a helium flushed ceramic discharge tube made of Al_2O_3. Due to the high temperature resistance of the ceramic, no special external cooling is necessary. Easy mounting of the discharge tube is provided by a graphite fitting. The microwave energy is focused into the plasma, while unwanted microwave modes are eliminated by partially shielding the discharge tube against electromagnetic field with a copper tube. Thereby the plasma discharge is limited to the unshielded region at the end of the discharge tube. As reflected microwaves may travel back through the resonator, leading

to detuning of the magnetron by destructive interferences, the original plasma source described in literature, contained a circulator eliminating these microwaves. The plasma can also be sustained without this component so that it was removed from the setup to save its high costs. Easy and fast maintenance is assured by a simple setup of the source. Optical detection is performed axially by end on viewing the discharge tube. The optic consists of two lenses focusing radiation on the detector or a fiber optics, which guides the light to the used spectrometer. Hyphenation to the GC is accomplished by a heated transfer-line. Thus, the capillary column ends right in front of the plasma, assuring a complete sample transfer without peak broadening caused by dead volumes.

Mini-MIP Source: A complete new microwave induced plasma source for element selective detection in GC (named MiniMIP) was developed by the *INP Greifswald* and the *Neoplas GmbH Greifswald*. In contrast to the system mentioned before, microwaves are guided to the plasma via a coaxial cable as shown in figure 3.14. By this, geometrical dimensions of the cavity may become smaller compared to a rectangular waveguide. To prevent microwaves reflected in the cavity from reentering and by this detuning of the magnetron, a circulator is mounted between magnetron and cavity. The plasma region is constructed similar to the source described above. The plasma is also sustained in a ceramic (Al_2O_3) discharge tube fixed axially in the resonator by a graphite fitting. To focus the electric field on the end of the discharge tube, it is surrounded

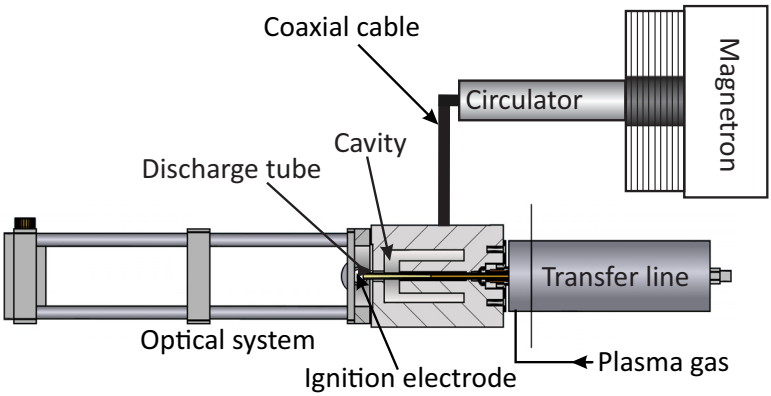

Figure 3.14.: *MiniMIP microwave induced plasma source using a coaxial cable for microwave transport.*

by a metallic cylinder. This cylinder and the inner diameter of the discharge tube limit the plasma dimensions to 6 mm in axial and 1.5 mm in radial direction.

For hyphenation with GC the plasma source is equipped with a heated transfer line allowing positioning of the capillary column directly in front of the plasma. Similar to the ASA source, the plasma gas is added at the end of the transfer line so that a complete mixing with the GC effluent is assured.

The optical system is mounted end-on so that the plasma is observed axially. The transfer optics consists of a fused quartz glass lens (f = 30 mm) which focuses the radiation on a fiber optics (0.22 numerical aperture). By this and usage of a coaxial cable, flexible positioning and mounting of the detector at the GC system is possible.

Table 3.5.: *Comparison of the used plasma sources.*

	ASA Plasma (no circulator)	**MiniMIP (INP)**
Magnetron	30-200 W	20-100 W
Plasmagas	He	He, Ar
Gasflow	100-200 mL/min	100-300 mL/min
Dopant	not provided	H_2/O_2 $\leq$10 mL/min
Discharge tube	Al_2O_3	Al_2O_3
	d_a=3.0 mm	d_a=3.0 mm
	d_i=1.5 mm	d_i=1.5 mm
Hyphenation	Transfer line	Transfer line

3.2.2. Comparison and Evaluation

As shown in table 3.5, both cavities have been constructed for operation at low microwave power (below 200 W). According to literature a low solvent tolerance is expected [92–95]. Hence, high absorption of provided microwave power generated by the magnetron is advantageous. Moreover, plasma power is a relevant parameter for the excitation of analytes in the plasma and its stable maintenance by this for sensitive detection [57, 71, 151].

Measurements of power absorption in both plasma sources were carried out at the *INP Greifswald*. For this purpose, a directional coupler was mounted between magnetron and waveguide or coaxial cable and cavity, respectively. By this setup a separate measurement of forward power

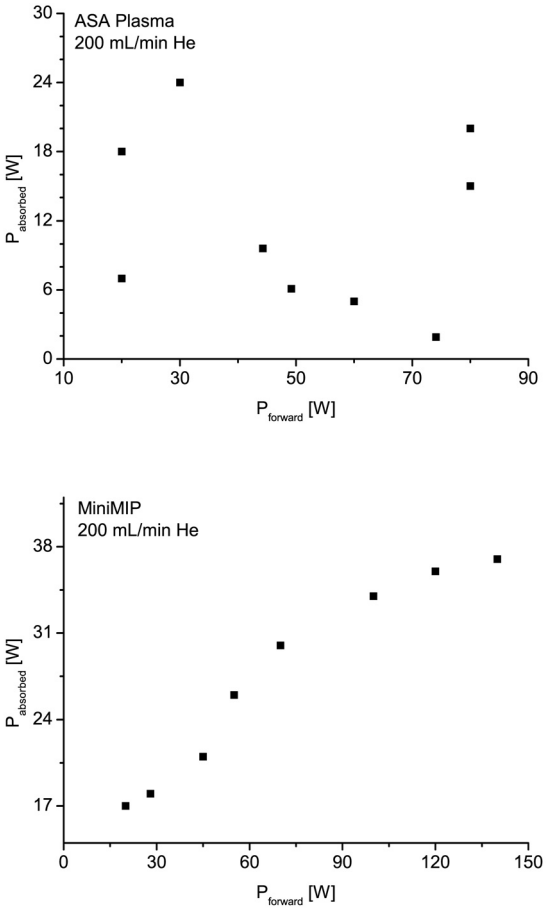

Figure 3.15.: *Comparison of the power absorption in the ASA (top) and the MiniMIP (bottom) plasma source.*

and reflected power was possible via the corresponding connection pin. Thus, absorbed power could be calculated as difference of both values. Results of these measurements are summarized in figure 3.15. While absorbed power in the MiniMIP source is continuously increased with increasing forward power, no trend in power absorption of the system consisting of a rectangular resonator without a circulator is visible. This should be attributed to detuning of the magnetron by the reflected microwave power or a destructive interference of forward and reflected microwave. However, the problem can be related to the omitted circulator in the ASA based plasma source.

Resulting from the low power absorption, the ASA plasma source is very susceptible to high solvent load. The plasma is extinguished by injection of more than 0.125 µL solvent. The MiniMIP can tolerate up to 1 µL solvent and reignites spontaneously after being extinguished by higher solvent load.

Beside stability, sensitivity of the system is an important criterion for analytical applications. Before the detection limits for mercury could be determined, plasma conditions of both excitation sources were optimized by injection of DMM (50 ng/mL Hg) dissolved in methanol. GC parameters were similar to those used for evaluation of the detectors optic system and have already been listed in table 3.2. Microwave power was adjusted to sustain a stable plasma discharge. Unfortunately for the ASA plasma a stable plasma discharge was only possible at 35 W and a helium gas flow rate of 150 mL/min. Above this power value strong

noise resulting from high microwave energy reentering the magnetron was observed. The MiniMIP source was operated with 60 W and a helium gas flow rate of 200 mL/min.
Detection limits were calculated according to equation 3.3 on page 88. For the rectangular resonator system an absolute detection limit of 0.3 pg according to mercury was achieved. By using the MiniMIP source an absolute detection limit of 0.4 pg was gained. Therefore, similar detection limits are provided. As the MiniMIP offers higher robustness it was used for further development.

3.3. Durability of Ceramic Discharge Tubes

An important factor for routine application is the high stability of the system assuring operation with a high uptime and calling for only little maintenance efforts. At the beginning of the development process, durability of the discharge tube was short, so that possible factors shortening the lifetime of the discharge tubes were evaluated to increase applicability of the detection system. To exclude material defects, unused discharge tubes were analyzed by the neighboring analytical service company *marcotech* with a scanning electron microscope. Resulting pictures are shown in figure 3.16. No cracks in the ceramic or other irregularities were visible that could cause preterm destruction. Figure 3.17 illustrates damages at discharge tubes after application at different plasma

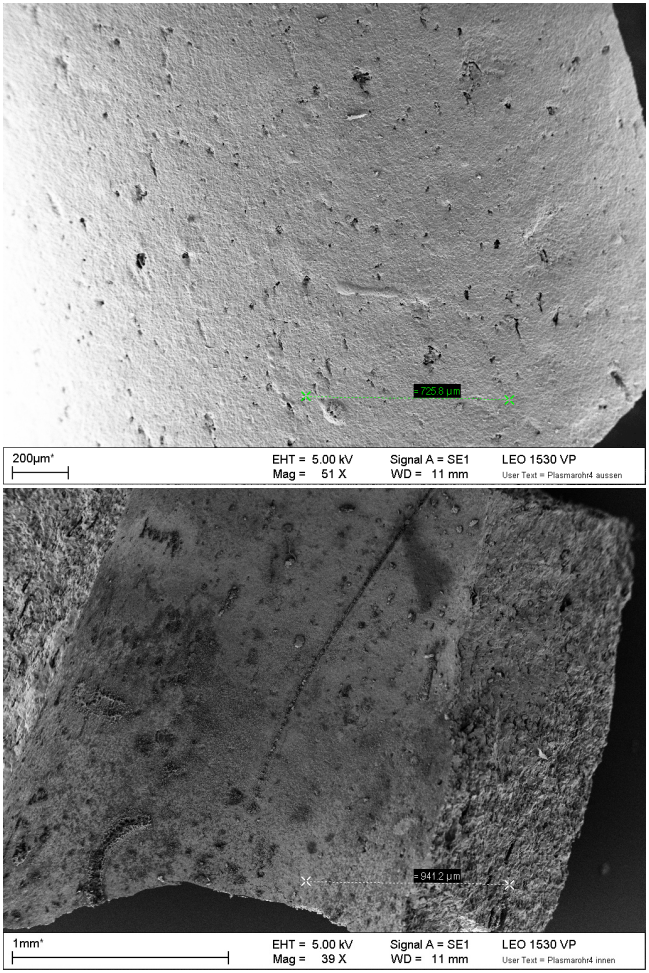

Figure 3.16.: *Scanning electron microscope pictures of an unused discharge tube. No cracks or other material defects are visible.*

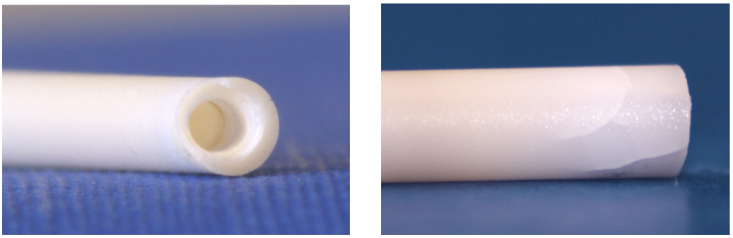

Figure 3.17.: *Discharge tube after operation with 5% of hydrogen as dopant (helium: 200-300 mL/min; MW power: 65 W; repeated solvent injection). The Material defects as consequence of the operation under these conditions are visible with the naked eye.*

conditions. Cracks in the ceramic and heavy erosion at the plasma position are visible. Correspondingly, operating conditions were evaluated to extend the discharge tube's lifetime.

3.3.1. Dopant Gas

High erosion of the discharge tube resulting from addition of hydrogen as dopant gas was already described by Estes *et al.* [100]. As a remedy against such erosion some authors recommended active cooling of the discharge tube with water or other cooling fluids, leading to increase the lifetime of the tube [71, 72, 94]. Unfortunately, a more complex setup is necessary for external cooling, complicating tube exchange and maintenance. In order to enable a simple and fast maintenance, our new detection system was constructed without requirements for cooling flu-

ids. In order to prove the applicability of the new system, the influence of dopant gases on the lifetime of the ceramic discharge tube was evaluated. The erosion resulting from high amounts (5%) of hydrogen added to the plasma gas is demonstrated in figure 3.17. Due to this erosion the inner diameter at the plasma position is increased, and the residual lower wall thickness is reducing the mechanical stability leading to a reduced lifetime. Besner *et al.* also reported peak tailing phenomena as a result of a changing flow pattern as consequence of this erosion [152]. Erosion was evaluated by plotting the lifetime of different discharge tubes running under similar conditions versus the used amount of dopant gas. Lifetimes less than 60 h are most frequently observed with hydrogen amounts above 4%. No significant differences in lifetime of discharge tubes used with pure helium plasmas and mixed gas plasmas with hydrogen concentration below 4% are observable. Hence, less than 4% hydrogen does not lead to higher erosion and shortened durability.

3.3.2. Plasma Source

To improve discharge tube's durability, minor changes of the plasma source have also been tested. One approach was to change the distribution pattern of the electromagnetic field particularly in the region of the discharge tube's walls. Lower field strength in the region close to the alumina walls should reduce heating of the wall. Therefore the diameter of the borehole on the front side of the cavity was increased from 3.3 mm to 3.7 mm. Hereby the microwave energy density at the tube wall was diminished. The resulting lower heating of the tube was

expected to lead to less erosion and longer discharge tube lifetime. Unfortunately only a few discharge tubes were running under same plasma conditions with different front hole diameters. Hence, results are not conclusive but a small improvement in durability of the ceramic tube could be assumed.

3.3.3. Solvent Load

Camman *et al.* reported a dependency of ceramic discharge tube lifetime from temperature shock resistance [151]. It is well known that high amounts of organic compounds - for instance the solvent vapor during a chromatographic solvent peak - may extinguish the plasma. As a consequence of this, the plasma and also the discharge tube are strongly cooled down. At reignition the resulting temperature shock caused by rapid heating of the alumina tube by the plasma may lead to cracks in the brittle material. In order to evaluate the plasma quenching effect of different solvent loads, the operation of the system using either splitless or split GC injection was further investigated. Certainly with discharge tubes used under splitless injection conditions, shorter lifetime could be observed compared to discharge tubes used in split injection mode.
The problem of low solvent tolerance is usually overcome by application of solvent venting systems [83, 92–95, 151]. For this purpose a Single-Column-Switching (SCS) System (*GERSTEL*) was installed behind the

capillary separation column to assure complete sample injection into the GC column. The applied system excludes possible mass discrimination effects expected for solvent venting in the injection port. Now maximum operation times above 600 h were gained.

3.4. Automation of the Detector

Nowadays automation is an important factor for application of laboratory systems as high sample throughput and high reproducibility can be provided and unattended operation becomes possible. Hence, a complete computer controlling of the new detection system was aspired. Moreover, important parameters should be monitored to avoid damage of system components and assure optimum analytical performance. Therefore following parameters have been considered during the required automation development:

- Controlling
  - Gas flows (plasma and dopant gases)
  - Ignition
  - Extinction
  - Shut-down in case of malfunction
  - Data acquisition parameters
  - Triggered measurements

- Monitoring
  - Microwave power
  - Gas flows
  - Plasma temperature

Microcontroller: To allow computer controlling of commercially available components not constructed for automation, a microcontroller was used. Due to its easy application based on simple software control via the implemented USB interface and the provided instrument library the *LabJack U12* controller available from *Meilhaus* (USA) was applied.

Digital Ports: The *Labjack U12* provides 20 digital I/O ports individual programmable as input or output channels. As digital signals are represented by a sequence of discrete values, two states are possible for these ports. True or false are represented by an electrical voltage set either to 0 V or to $+5$ V. Therefore these ports are usable for switching of components or accepting external trigger signals.

Analog Ports: In contrast to digital signals, analog signals can have any values. The two analog output ports can be set to voltages between 0 and $+5$ V with a 10-bit resolution (1024 increments). Moreover, the microcontroller provides eight analog input ports which are configurable either as 8 single-ended ports with an input range of ± 10 V or four differential ports with an input range of 20 V. The resolution of each

input port is 12-bit (4096 increments). Thus, provided analog ports are suitable for controlling and precise readout of voltages fed to components.

3.4.1. Controlling

Gas flows: Plasma conditions and the resulting analyte excitation is strongly depending on plasma gas flow and its composition. Therefore, automatic controlling of various components is essential to provide sensitive and reproducible detection system operation. While total plasma gas flow is affecting the residence time of analyte components in the plasma, dopant gases like hydrogen and oxygen are often applied to improve excitation conditions for various elements [50, 149, 152]. Chemical interferences like the formation of high melting oxides can be avoided by transformation to volatile hydride species. As a consequence high blank values and bad sensitivities resulting from the inefficient excitation can be reduced [149]. In contrast oxygen is usually applied to minimize deposition of elementary carbon. It may reflect microwave energy and thus leads to an unstable plasma discharge. However the low gas flow rates are to be controlled precisely.

Therefore, digital mass flow controllers (*Bronkhorst HIGH-TECH*) were used to control the plasma and dopant gas flow rates. The controllers for hydrogen and oxygen have been calibrated for the gas flow range from 0 to 10 mL/min, whereas the helium mass flow controller provides gas

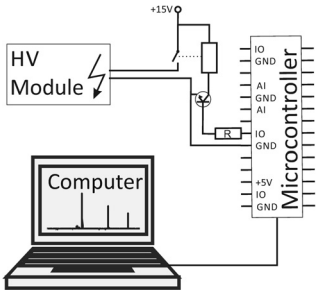

Figure 3.18.: *Circuit diagram for computer controlled ignition of the plasma.*

flows up to 300 mL/min. The used mass flow controllers were equipped with RS-232 interfaces allowing for simple computer controlling via the delivered instrument libraries.

Ignition: In a cold helium gas stream the amount of free charge carriers is too low for self ignition of the plasma. In consequence the essential charges for plasma ignition at a given electromagnetic field strength need to be formed by an electrical spark. Such ignition spark was generated by a commercial available 5 kV high-voltage-module (*Hivolt* G50R; output: 0-5 kV, 0.3 mA). Time period of the ignition spark is controlled via the developed software, as discussed in chapter 3.6. The circuit diagram is shown in figure 3.18. As depicted switching of the 15 V power supply for the high-voltage-module is achieved by a simple relay circuit via an I/O port of the microcontroller.

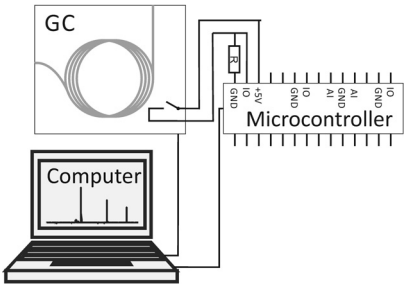

Figure 3.19.: *Circuit diagram for triggered measurements.*

Shut-down in Case of Malfunction: Extinction of the plasma by switching-off the magnetron in case of a malfunction is accomplished by controlling the supply-voltage of the magnetron via a solid-state-relay. In contrast to electromagnetic relays these devices work similar to a transistor without moving components and can be directly controlled via an I/O output port of the used microcontroller. This approach allows for software controlling even if the power-supply feeding the magnetron does not provide an adequate software communication interface. Monitored parameters used for the detection of an instrumental malfunction are the reflected power and the light intensity of the plasma.

Triggered Measurement: For reproducible retention times and applicability for long sample sequences, automated start of the measurement is essential. An appropriate output at the used *Agilent* GC-system is the "Event" port for controlling external devices as it includes two passive contact closures. Connection to this port offers an easy opportunity to

detect this remote start signal via an I/O-port of the microcontroller. The circuit diagram is demonstrated in figure 3.19. As shown, defined true/false states are assured by applying +5 V DC and a pull-down resistor, providing 0 V as false state.

Detection Parameters: Beside plasma conditions important detection parameters in OES are related to the detection system. Detection is accomplished by a commercial available CCD spectrometer which is software controlled via its USB connection to the system computer. All relevant parameters like exposure time and internal spectrum averaging are directly adjustable by use of the corresponding instrument library, providing these parameters.

3.4.2. Monitoring

Power: Microwave forward power and the amount of energy reflected by the plasma source are essential information to assess plasma properties and identify eventual problems. Therefore, these values should be monitored during application of the plasma source. The circulator used to prevent reflected microwave energy from re-entering the magnetron provides two electrical contacts for monitoring of both forward and reflected microwave energy. A rectifier-diode converts microwave power to an electrical voltage that is proportional to the microwave energy applied. This resulting voltage is measured with the analog-input port of

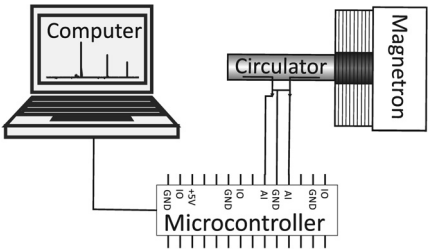

Figure 3.20.: *Circuit diagram for monitoring of forward- and reflected microwave power.*

the used microcontroller. Subsequently microwave power is calculated with an appropriate polynomial calibration function, which is unique for every rectifier-diode. The electric circuit is summarized in figure 3.20.

Gas Flows: In contrast to most other components used for the plasma detector, the utilized digital-mass-flow-controllers provide a RS-232 interface. Hence, direct connection with the computer allows continuous read out of current gas flows by use of the corresponding instrument library.

Temperature: As mentioned in chapter 2.1.1 plasma temperatures are usually calculated from the emitted spectrum using the *Boltzmann* equation. In order to measure the spectral features such as line intensities, high resolving monochromators are necessary. Due to the fact that the small CCD spectrometer used in the developed system provides only

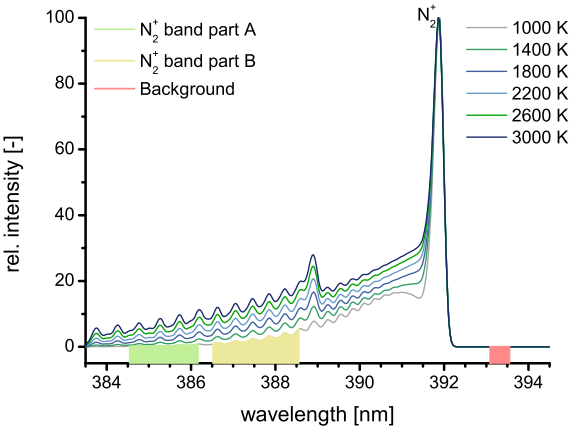

Figure 3.21.: *Simulation of the appearance of the N_2^+ emission at 391.4 nm including vibrational levels.*

limited resolution, common methods used for temperature calculation are not suitable. Thus, for a rough online temperature estimation a new approach is required.

In chapter 2.1.1 different temperatures defined according to local-thermal-equilibria (LTE) have been discussed. As mentioned the rotational temperature in a plasma is often calculated via N_2 emission bands and approximates the kinetic gas temperature. Therefore, the behavior of the N_2^+ emission band at 391.4 nm in dependence of changing gas temperatures has been simulated with the free software spectroscopy tool LifBase 2.1. The results are shown in figure 3.21. In contrast to the band head, that does not change significantly, the flank resulting

from rotational levels increases with higher gas temperature (see figure 3.21). This predictable, temperature dependant behavior was utilized for a rough temperature estimation by measuring the ratio of two integrals at different positions of the band. Due to the background radiation in the observed plasma, moreover a spectral region for background measurement has been defined and the average value was subtracted from all data points inside the integrals. The integrals of the spectral ranges highlighted in figure 3.21 and resulting integral-ratios are listed in table 3.6. As expected the ratios are increasing with temperature. Thus, a polynomial fit allows to calibrate the correlation between modelled temperature and integrals from the emission band. According to this, the temperature inside the plasma can be calculated using equation 3.1. Due to the used molecular band, the resulting temperature can be interpreted as rotational temperature.

$$\begin{aligned} T &= 30357.2 \cdot r^3 - 12834.5 \cdot r^2 + 6070.1 \cdot r + 436.9 \\ r &= \frac{Int.(A)}{Int.(B)} \end{aligned} \tag{3.1}$$

The approach was tested by means of a spectrum collected from the new plasma source. High accordance of the simulated spectra shown in figure 3.21 and the sampled spectrum is apparent from figure 3.22. The resulting ratio of 0.3328 correlates with a rotational temperature about 2200 K. This value is in good agreement with results gained with common methods described in chapter 5.2.

Table 3.6.: *Integrals of two regions of the N_2^+ emission band used for a rough estimation of the rotational plasma temperature.*

Temperature	Int.(A)	Int.(B)	Int.(A)/Int.(B)
1000 K	5.293	47.14	0.1123
1400 K	18.67	91.28	0.2046
1800 K	38.48	137.4	0.2801
2200 K	62.18	183.6	0.3387
2600 K	88.32	229.5	0.3849
3000 K	115.9	247.4	0.4224

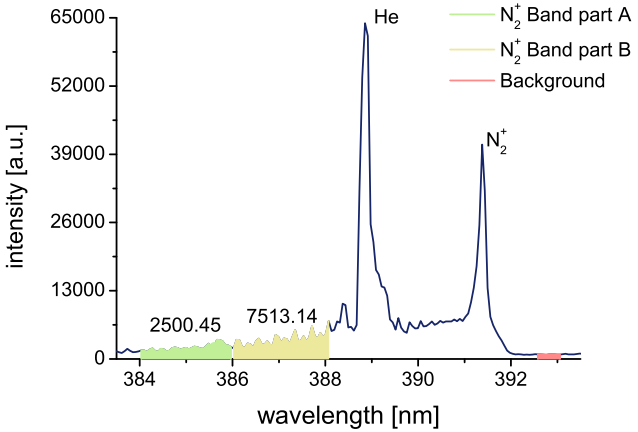

Figure 3.22.: *Spectrum of the new MIP source. The highlighted integrals (Int.(A)=2500.45) and Int.(B)=7513.14 were used for temperature calculation.*

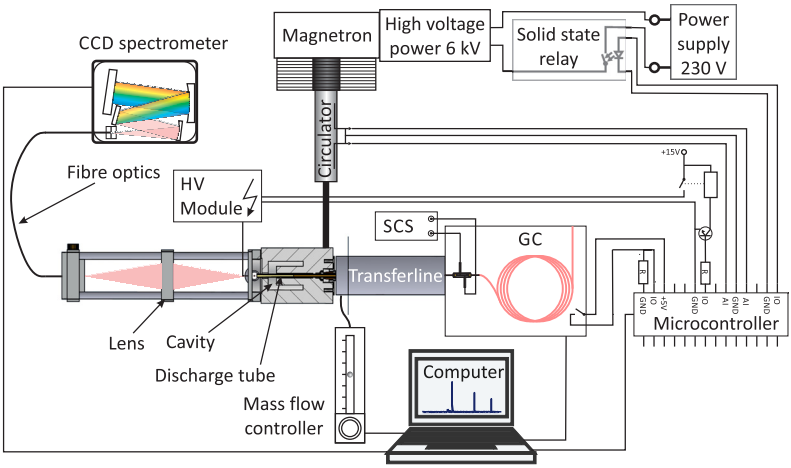

Figure 3.23.: *Complete connection diagram of the new microwave induced plasma emission detector.*

3.5. Final Setup

The final setup is summarized in figure 3.23. The gas chromatographic system consists of a *Hewlett-Packard* GC (HP 6890) equipped with a programmable temperature vaporization (PTV) inlet (*GERSTEL* CIS 4) and a multipurpose autosampler (*GERSTEL* MPS2). To protect the plasma against high solvent load, a Single Column Switching System (*GERSTEL* SCS) was used. It was installed between the capillary column and the transfer line and offered the opportunity of venting the

solvent peak. The GC was controlled with the GC ChemStation (Rev. B.02.01-SP1 [260]). All *GERSTEL* components were controlled via the *GERSTEL* Maestro Software (Version 1.4.8.4).

To fulfill the demand of complete automation the developed detection system is linked with the used GC components via the computer. Therefore it was necessary to develop a homemade software to allow an easy and user-friendly application of the detector, fully controlling the options provided by the technical setup. Different tools to control plasma and data acquisition parameters, monitoring system performance and data evaluation were necessary.

3.6. Software

Development of the software was performed with the graphical programming environment LabVIEW 2009 from *National Instruments*. As many functions are predefined, the corresponding commands are easy available even for untrained users.

A flowchart of the complete software is prompted in figure 3.24. As shown, at software start, the spectrometer is initialized by loading the corresponding instrumental library and the related calibration file. In addition, the plasma power supply is switched on. The main program is organized in two parallel "while loops" being executed repeatedly until a boolean statement is set true. The first loop is responsible for synchronization with the gas chromatographic system. It waits for trigger signals and transfers these to the second loop. The second loop contains the whole code for controlling, monitoring, data acquisition and data evaluation. This separation of synchronization and main processes assures that all trigger signals coming from the chromatographic system are recognized. A trigger signal starts the acquisition loop, which collects data for a defined period. Its structure will be discussed in section 3.6.2. As it is running in the main loop, neither data evaluation nor controlling or monitoring of the system is possible during data acquisition. Hence, the complete processor capacity of the PC is available for the acquisition process, assuring a high and particular constant data acquisition rate. After measurement has finished the main program loop continues.

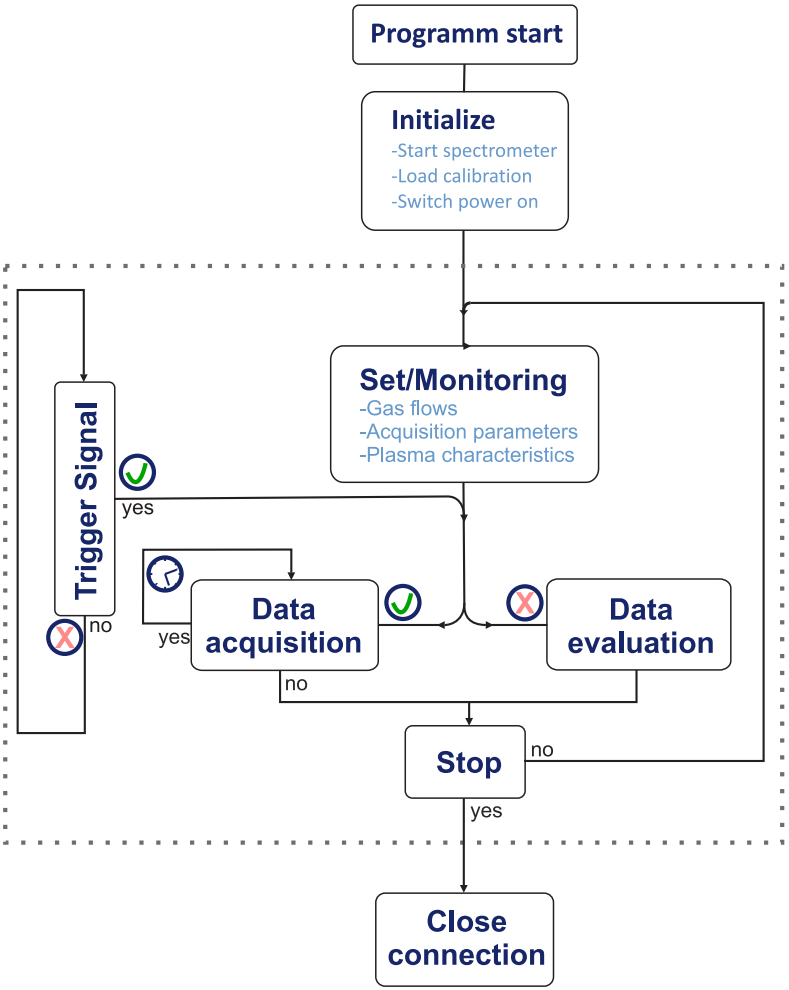

Figure 3.24.: *Flowchart of the purpose made software.*

The following sections will deal with the above mentioned functions of the software. Herein the graphical user interface (GUI) and the corresponding program code will be explained in detail.

3.6.1. Controlling and Monitoring

For a better structure of the GUI, the different functions of the software are organized in sub-panels. The control panel is shown in figure 3.25. Selected wavelengths are global parameters as they are necessary for data acquisition as well as for data evaluation. So the selection panel is located on the left side of the GUI. In consequence it is available in all selected function panels. In the upper region of the control panel a schematic setup of the detector is shown. Numerical values like gas flows and acquisition time are directly typed into the corresponding input boxes. The returned gas flow values are visualized via different sliders representing the different gases. To avoid an over saturation of all relevant detection wavelengths, the exposure time is completely controlled and adjusted by the system software.

To change the plasma and data acquisition conditions while processing a sample batch, above mentioned parameters may also be automatically set. Therefore it is necessary to load a sequence file, which contains the corresponding directory of the method files. Sequence files as well as method files are ASCII CSV files containing relevant parameters in a predefined order.

For igniting the helium plasma, first maximum plasma gas flow (He: 300 mL/min) is initiated and the system is flushed for 30 s. Sub-

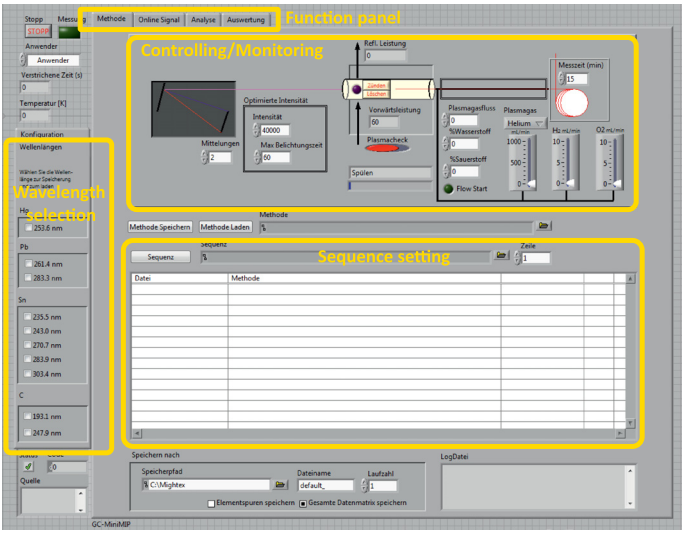

Figure 3.25.: *Graphical user interface for controlling and monitoring the plasma parameters.*

sequently the high voltage module is energized for 0.5 s so that the resulting spark ignites the plasma discharge. To assure equilibration of the plasma and avoid thermal shocks to the discharge tube, the system retains for 30 s with maximum gas flow before setting those gas flow value that shall be used during detection mode.

Strong heating of the cavity would lead to distortion and thus damaging of the plasma source. Therefore the magnetron needs to be switched-off at unexpected plasma extinction. Hence, forward and reflected microwaves power is monitored as described in chapter 3.4.2. Power values are obtained by a calibration function individually calculated for the used

rectifier-diode. Under normal operation conditions maximum 20% of the microwave's power is reflected in the plasma source. An extinguished or wrongly running plasma is easy detectable via the ratio of forward and reflected power. The software automatically stops the power supply of the magnetron in case of an unexpected increase of the reflected microwaves power above a level of 60%.

3.6.2. Data Acquisition

All relevant data acquisition parameters are set in the related control panel. Thus, the acquisition GUI just offers online observation of the collected data. As already shown in figure 3.24, data acquisition is organized in a separate "while loop" so that plasma and spectrometer parameters once transferred to this loop at its initiation are fixed during the acquisition process. Acquisition time is read-out within this loop in every cycle so that the time may be changed during the acquisition process.
As shown in figure 3.26 the collected spectrum is always processed in different ways:

- Optionally it is saved in an array to enable evaluation of the performed background correction and recalculate a background corrected chromatogram, after data acquisition is finished.

- To adjust the exposure time, the intensities of the selected detection wavelength are investigated. Correct adjustment is assured by

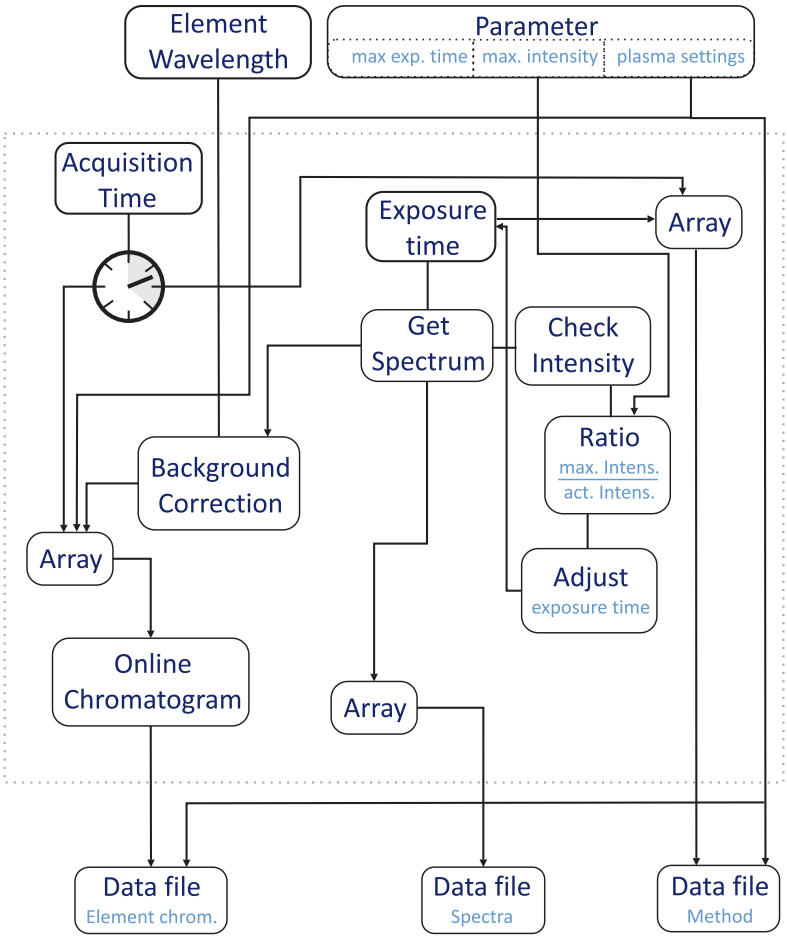

Figure 3.26.: *Flowchart of the data acquisition loop from the software.*

calculating the ratio of maximum permitted intensity and sampled intensity. Multiplication of the used exposure time with this ratio leads to the exposure time set for the next collected spectrum.

- For generation of an online chromatogram, the spectrum first need to be normalized according the used exposure time. Necessity can be explained from the changing absolute intensities in the spectrum, when the exposure time is automatically adjusted to avoid over saturation. After normalization, the background correction is performed as described in chapter 3.1.2. To allow a direct plotting of the chromatogram, a time stamp is added to each element specific intensity value and those data stored in an array. The element specific online chromatogram is obtained by plotting this array.

A recalculation of the element chromatograms during data evaluation requires a normalization of the raw spectra according to the used exposure times. Therefore all exposure times are linked with specific time stamps and written to a separate array.
After acquisition is finished, plasma- and sampling parameters are added to the online chromatogram- and the exposure time array for documentation. The structure of the resulting files is visualized in figure 3.27. According to further processing, the three arrays are saved to the hard disk in different data formats. The background corrected chromatogram file is saved as ASCII-txt-file, a format that can be opened in various software applications providing a flexible data evaluation. The exposure time array and the spectra array are stored as binary files in order

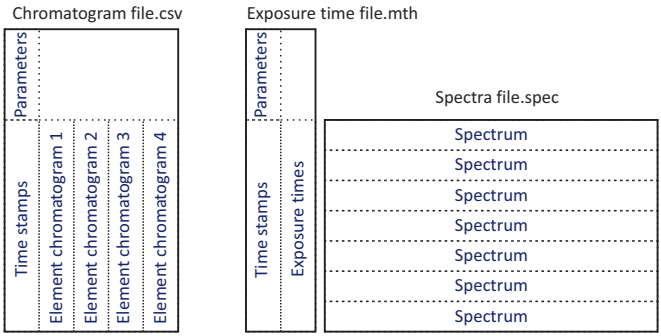

Figure 3.27.: *Structure of the different files saved after data acquisition.*

to assure a fast storage with minimum memory requirement. Nevertheless, this file occupies quiet significant storage space on hard disk drive. To reduce the required space on hard disk, it is possible to save just the chromatogram file. In turn, the opportunity of chromatogram recalculation or evaluation of the spectral background is lost.

3.6.3. Post Data Evaluation

Another important step is the evaluation of the collected data. To simplify this step, the software contains different tools for a fast and easy data handling. The responsible GUI is shown in figure 3.28. The different provided functions "Background Correction", "Signal to Noise", "Limit of Detection" and "Integration" are organized in different subpanels. In the upper region, the software offers a data explorer which is independent from the chosen data processing tool. Thus, data are

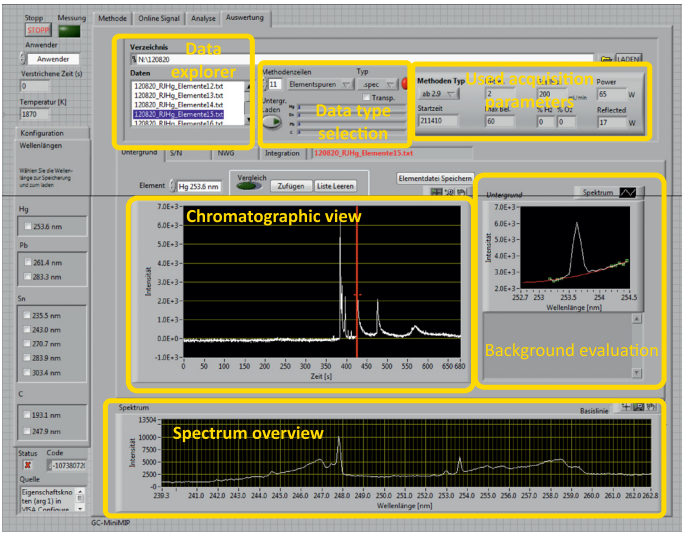

Figure 3.28.: *Graphical user interface to evaluate the spectral background and the applied background correction method.*

loaded by selecting the corresponding file-name. Supported file formats are the above mentioned sampled chromatogram txt-files and the spectra-files. Moreover, the software is able to load previously exported ICP-MS data stored in CSV-format (e.g. such as the data storage provided by *Agilent* ChemStation). In this context, signal-to-noise investigation, calculation of the detection limit and peak integration are applicable for any kind of chromatographic data stored in txt- or CSV-fromat.

Chromatogram txt-files: As visualized in figure 3.27, the chromatorgam txt-files are small and just contain the sampled element chro-

matograms making the loading process fast. To evaluate the spectral background the corresponding spectra-file can be loaded. Due to their higher memory requirements, the loading process is slower. As the background correction is not reprocessed during loading these files, only wavelengths observed during data acquisition are available. According to its properties, this data format is best for evaluation of great sample batches in routine analysis.

Spectra spec-file: All spectral information are stored in the spectra spec-files making a new background correction and calculation of elemental chromatograms necessary. This step requires high processor capacity, slowing the loading process. In turn, information about spectral background and the performed correction are directly available. Moreover, it is possible to analyze elements, not previously selected for data acquisition but perhaps becoming interesting afterwards. Hence, this data type is optimum for method development and a small number of unknown samples.

ICP-MS CSV file: Due to the lack of available software solutions for evaluation of GC-ICP-MS data, the opportunity to load these data was implemented in the developed software. Beforehand it is necessary to export the ICP-MS data to CSV-files. The *ChemStation* software saves the exported CSV-files in the corresponding sample folder. As these files may contain various chromatograms of different isotopes, it is necessary to select the related column to be loaded. For a simple drift correc-

tion, the opportunity to calculate the ratio of two ion chromatograms is implemented. The data evaluation routine offers a simple internal standard drift correction of the ion-chromatogram.

Background Correction: Evaluation of the spectral background can only be done in post-run data evaluation, after loading the corresponding spectra spec-file. The sub-panel to evaluate the spectral background contains three charts (see figure 3.28). The one in top left displays the selected element chromatogram. Using the cursor, the operator can select the spectrum corresponding to the chromatographic data point. The selected spectrum is displayed in the lower section of the sub-panel, showing the whole sampled spectrum and thus giving an overview of possible interfering molecular bands or other interfering emissions from the plasma source. The chart on the right hand side shows the spectral range around the observed elemental wavelength. Moreover, data points used for background correction are highlighted and the resulting polynomial function for background calculation is plotted. Therefore, a simple evaluation of the applied background correction by visual inspection is possible. In addition to that the software calculates the gas temperature of the plasma, according to the method described in section 3.4.2..

For a fast comparison of different samples it is possible to store the currently loaded chromatogram internally and overlay it with a second, new loaded one. This overlay function is suitable for a rough estimation of peak heights for example to assess reproducibility of sample preparation or the chromatographic system.

As shown in figure 3.29 in the lower section of the sub-panels for signal-to-noise ratio estimation, calculation of the detection limit and peak integration, a table appears. All results of the aforementioned functions are represented in this table including information about used detection wavelength, retention time and used evaluation tool. These results can be exported as tab separated CSV-file for further data processing. Despite the performed spectral background correction, the position of the chromatographic baseline may be different from zero, so that it has to be subtracted prior to further data evaluation. The software provides two methods for chromatographic baseline subtraction. In most cases it is suitable to use the median of the chromatogram as baseline. In case of high peak loaded chromatograms, in worst case additionally with strong tailing, this approach is not sufficient. Therefore, the baseline needs to be calculated for every single peak on the basis of the selected peak limits previously defined by the user.

For routine analysis with great sample numbers a batch processing option is included.All files within the batch are automatically loaded in the order displayed in the explorer and the results of the selected evaluation tool are stored to the results table.

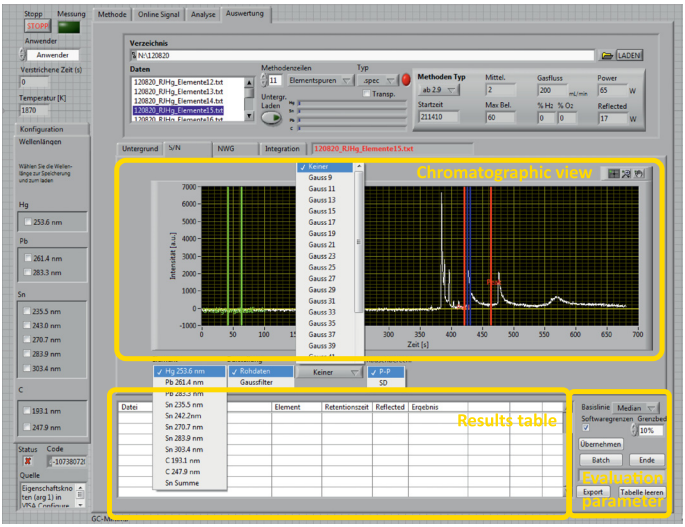

Figure 3.29.: *GUI for estimation of the signal to noise ration of a chromatographic peak.*

Signal-to-Noise Ratio: The signal-to-noise ratio of a chromatographic peak is usually calculated according to equation 3.2, where H is the peak height considering the chromatographic baseline and h_n is the greatest fluctuation in a period of five times the full width at half maximum (FWHM) of the peak.

$$\frac{Signal}{Noise} = \frac{2H}{h_n} \tag{3.2}$$

To simplify signal-to-noise ratio determination for the user, required input parameters to be entered were minimized during software development. After setting background and peak position, the software automatically identifies the peak maximum and calculates the FWHM. Sig-

nal-to-noise ratios are displayed in the results table. To gain meaningful results, it is necessary to check that range of retention time defined as instrumental blank is free of chromatographic signals.
To enhance the visual inspection possibility of the user, different graphical representation forms of the chromatogram can be selected. Details will be discussed in the section "Display options" on page 90.

Limit of Detection: The sub-panel for calculation of the limit of detection from a chromatographic peak, offers two options to define the peak window limits. The first one is an automatic selection of the peak window limits by the software. For this purpose, the algorithm developed to find the FWHM was extended to find position with lower percentage intensities of the peaks maximum. Provided are values of 10%, 20%, 25% and 50%, so that even window limits for not completely separated peaks can be located by the software. The advantage of software calculated peak window limits is the higher reproducibility. Moreover, even in presence of small variations in retention time, peak window limits do not have to be readjusted by the user. Thus, batch processing becomes possible. Alternatively, peak window limits may be defined by the user, an option that may be advantageous in case of poorly separated, strongly tailing peaks.
The limit of detection is calculated from the peak area according to equation 3.3 [153, 154].

$$x_{(DL)} = \sigma \cdot \frac{SD_{blank}}{b} \tag{3.3}$$

Thus, the detection limit ($x_{(DL)}$) depends on the standard deviation of a blank (SD_{blank}), the sensitivity b (slope of the calibration curve) and the uncertainty factor σ (usually $\sigma = 3$). To enable the calculation of blank's standard deviation the software sets the range of the blank 10 times longer than the corresponding signal peak. In this region, 10 integrations are performed and SD_{blank} is calculated from the resulting area values. Sensitivity is estimated by a linear fit of the blank's mean area and the peak area for a given analyte amount. The result is displayed in the results table. As already described for the signal-to-noise ratio calculation sub-panel, the chromatogram can be represented in different forms to improve visual inspection of the chromatogram (compare page 90).

Peak Integration: Certainly, evaluation of the peak areas is the most important step in chromatographic data analysis. Therefore, the software solution provides a powerful tool for peak integration. Most of the features like automated selection of peak window limits in a predefined range, auto-selection of the chromatographic baseline, batch-processing and the choice of different chromatogram representations have already been discussed in previous sections. Additionally, the integration tool supports up to 20 different regions for automated peak search and subsequent integration. In case of a baseline changing over retention time, the baseline can be defined separately for each peak search section. As the integration process is completely automated, the software is suitable

for the evaluation of chromatograms with a high amount of different analyte signals and a great number of sampled data in a short time by just one click.

Display options: To improve the signal-to-noise ratio after data acquisition, different approaches for noise reduction are possible. The simplest method is use of the moving average to smooth the noisy data. As an unweighted averaging of the data points along the time axis is performed, the desired noise reduction is achieved in connection with an undesired signal intensity reduction and the broadening of the chromatographic peak. Better results are obtained by applying improved methods using convolution with filter functions. The basic concept of filter functions is the reduction of high frequency information characterizing the noise, though essential information located in lower frequencies is kept. Most often used are Gaussian functions or Fourier transformation [155–159]. As already mentioned before, smoothing of chromatographic data is extremely simplified in the software. So Gaussian functions with different widths are selectable to allow convolution with raw chromatograms. The general function used for generation of these Gaussian functions is summed up in equation 3.4.

$$\phi(n) = e^{-\frac{1}{2}\left(\frac{\alpha \cdot n}{\frac{N}{2}}\right)^2} \tag{3.4}$$

In this context $\phi(n)$ is the density function. N represents the width of the Gaussian curve, while α is a value inversely proportional to the mathematical standard deviation of the Gaussian curve. In figure 3.30

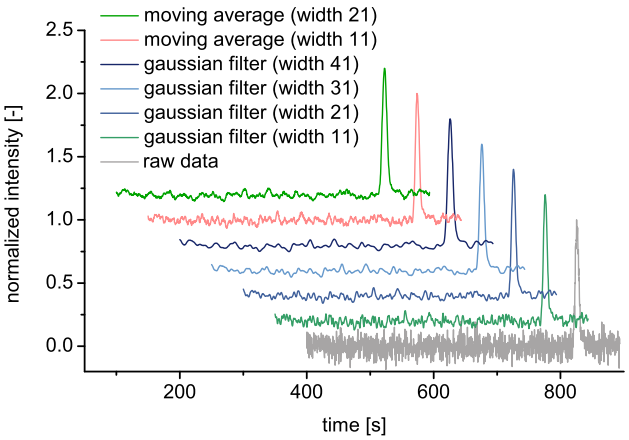

Figure 3.30.: *Influence of different smoothing approaches and filter width on the shape of the chromatogram.*

one chromatogram of dibutylmercury smoothed with different moving average width as well as Gaussian functions is shown. The improvement of the signal-to-noise ratio is obvious for the moving average and the Gaussian filter function. Moreover, peak broadening is negligible for both tested methods and applied width. To investigate the enhancement of the limit of detection by smoothing, signal-to-noise ratios for different width of the Gaussian function and moving average length were calculated. Results are shown in figure 3.31. As shown in figure 3.31, signal-to-noise ratio improvement for an optimized moving average is about 5.7 while an optimized Gaussian filter allows an improvement about 7.4. The found optimal Gaussian filter width in this case is 35

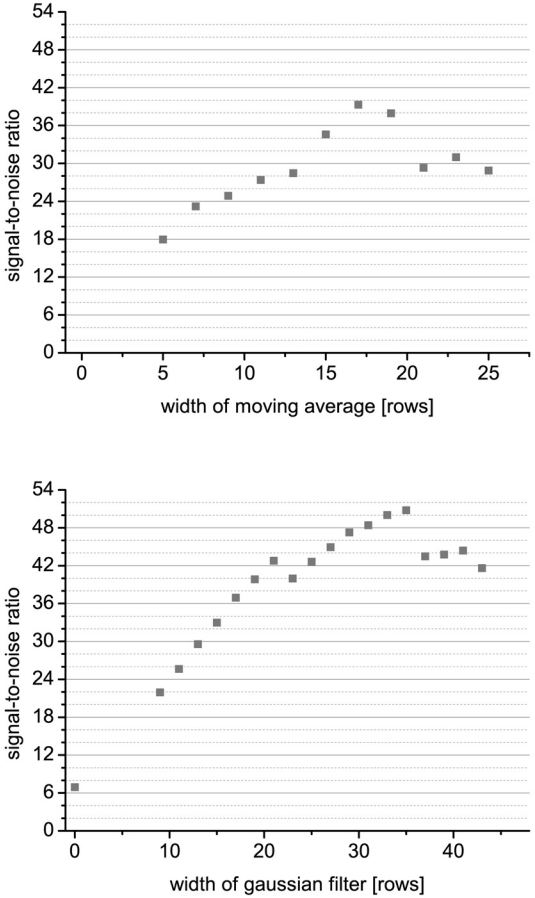

Figure 3.31.: *Dependency of the signal-to-noise ration from the moving average width and different filter's width.*

points correlating with a half width of 17 points. This filter length fits well to the detected chromatic peak width. According to this observation, highest signal-to-noise ratio values could be expected when using the Gaussian filter with a filter length corresponding to the chromatographic peak width. This result is slightly differing from those reported for the application of Fourier transformation as filter function, for which different authors observed optimum performance when filter's FWHM was about 60% of FWHM of the chromatographic peak [158,159]. Anyhow, to obtain best sensitivities filter width has to be adjusted according to peak width. Thus, optimum sensitivities for all chromatographic peak can only be ensured by selection of the filter's width according to the observed chromatographic peak width.

$$Int_{(k)} = \sum_{n=1}^{k} Int_n \tag{3.5}$$

Int$_{xx}$ represents the intensity while k and n are enumerators.

The visualization of the smallest peaks requires a completely different data handling. A plot of the cumulated intensities, calculated according to equation 3.5, results in a rising or falling function, if the chromatographic baseline is unequal to zero. This fact is also observable in figure 3.32 (data in light blue). The algebraic sign of the slope is depending on the absolute value of the chromatographic's baseline. By subtracting the median calculated from the raw data the slope of the cumulated sum is almost zeroed. Hence, chromatographic peaks are appearing as well defined steps in the chart (compare figure 3.32 dark

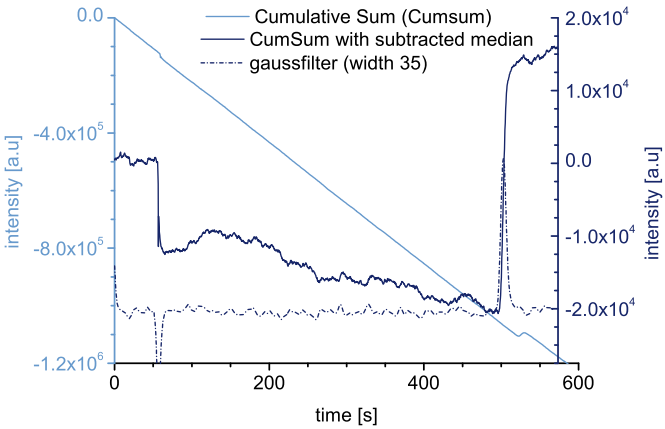

Figure 3.32.: *Comparison of a chromatogram in conventional shape and the cumulated representation.*

blue). A comparison of the plotted cumulative sum with a smoothed chromatogram (dark blue dash dots) illustrates the power of this way of data presentation.

4. System Optimization

As already mentioned in former chapters, low detection limits and high reproducibility are only achievable by optimization of instrumental parameters. As cavity and discharge tube dimensions as well as spectral resolution of the optical system are given by the used technical setup, only some plasma parameters are available for adjustment. Especially for multi element detection knowledge of optimum gas flows, dopant gases and applied microwave power is essential for achieving highest analytical performance. With respect to detection, the observation position within the plasma is important as different elements may be excited in different plasma regions [74, 83, 100, 160, 161]. For system optimization, all mentioned parameters have been optimized with respect to best signal-to-noise ratios using a response surface mapping method changing one parameter at time.

4.1. Gas Flows

First the influence of changing plasma gas flows on signal-to-noise ratios was investigated. As residence time of element atoms in the plasma is

Table 4.1.: *Instrument parameters for optimization purpose.*

GC		**Setting**
Injection	Vol.	1 µL
	Mode	Split 10:1
	Start Temp.	145 °C (0.2 min)
	Ramp	12 °C/s
	End Temp.	240 °C (8.0 min)
Column	Type	HP-1
		(30 m; 0.32 mm; 3.00 µm)
	Gas	Helium
	Press.	const. 162.9 kPa
Oven	Isotherm	160 °C (15 min)
SCS	Cut ON	at 1.0 min (25 kPa)
	Cut OFF	at 2.0 min
Transferline	Temp.	200 °C

depending on the velocity of the plasma gas inside the discharge tube, high gas flows may cause less efficient excitation than possible. Moreover, high gas flows reduce gas and discharge tube temperatures compromising atomization and excitation efficiency. Both effects are reducing intensities and detection power [71, 100, 160]. Reducing the plasma gas flow is resulting in higher residence time and higher temperature inside the plasma. Hence, higher intensities are expected. Unfortunately, increased plasma temperature is resulting in higher erosion of

the discharge tube, leading to reduced lifetime and increased spectral background. Moreover, higher temperatures enhance ionization rates of the analytes in the plasma and therefore decreases intensity of atomic emission lines.

To change plasma characteristics, small amounts of different dopant gases can be added to the plasma gas. As already mentioned, the element tin tends to form high melting oxides that cannot easily be dissociated by low power plasmas and therefore, is not available for atomic emission. Since such high melting compounds accumulate in the discharge tube, not only sensitivity is decreased but also peak tailing and subsequent memory effects can be observed. To overcome these problems, hydrogen is commonly added to the plasma gas to generate volatile hydride species and bind free oxygen as hydroxide [100, 149, 152, 162]. Beside possible positive effects the most severe disadvantage of the addition of hydrogen is an increased deposition of elemental carbon in the discharge tube resulting from the reducing environment. As result of deposition within the discharge tube, peak tailing has been observed. Moreover, elemental carbon reflects microwave energy, and thus reduces the power transfer into the plasma. The result is a signal drift during long term measurements. To reduce this effect often addition of oxygen to the plasma gas is proposed [46, 57, 97, 149, 152].

In the first optimization step, the influence of total gas flow and the amount of hydrogen on the detection performance were investigated. For this purpose, microwave power was adjusted to 95 W and the total gas flow was varied in a range from 300 to 100 mL/min with decre-

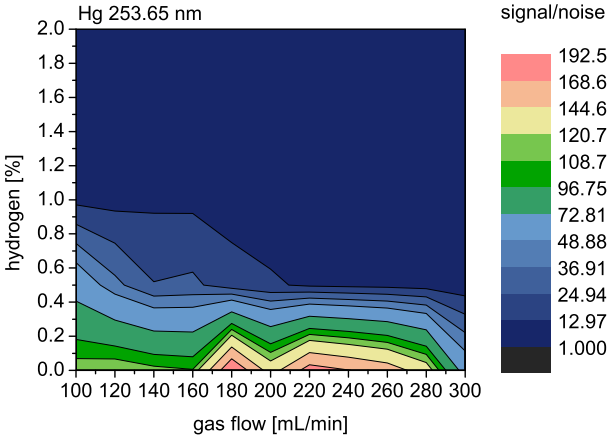

Figure 4.1.: *Image of the signal-to-noise ratio dependency for Hg detection from the plasma gas flow and its hydrogen content.*

ments of -20 mL/min. The hydrogen amount was altered from 2.0% to 0.0% with decrements of -0.5%. To investigate multielement capability of the mixed gas plasma the effects on mercury and tin detection were evaluated, respectively.

Mercury: Mercury signals were generated by repeated GC injection of DBM (10 µg/mL calculated as Hg) dissolved in methanol. Relevant GC parameters are listed in table 4.1. Results are summarized in figure 4.1. It is obvious that the signal-to-noise ratio for mercury is strongly de-

creased by addition of hydrogen. Best sensitivities are gained at a total gas flow between 180 and 240 mL/min. As expected, low gas flows are beneficial to gain high signal-to-noise ratios.
Due to the fact that hydrogen has shown no positive effect on mercury detection, the influence of added oxygen was investigated in the next step. Total gas flow was changed in established manner in the range between 300 and 100 mL/min with decrements of -20 mL/min. The amount of oxygen was changed between 2.0 and 0.0% with decrements of 0.5%. The resulting signal-to-noise ratio map is shown in figure 4.2. Accordingly, signal-to-noise ratio is strongly decreased with increasing oxygen amounts as it has been observed in experiments performed with hydrogen. Thus, it could be assumed, that addition of molecular gases lowers sensitivity of mercury detection for the used system. Background band emission intensities are reduced with added dopant gases. So an incomplete excitation could be assumed due to fact that additional breaking processes of molecule bond are absorbing plasma energy. Moreover, molecular species tend to absorb a lot of microwave energy by excitation of vibrational modes [163].

Tin: To generate a tin signal, TTET (100 µg/mL calculated as Sn) dissolved in methanol was repeatedly injected into the plasma via the GC. Parameters are equal to those used for mercury optimization and are summarized in table 4.1. The resulting signal-to-noise ratio maps for the most suitable tin detection wavelenghts 270.65 nm and 284.00 nm are shown in figure 4.3. The positive effect of added hydrogen on tin sensitivity is obvious. Remarkable is the local maximum at a total gas

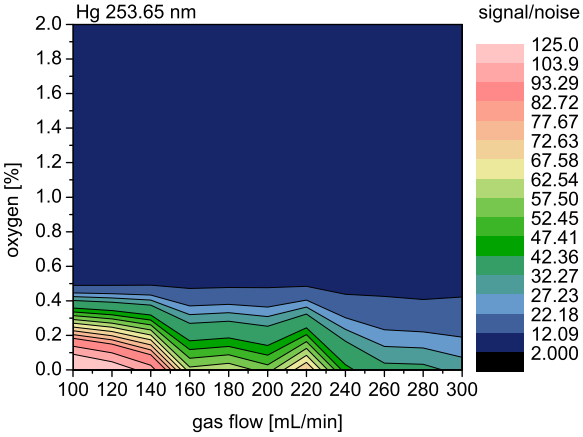

Figure 4.2.: *Influence of added oxygen in the plasma gas on the signal-to-noise ratio of mercury.*

flow of 160 mL/min and a hydrogen amount of 1%. Hence, for sensitive detection of tin, gas flows need to be accurately fixed at these values.

As these plasma conditions promote deposition of carbon in the discharge tube the effect of additional oxygen to the plasma gas was evaluated. For this purpose an additional oxygen amount between 0.0% and 2.0% was applied with 0.5% decrements. The total gas flow of helium and hydrogen were adjusted to their optimum values 160 mL/min and 1.0%, respectively. Subsequently the signal-to-noise ratios of two tin emission lines were analyzed. Results are shown in figure 4.4 and illustrate the negative influence of added oxygen. Obviously the addition of oxygen undoes the positive effect of hydrogen on tin detection.

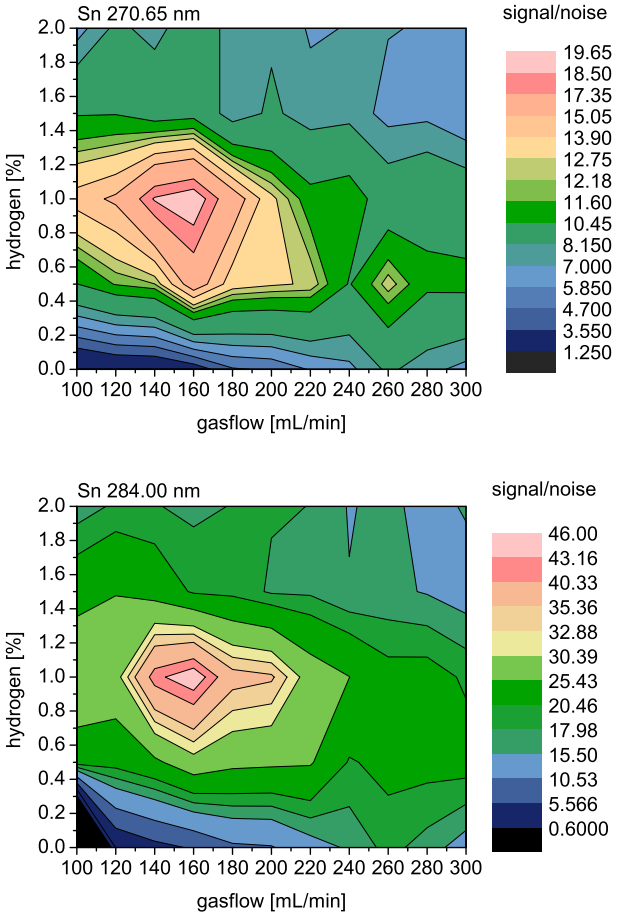

Figure 4.3.: *Signal-to-noise ratio dependency on helium plasma gas flow and hydrogen content of the plasma gas.*

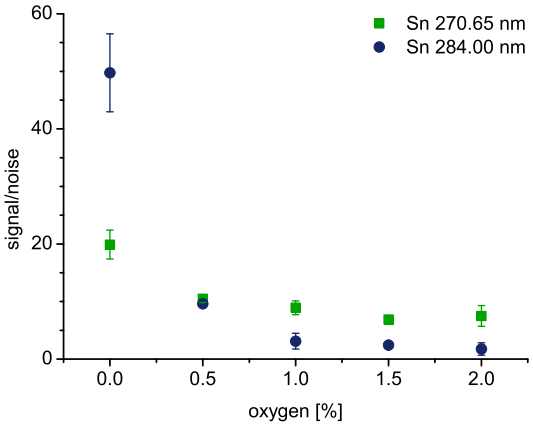

Figure 4.4.: *Influence of added oxygen on the signal-to-noise ratio of tin emission.*

Therefore, optimum gas flow rates for tin detection are a plasma gas flow rate of 160 mL/min with 1% of hydrogen added. The addition of oxygen should be avoided.

4.2. Plasma Power

Another important parameter affecting the sensitivity is the applied microwave power. It can be assumed that increased power results in increased emission intensities. However, the spectral background radiation is also increased partly resulting from the material eroded from the discharge tube. Moreover, at high power levels ionization may occur

reducing the population of atomic levels and therefore the intensity of atomic emission lines. Accordingly, the influence of the applied power on the response of the MIP-OES system is complex and need to be optimized [56, 70, 71, 73, 100].

Mercury: To find possible interrelation-ships between the applied microwave power, the composition or flow of the plasma gas and the signal-to-noise ratio, all parameters have been evaluated in one response surface mapping experiment. Therefore, the plasma gas flow was successively adjusted between 300 and 150 mL/min with decrements of 50 mL/min whereas the hydrogen amount was adjusted from 1.5% to 0.0% with decrements of 0.5% respectively. The lower gas flow rate limit was set to 150 mL/min as high thermal stress of the source was assumed at lower gas flow levels in combination with high microwave power levels. Parallely, the microwave forward power was varied between 60 W and 96 W with increments of 12 W. As before the mercury signal was generated by repeated GC injection of DBM (10 µg/mL as Hg) dissolved in methanol. Relevant GC parameters are listed in table 4.1. By this, the signal behavior at different gas flows and gas compositions was proved. Observed signal-to-noise ratios for mercury increases with the applied microwave power. According to optimized parameters mentioned above, best detection limits for mercury were obtained at low gas flows without dopant gases at maximum microwave power (He 160 mL/min; P $\geq$96 W).

Tin: Simultaneous to the optimization of the applied power for mercury, the influence on tin detection was investigated. As already mentioned for mercury, the plasma gas flow was varied from 300 mL/min to 150 mL/min with decrements of -50 mL/min. As already mentioned, the lower gas flow rate limit was set to 150 mL/min to avoid thermal stress to the source at lower gas flow rates with high microwave power levels. Simultaneously the hydrogen amount was adjusted from 1.5% to 0.0% with decrements of -0.5%. Investigated power levels were 60 W, 72 W, 84 W and 96 W. The signal-to-noise ratios resulting from the injection of TTET (100 µg/mL calculated as Sn) dissolved in methanol were calculated from the chromatogram. In this experiments the local signal-to-noise maximum was reproduced at a total gas flow rate of 150 mL/min with 1% of hydrogen. Moreover, it was observed that high microwave power is required to provide low detection limits. In this context no wavelength dependency of the calculated signal-to-noise ratios at different plasma conditions was observed.

4.3. Sampling Position

Technical setup: From the work of Quimby *et al.* and Tanabe *et al.* it is known that element emission intensities show a certain spatial distribution within the plasma [83, 160], making detection power depentent on the observed zone. In order to study such relationship, experiments have been carried out to investigate the spatial distribution of mercury and tin emissions in the plasma and its influence on

the detection power of the new plasma source. To gain highly sensitive element specific and spatial resolved plasma intensities, the optical system including spectrometer, fiber optics and lens system was removed from the detector. Instead a high resolution 750 mm grating imaging monochromator (Acton SP2750; *Princeton Instruments*, Grating 1800 lines/mm, Czerny-Turner) equipped with an intensified CCD camera (ICCD; PI-MAX 3 1024i; *Princeton Instruments*, 1024 x 1024 pixel) was used for plasma diagnostics using an imaging approach to generate a monochrome image of the plasma zone that was observed axially. To reduce the image distortion, a sub stage iris aperture was applied between the focus lens (f = 40 mm) and entrance slit of the spectrometer. The spatial distribution of the intensities of atomic emission lines was investigated under optimized plasma conditions by continuously adding small amounts of vaporized elemental mercury or TTET to the plasma gas. Background emission was eliminated from the recorded image by subtraction of the intensities of a background image from the plasma, recorded at same plasma and camera operation conditions but without sample injection.

Results and Discussion: The resulting images for mercury, collected at a helium gas flow of 200 mL/min and 95 W microwave power, are shown in figure 4.5. Reduced mercury emission intensities were observed in the center of the plasma compared to the boundary areas of the plasma. Such observation has already been described by Tanabe *et*

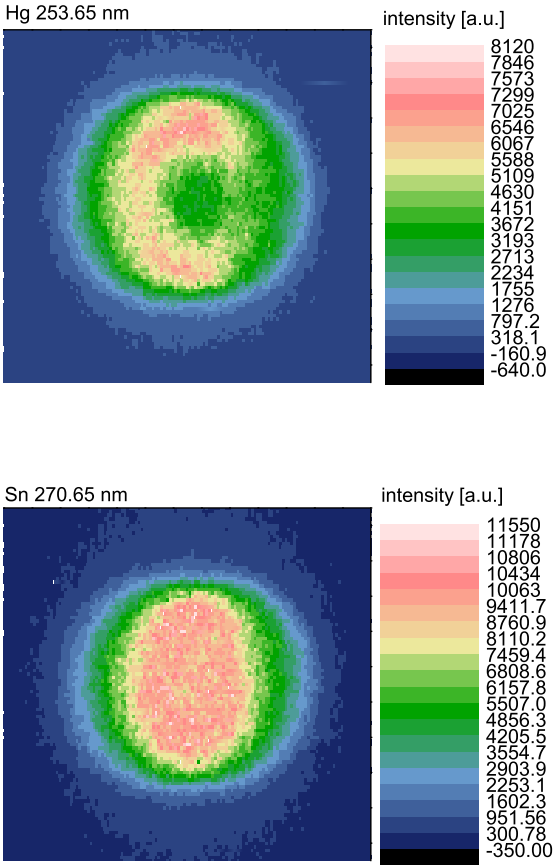

Figure 4.5.: *Spatial distribution of mercury (top) and tin (bottom) emission in the plasma source.*

al. using similar plasma conditions [160]. They explained this emission profile by the high ionization rate in the plasma center, resulting in reduced intensity at the atomic emission line.

In contrast to the atomic mercury emission, the emission intensity of the atomic tin line at 270.65 nm is homogeneously distributed over the cross-section of the discharge tube refering to figure 4.5. In this context, ionization does not explain the emission profile easily. According to the changed gas flow of 150 mL/min and 1% hydrogen used for tin detection, maybe the added diatomic hydrogen absorbs microwave energy mainly required for dissociating the hydrogen atoms. This energy is lost for the ionization processes of tin [152,162,163]. However, with 7.34 eV, the first ionization potential of tin is significant lower compared to that of mercury (10.44 eV). Therefore, other reasons than ionization seem to cause the effect. According to the relative high amount of mercury vapor introduced into the plasma, also self-absorption processes could cause the low emission intensity in the center of the displayed cross-section. It could be expected, that the abundance of element atoms is highest in the center of the optical path, so that the expected absorption has a maximum in the central area observed. While the used mercury emission line at 253.65 nm is a resonance line, resulting from electron relaxation to the ground state, the measured tin detection wavelength is no resonance line but corresponds to transitions between higher electronic excitation states. Since the related lower excitation state of tin

is not or minimum populated and can therefore not significantly absorb light of the corresponding transition wavelength, self-absorption is not expected [164]. Nevertheless, further investigations are required to understand the different spatial emission intensity distribution.

5. System Characterization

The developed plasma detection system was characterized according to its physical and analytical properties. Physical characterization of the plasma source was done by the "*Institute for Plasma Research and Technology*" *INP Greifswald*, including parameters like electron density and different plasma temperatures. Analytical characterization of the entire detector, consisting of plasma source, optical system and software has been performed in the framework of this thesis. Evaluated parameters were selectivity, linearity within the working range and limits of detection for all selected detection wavelength of mercury and tin discussed in chapter 3.1.1.

5.1. Electron density

Electron number density n_e is an important parameter for theoretical description of plasma sources. The high-energy electrons play a specific role in analyte excitation [55, 69]. Therefore, the electron number density in the new MIP source had to be determined in order to optimize and characterize the source. The measurements were per-

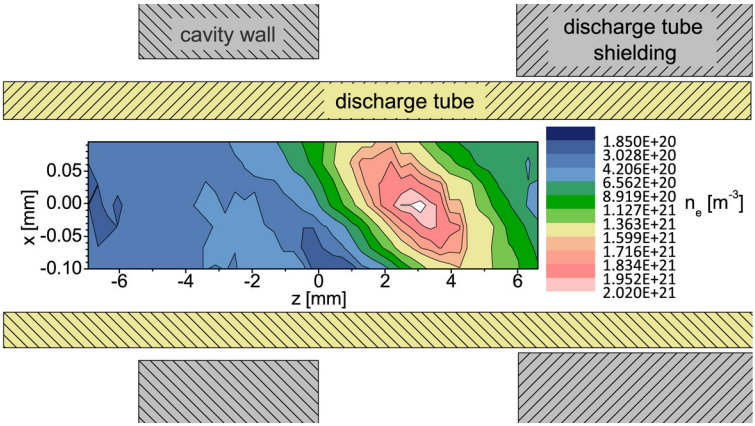

Figure 5.1.: *Spatial distribution of the electron density (n_e) inside the plasma. Axial direction was defined as z. Thus, the gas flow is directed from high to low z-values. Radial dimensions of the discharge tube and cavity walls are distorted.*

formed by precise determination of the Stark broadening of the H_β-line at 486.13 nm [67, 69, 72, 77, 165]. To gain high spatial resolution of the electron number density inside the plasma zone, the optical setup was adjusted as described in literature [166]. Just in short, the optical system consisted of two achromatic lenses and some aperture. The plasma radiation was conducted through a fiber optics from the image plane to a Czerny Turner monochromator (SpectraPro-500i; *Acton Research Corporation*; Grating 2400 lines/mm) equipped with line scan camera (TCE-1304-UW, *Mightex Systems*; 3648 pixel). By directing the focus of this system, a spatial resolution about 400 µm in axial direction

and about 50 µm in radial direction was achieved. Due to the fact that measured electron densities should be compared to a theoretically model of the plasma source, investigation was performed at a plasma gas flow of 200 mL/min Ar. Therefore, no conclusions on excitation characteristics of the new source running with He could be drawn from calculated electron densities. Nevertheless, comparison with other MIP sources described in literature is possible. As shown in figure 5.1, a maximum electron density of 2.1 x 10^{21} m^{-3} was found. This value is in good agreement with data collected from the theoretical model of this plasma source [166]. For the new sources operated with helium as plasma gas, a lower electron number density could be assumed according to the higher ionization energy of helium [56]. These data are in good agreement with other microwave induced plasma sources published in literature, taking into account that published values mostly represent mean values in the plasma due to the low spatial resolution used for their data collection [67, 69, 72, 74, 152].

In axial direction the plasma extends over a length of about 6 mm between cavity wall and shielding of the discharge tube. As shown in figure 5.1, the plasma discharge sustained in argon is not symmetric but tilted inside the discharge tube and indicates that the electomagnetic field distribution inside the resonator is orientated similar.

5.2. Plasma Temperature

In chapter 2.1.1 the necessity of defining different temperatures to describe a plasma has been mentioned and explained by the non equilibrium state of MIPs. As the gas temperature has a direct influence on vaporization, dissociation, atomization and further processes of sample components in the plasma it was further investigated for comparison with microwave plasma sources described in literature [55, 56].

5.2.1. Rotational Temperature

As commonly applied in plasma diagnostic for MIPs, gas temperature was estimated by calculating the rotational temperature (T_{rot}) from measured intensities of a molecular band of nitrogen (N_2^+ 391.44 nm, first negative system) present in the plasma. For the according temperature determination the emission profile of the molecular band was calculated theoretically as a function of the gas temperature [63, 68, 69, 162, 167]. The most suitable temperature was found by adjusting the theoretical to the actually measured emission profiles. The required spectral resolution necessary for resolving vibrational and rotational modes of the emission band was provided by a Czerny-Turner monochromator (SpectraPro-500i; *Acton Research Corporation*; Grating 2400 lines/mm) equipped with line scan camera (TCE-1304-UW, *Mightex Systems*; 3648 pixel). Dependency of T_{rot} from absorbed power and helium gas flow was investigated in a range from 18 to 40 W and 100 to 800 mL/min, respectively. As results shown in figure 5.2 il-

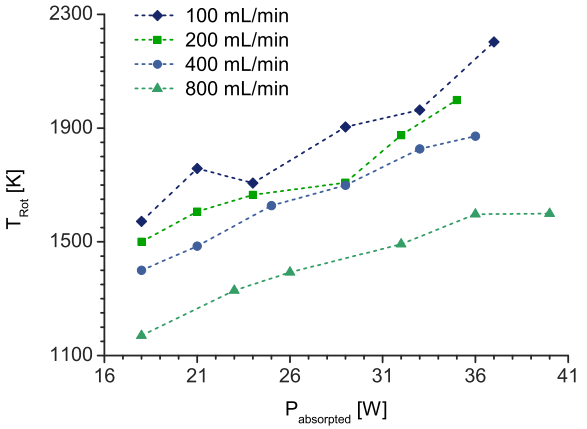

Figure 5.2.: *Rotational temperature (T_{rot}) of the plasma at variied plasma gas flows (He) and microwave power levels.*

lustrate, T_{rot} decreases with increasing plasma gas flow and increases with higher power levels. This observation is in accordance with data reported by Cotrino *et al.* [69]. The observed rotational temperatures at the usually used gas flow rate of 200 mL/min of He are within the range of 1500-2100 K. These values are very similar to temperatures measured in MIPs used by other researchers [67, 69, 72, 74, 152].

5.2.2. Kinetic Gas Temperature

Beside this established method of gas temperature approximation via the rotational temperature, it was also determined by laser absorption spec-

trometry (LAAS) with an acousto-optically modulated (AOM) laser. To allow the absorption experiment, the discharge tube fixture and transferline were replaced by a polytetrafluoroethylene (PTFE) component with a glass window at the end and a lateral gas connection. By this setup it was possible to guide the laser radiation through the plasma zone and to calculate the gas temperature according to the helium transition line at 667.81 nm. Details have been described by Baeva *et al.* [166]. The kinetic gas temperature of $T_{gas} = 1800$ K obtained in this way for the MIP operated at 20 W microwave power and a He gas flow rate of 200 mL/min is in good agreement with the rotational temperature ($T_{rot} = 1600$ K).

5.3. Analytical Performance Parameters

In analytical routine application, parameters like selectivity, sensitivity and linearity are of importance. Therefore, selectivity, linearity within the working range (LDR) and limits of detection (LOD) for detection of mercury and tin species were evaluated using the setup described in chapter 3.5.

Table 5.1.: *Analytical figures of merit.*

Wavelength		**Selectivity.**	**LDR**	**$LOD_{Observed/Lit.}$**
	[nm]	vs. carbon	*[ng]*	*[pg]*
Hg	253.7	159000	5	0.8/1.4 [168]
Sn	235.5	-12	50	801/-
	243.0	-87	50	372/-
	270.7	-215	50	280/5 [169]
	283.9	-1352	50	98/96 [152]
	303.4	-	50	183/0.5 [7]

5.3.1. Selectivity

The selectivity specifies the interference of an analyte signal by other species. Due to the high carbon amount of most matrices, selectivity is commonly evaluated versus carbon [57, 100, 161, 168]. Usually it is calculated according to equation 5.1 [57, 161].

$$S_{Analyte/Carbon} = \frac{b_{Analyte}}{b_{Carbon}} \tag{5.1}$$

Herein $S_{Analyte/Carbon}$ is the selectivity of the analyte emission line versus carbon, while b_{Carbon} and $b_{Analyte}$ are the slopes of the calibration curves of the interfering species and the analyte at the investigated detection wavelength.

To calculate selectivities for mercury and tin emission lines accessible with the new detection system, solutions of DBM (0.80 µg/g as Hg) or TTET (6.05 µg/g as Sn) in hexane spiked with different amounts

of carbon (0-100 µg/g as decane) were injected and separated via the GC. The usage of hexane instead of methanol as solvent was required due to the insolubility of decane in methanol. The resulting selectivities for mercury and tin are listed in table 5.1. The calculated selectivity for mercury is very high, although detection is interfered by an unknown carbon containing species as already discussed in chapter 3.1.4.
The found selectivities for tin are quite worse compared to mercury. All available detection wavelength show negative values resulting from over saturation of wavelengths used for background definition. As in literature selectivities up to $3{\cdot}10^8$ for tin against carbon have been reported [168], further improvements in future are expected by modification of the algorithm to adjust the exposure time of the used spectrometer.

5.3.2. Limit of Detection

The limit of detection (LOD) is defined as the lowest amount of the target compound that can be differentiated from blank value with a certainty of 99%. As already discussed in chapter 3.6.3 on page 88, the LOD is commonly calculated by means of equation 3.3. Accordingly, the limit of detection is calculated as multiple of the background's standard deviation. Usually, for the uncertainty factor, values between two and three are applied [57, 71].
Detection limits for mercury and tin have been calculated from chromatogramms obtained by injection of DBM (100 ng/mL as Hg) or TTET (100 µg/mL as Sn) both dissolved in methanol and obtained

Table 5.2.: *Instrument parameters used for evaluation of the analytical figures of merit.*

GC		**Setting**
Injection	Vol.	1 µL
	Mode	Split 10:1
	Start Temp.	145 °C (0.2 min)
	Ramp	12 °C/s
	End Temp.	240 °C (8.0 min)
Column	Type	HP-1
		(30 m; 0.32 mm; 3.00 µm)
	Gas	Helium
	Press.	const. 162.9 kPa
Oven	Isotherm	160 °C (15 min)
SCS	Cut ON	at 1.0 min (25 kPa)
	Cut OFF	at 2.0 min
Transferline	Temp.	200 °C
Plasma		
	Power	95 W
	Gasflow	200/150 mL/min (Hg/Sn)
	Hydrogen	0.0/0.5% (Hg/Sn)

under the chromatographic conditions listed in table 5.2. The standard deviation of instrumental blank signals was obtained by evaluating chromatographic ranges without chromatographic peaks. Previously, it was controlled that the statistical characteristics of these ranges in the chromatogram were identical in terms of intensity and noise values to those at the analyte peak's retention time so that instrumental blanks could be estimated on the chromatographic baseline. Results are summarized in table 5.1.

Though excitation characteristics of the plasma source are similar to previously described MIP sources, the detection limit for mercury could be improved in comparison to previously described MIP sources. It could be assumed that the improvement is gained by advanced in data sampling devices and data processing in comparison to earlier work. Detection limits for tin are higher compared to those described in literature, although similar plasma conditions have been applied. However, in contrast to previously described systems a ceramic discharge tube was applied instead of a fused quartz glass tube. Therefore, a loss in detection power for tin, may be related to interactions of the sample with the Al_2O_3 or its inclusions. The effect of changed discharge tube materials need to be investigated in future.

5.3.3. Working Range

Quantification can be best achieved, for detection systems providing a linear correlation between amount of analyte and detector signal. At high analyte concentrations in the plasma, linearity may be disturbed by

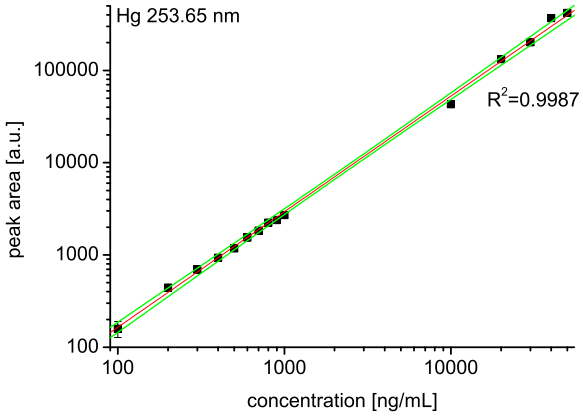

Figure 5.3.: *Working range of the developed detection system for mercury. Linearity has been proven by the Mandel test.*

self-absorption or over-saturation of the detector device. The working range of a system is the concentration range for which linear response can be obtained. A wide working range is an important qualifier, assuring broad application and reducing sample dilution and other concentration adjustments. Linearity within the working range of the developed detection system has been verified by GC injection of solutions containing DBM (0.1-50 µg/mL as Hg) or TTMT (5-500 µg/mL as Sn) dissolved in methanol with increasing concentrations. The linearity was estimated by plotting the peak area vs. the concentration. Linearity of the response was evaluated by the Mandel test [170]. Results for mercury and tin are shown in figure 5.3 and figure 5.4, respectively. Even

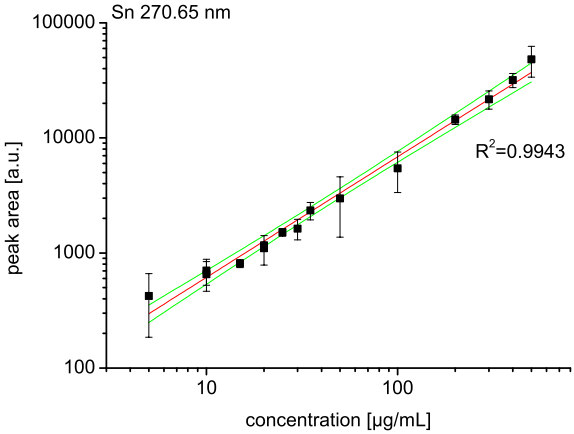

Figure 5.4.: *Working range for detection of tin. Linearity has been proven by the Mandel test.*

at high concentrations no flattening of the calibration curve can be observed, indicating that the linear dynamic working range of the detection system is wider than the concentration range tested here. Due to the application of capillary columns in GC, high analyte amounts are expected to force overload effects. The resulting peak broadening would limit quantification of high concentrations with acceptable chromatographic resolution.

6. Method Validation

Validation of the new detection system was performed by investigation of two certified reference materials as well as by participation in an interlaboratory study. For mercury the certified reference material IRMM BCR-464 (tuna) with a certified content of methylmercury and total mercury was used. The reference material IRMM BCR-646 (fresh water sediment) provides certified contents of tributyltin (TBT), dibutyltin (DBT), monobutyltin (MBT), triphenyltin (TPhT), diphenyltin (DPhT) and monophenyltin (MPhT).

6.1. Procedures

6.1.1. Treatment of Glass Vials

To avoid possible species loss resulting from adsorption at active glass surface, all glass vessels have been silanized before usage [122]. For this purpose, the glass vials were heated for 12 h at 80 °C. To simplify the handling, vials up to 2 mL volume were placed in a 1 L Erlenmeyer flask before. Afterwards, 1.5 mL of hexamethyldisilazane (HMDS) per 100 vials or 1 µL HMDS per mL of vessel volume were added, respectively.

Vessels were sealed and heated for another 12 h at 80 °C. After removal of remaining HMDS with methanol, all vessels were dried before usage.

6.1.2. Preparation of Activated Copper

The copper powder (average particle size: 63 µm) used for removal of sulfur from the sample extract was activated by addition of HCl (50%) and subsequent temporarily stirring (30 min reaction time). Afterward, HCl was decanted and the activated copper was washed with solvents of decreasing polarity ending with hexane.

6.1.3. Preparation of Derivatization Reagent

As tetra alkylborates are air sensitive and partially hygroscopic, small amounts (ca. 1 g) of sodium tetraethylborate (STEB) and sodium tetra phenylborate (STPhB) were weighted into glass vials (20 mL) under Ar atmosphere. The vials were stored in the fridge at -20 °C till usage. Solutions (10%) were prepared prior to analysis by dissolution of the salt in an appropriate amount of THF (HPLC grade without stabilizer).

6.1.4. Preparation of Stock- and Spiking Solutions

Mercury: Stock- and spiking solutions of mercury were prepared in graduated flasks made of polymethylpentene (PMP) to avoid analyte loss by adsorption on the surface. Standards listed in table 6.1 were weighted in the flask and subsequently filled up to the calibration mark with i-propanol (*"STOCK" solution*). To ensure traceability, solvent

Table 6.1.: *Concentrations of stock and high and low concentrated spiking solutions of all used mercury species.*

	Species	$m_{Std.}$	$m_{Solv.}$	$Conc._{Hg}$
STOCK	MeHgCl	12.20 mg	8.0315 g	1.517 mg/g
	EtHgCl	16.80 mg	8.0645 g	2.079 mg/g
	BuHgCl	14.90 mg	8.0523 g	1.847 mg/g
HIGH	$MeHg^+$	0.7757 g	98.8114 g	9.526 µg/g
	$EtHg^+$	0.7742 g	98.8265 g	12.35 µg/g
	$BuHg^+$	0.7807 g	98.8211 g	10.00 µg/g
LOW	$MeHg^+$	2.4919 g	22.5281 g	1.054 µg/g
	$EtHg^+$	2.4694 g	22.4263 g	1.360 µg/g
	$BuHg^+$	2.4838 g	22.7757 g	1.091 µg/g

weight was taken. According to the varying amount of mercury species expected in the different samples, two spiking solutions were prepared for every standard. For high-concentrated spike solutions (*"HIGH" solution*) an appropriate amount of every stock solution was weighted in a graduated flask and filled up with deionized water. Subsequently the weight of the solvent was taken for calculation of the resulting concentration. The low-concentrated spiking solutions (*"LOW" solution*) were prepared in the same way from the high concentrated spiking solutions. Resulting concentrations are summarized in table 6.1.

Table 6.2.: *Concentrations of stock solutions for tin.*

Standard	$m_{Std.}$	m_{MeOH}	$Conc._{Sn}$
MBTCl	19.60 mg	7.8716 g	1.045 mg/g
DBTCl	25.50 mg	7.9851 g	1.244 mg/g
TBTCl	27.70 mg	7.8502 g	1.282 mg/g
TTBT	30.70 mg	7.8841 g	1.326 mg/g
MOTCl	33.40 mg	7.8717 g	1.483 mg/g
DOTCl	35.80 mg	7.8664 g	1.293 mg/g
MPhTCl	19.20 mg	7.8480 g	0.959 mg/g
DPhTCl	32.10 mg	7.9777 g	1.384 mg/g
TPhTCl	36.60 mg	7.8395 g	1.431 mg/g
TPTCl	23.70 mg	7.8613 g	1.241 mg/g
TTPT	25.70 mg	7.8858 g	1.268 mg/g

Tin: Stock solutions for all tin species listed in table 6.2 were prepared by weighting the species in silanized graduated glass flasks (10 mL). Thus, increased blank levels from plastics were avoided. After filling up to the calibration mark with methanol, solvent weights were taken to ensure traceability. Resulting concentrations of the stock solutions are summarized in table 6.2. Due to the high number of tin species, mixed spiking solutions were prepared to simplify calibration and spiking of the samples with internal standard (*"IS" solution*). According to the different amounts of tin species, three spiking solutions were prepared (main components: *"MAIN" solution*; trace components: *"TRACE"*

Table 6.3.: *Concentrations for tin spiking solutions.*

Spike	Species	$m_{Std.}$	m_{MeOH}	Conc.
IS	TPT	66.0 mg	15.6832 g	5.27 µg/g
	TTPT	12.2 mg		1.03 µg/g
MAIN	MBT	185.6 mg	15.3871 g	12.21 µg/g
	DBT	155.7 mg		12.19 µg/g
	TBT	153.8 mg		12.42 µg/g
PRE	TTBT	74.9 mg	9.3456 g	12.6 µg/g
	MPhT	109.6 mg		13.4 µg/g
	DPhT	72.7 mg		12.8 µg/g
	TPhT	71.1 mg		13.0 µg/g
	MOT	68.8 mg		13.0 µg/g
	DOT	65.6 mg		10.8 µg/g
TRACE	**PRE**	154.1 mg	15.6082 g	
	TTBT			124 ng/g
	MPhT			131 ng/g
	DPhT			126 ng/g
	TPhT			127 ng/g
	MOT			127 ng/g
	DOT			106 ng/g

solution; intermediate dilution for trace solution: *"PRE" solution*). For this purpose appropriate amounts of stock solutions were weighted into graduated glass flasks and filled up with methanol. Resulting concentrations of the spiking standards are calculated according to the solvent's weight. Results are listed in table 6.3.

6.1.5. Moisture Measurements

Determination of water content of freeze dried and cryo milled samples was performed directly before further sample preparation. Moisture measurement became necessary because all samples were stored at -20 °C, resulting in slightly increasing water contents with storage time due to humidity condensation on unsealed samples.

Because in drying methods apart from water also other volatile components may be lost, the drying loss is not necessarily equal to the water content. Moreover, this method is very time consuming. Therefore, determination was performed by means of volumetric Karl Fischer titration using an automated system from *Metrohm* (901 Titrando). A single-component solution (Hydranal® Composite 5) containing iodine, sulfurdioxide, imidazole and methanol was used as titrant. As the titer of the titrant solution may vary resulting from humidity it was checked before measurement by using sodiumtartrate-pentahydrate for cross checking. Titer measurements as well as sample moisture measurements were performed according to the procedure described below. The titration vessel was filled with methanol and titrated till dryness. Subsequently sodium tartrate or sample (ca. 100 mg) were added and

the titration started. Titer of the reagent solution and samples were analyzed in triplicate. The resulting moisture amount in the tuna reference material BCR-464 was calculated as 6.41% (weight/weight). The water content in the tuna material analyzed within the interlaboratory study was 8.81% (weight/weight). The detection limits of volumetric Karl Fischer titration are approximately 100 µg/g of water in the sample. As water contents of all tin samples analyzed within this work were found to be below this value, they have not been considered for quantification.

6.1.6. Mercury Speciation Analysis

The method used is based on an in-house method from the *Federal Institute for Material Research and Testing* (BAM), Berlin. It has been develop by T. Sommerfeld for speciation analysis of mercury in fish meal [171]. A scheme of the procedure is shown in figure 6.1. Sample tissue (CRM: 0.2 g; Sample: 0.3 g) was placed in a heat and pressure resistant centrifugation tube. For calibration purpose sample was replaced by appropriate amounts of species standards. Butylmercury as well as ethylmercury (CRM: 100 µL High-Spike; Samples: 250 µL Low-Spike) were added as internal standard. For enhancing accuracy, spike weights were taken and glacial acetic acid (5 mL) was added for digestion. Microwave digestion was carried out for 20 min at 50 W. Ultrasonic-assisted extraction followed this procedure for 60 min. The extracts were allowed to cool down and a mixture of methanol, water and acetic acid (15 mL; 1/1/1.5) as well as NaOH (15 mL; 2 M) were

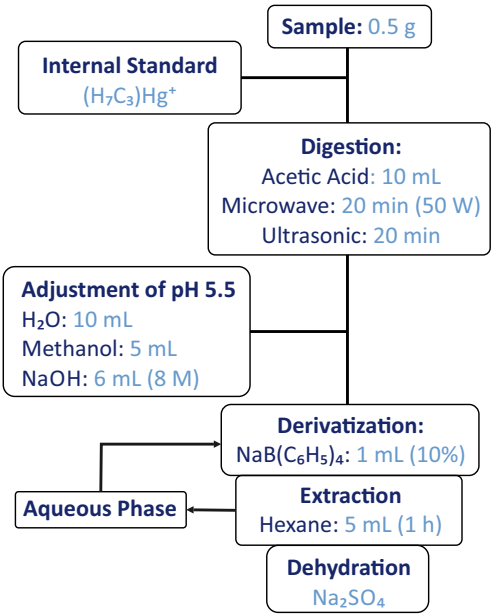

Figure 6.1.: *Scheme of the sample preparation method used for mercury speciation analysis.*

added to adjust the pH to 5.5. Derivatization and solvent extraction were carried out twice by addition of STPhB (0.5 mL 10% in THF) and hexane (5 mL) and subsequent shaking of the mixture for 60 min. Phase separation was executed by centrifugation (10 min, 3500 rpm). The organic phases were collected with a glass pipette, combined and dried with Na_2SO_4 prior to measurement.

6.1.7. Tin Speciation Analysis

Sample preparation was performed according to ISO DIS 23161.2: 05.2007. The work flow is visualized in figure 6.2. After addition of internal standard solutions (IS-Mix, 100 µL, table 6.3) and taking its weight, the sample (CRM: 1.5 g; Samples: 3 g) was extracted with glacial acetic acid (5 mL) assisted by ultrasonic treatment (30 min). As already described for mercury speciation analysis, for calibration purpose sample was replaced by appropriate amounts of mixed species standards listed in table 6.3. Solids and solution were separated by centrifugation (10 min; 4000 rpm), followed by a second ultrasonic treatment (30 min) assisted extraction of the precipitate with a mixture of acetic acid, methanol and water (15 mL; 1/1/1). Both centrifugates were combined and the pH adjusted to 4.5 by addition of NaOH (15 mL; 2 M) and water (5 mL). Species were derivatized and solvent extracted twice by addition of STEB (0.5 mL; 10% in THF) and hexane (10 mL) with subsequent shaking (60 min). Both organic phases were combined, dried over Na_2SO_4 and concentrated to 1 mL. The removal of sulfur from the sample extract was carried out by treatment with activated copper (63 µm). Cleanup was performed by adsorption chromatography with florisil®. The column was first rinsed with hexane (10 mL). After sample application, non polar species were eluted with a mixture of hexane and dichloromethane (20 mL; 9/1). Prior to analysis, the cleaned sample extracts were concentrated to 0.5 mL by means of a nitrogen gas flow.

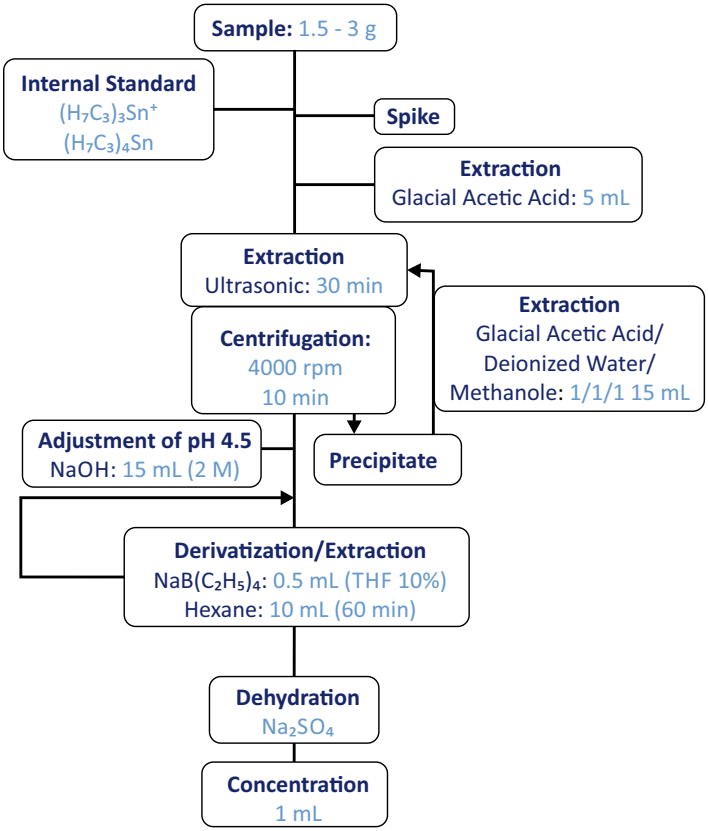

Figure 6.2.: *Sample preparation method used for tin speciation analysis.*

6.2. Instrumentation

6.2.1. GC-MIP/OES

The technical setup of the used GC-MIP/OES has already been discussed in chapter 3.5.

6.2.2. GC-ICP/MS

As GC-ICP/MS is well established for analysis of organometallic species, it was used for reference measurements to prove accuracy of the new developed detection system. The used system consisted of a gas chromatograph (*Agilent* 6890N) equipped with split/splitless inlet and an automatic liquid sampler (*Agilent* 7683B). Detection was perfomed with an *Agilent* 7500ce ICP/MS system. Hyphenation was accomplished via a heatable (to 300 °C) transferline (*Agilent*). It contained an untreated fused quartz capillary, which was connected to the GC column via a glass seal column connector (*Supelco*). Thus, GC effluent were efficiently guided to the plasma and interactions of sample with hot metal components in the transferline were avoided. To assure a complete effluent transfer to the plasma, ICP injector gas flow was heated in the GC oven and guided through the transferline. If necessary, oxygen required to avoid carbon deposition at the sampler cone was added to the injector gas flow. The transferline was connected to the plasma in two different ways.

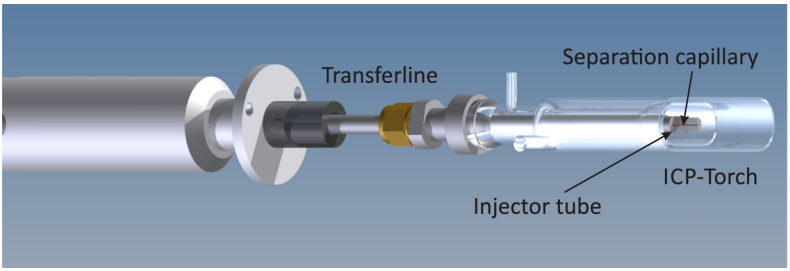

Figure 6.3.: *Direct hyphenation of GC with ICP/MS.*

Dry Plasma: In this setup, a special torch (*Agilent*) without injector tube was used so that the end of the transferline was directly connected to ,the torch and replaced the injector tube, as shown in figure 6.3. Thereby the gas chromatographic capillary ended directly in front of the plasma providing a maximal sample transfer. To allow for element selective tuning, elementary mercury vapor was injected via the transfer capillary into the plasma [172] to achieve optimized conditions for mercury detection. With dry plasma conditions, oxygen (150 kPa) was added to avoid carbon deposition at the sampler cone.

Wet Plasma: As already mentioned in chapter 2.3, hyphenation of GC-ICP/MS using the wet plasma mode does not require special torches or injectors. Hyphenation was accomplished by mounting the transferline at an additional gas inlet above the cyclone spray chamber as illustrated in figure 6.4. Due to the fact, that no commercial hyphenation kit for connection of the used components was available, an adapter has been built by the mechanical workshop of the IAAC. A PFA MicroFlow

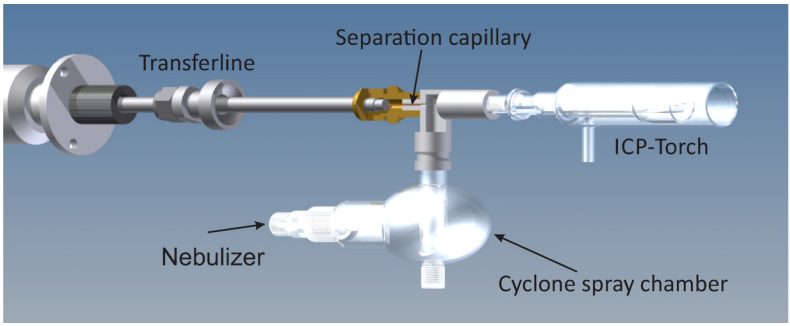

Figure 6.4.: *GC-ICP/MS hyphenation via a cyclon spray chamber.*

nebulizer (*AHF*) was used for liquid sample introduction. Besides the advantages of the wet plasma mode already discussed in chapter 2.3, Davis *et al.* reported increased signals during usage of a wet plasma [27]. They explained the higher sensitivity by an increased electron number density in the plasma channel resulting from the introduced hydrogen from water. In consequence, heat transfer in the plasma is improved and thus ionization increased.

6.3. Certified Reference Materials

6.3.1. Mercury Speciation Analysis

A first validation of mercury speciation analysis with the new detection system was performed by analysis of the certified reference material

Table 6.4.: *Analytical results for BCR-464.*

	$MeHg^+$ [mg/kg]	**Recovery**
Certified value	5.50 ± 0.17	-
GC-MIP/OES	5.37 ± 0.13	97.6%
GC-ICP/MS (dry mode)	5.46 ± 0.23	99.3%
GC-ICP/MS (wet mode)	5.48 ± 0.22	99.6%

BCR-464. This tuna material provides a certified content for methylmercury ($MeHg^+$) of 5.50 ± 0.17 mg/kg and a certified mass fraction of total mercury of 5.24 ± 0.10 mg/kg.
Samples were treated according to the procedure described under 6.1.6. According to the certified $MeHg^+$ content and the samples weight of circa 200 mg, an absolute amount in the reaction vessel of 1.07 to 1.13 µg was expected for $MeHg^+$. Thus, $MeHg^+$ was calibrated in a range from 0.80 to 1.2 µg. According to literature the remaining mercury content in the fish material is present in the form of inorganic mercury Hg^{2+} [28, 37, 47, 173, 174].

To ensure correct results, samples were prepared and analyzed in triplicate. ICP/MS reference measurements were performed with direct hyphenation (dry plasma) and via a cyclone spray chamber (wet plasma). All relevant GC, MIP and ICP conditions are shown in table 6.5 and table 6.6.

The results are summarized in figure 6.5. In top, a chromatogram collected with the new MIP/OES detection system is shown. The chro-

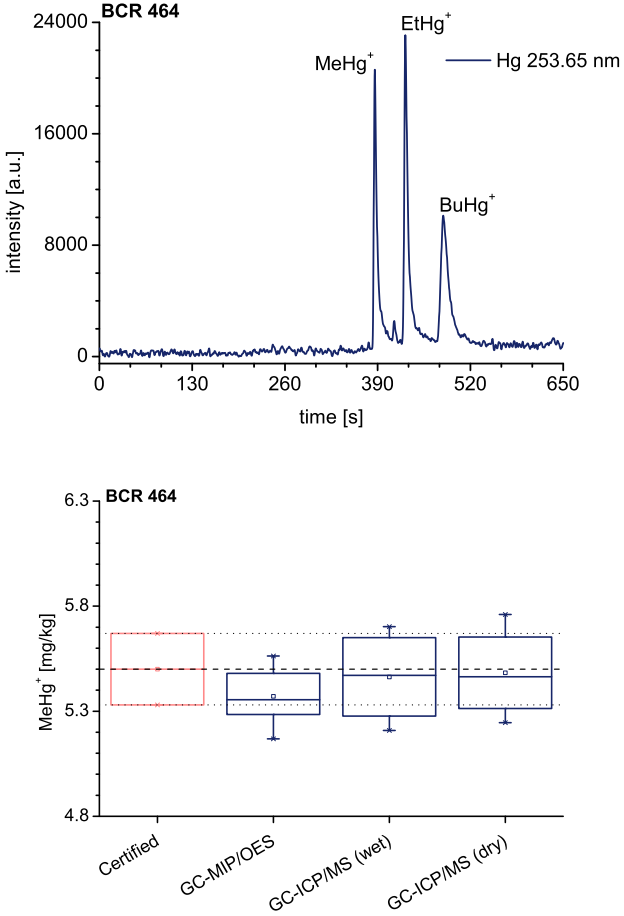

Figure 6.5.: *Top: MIP/OES Chromatogram of the tuna material BCR 464 smoothed with a Gaussian filter. Bottom: Validation results for mercury using the certified reference material BCR 464 (tuna).*

Table 6.5.: *Gaschromatographic parameters used for speciation analysis of mercury in fish matrices.*

Injector		
	PTV[I]	**Split/Splitless**
	Splitless: 0.5 min	0.5 min
	Inj. Vol.: 1 µL	1 µL
	Temp.: 60 °C (0.0 min)	250 °C
	12 °C/s	
	- 270 °C (10 min)	
GC		
	Column:	HP-1 30 m; 0.25 mm; 0.25 µm
	p(front):	154 kPa (const.)
	Temp.:	60 °C (3 min)
		30 °C/min - 250 °C (0 min)
		60 °C/min - 310 °C (1 min)
Transferline		
	Temp.:	250 °C
Solvent vent		
	SCS	**ICP/MS**
	Cut: 0.0 min (off)	-
	0.5 min (on)	-
	3.5 min (off)	-

[I] Programmed Temperature Vaporizer

Table 6.6.: *Detection parameters used for mercury analysis.*

MIP		
Plasma		
Power:	65 W	
He flow:	200 mL/min	
H_2 flow:	0 mL/min	
O_2 flow:	0 mL/min	
Detection		
Integration:	60 ms	
Spectra averaging:	2	
Wavelength:	253.65 nm	
ICP/MS		
Plasma	**wet**	**dry**
RF-Power:	1200 W	1200 W
Sample depth:	5 mm	5 mm
Coolant gas:	14.0 L/min	14.0 L/min
Carrier gas:	0.95 L/min	0.75 L/min
Makeup gas:	0.30 L/min	0.27 L/min
Oxygen:	-	150 kPa
Mass spectrometer		
Isotopes:	^{202}Hg	^{202}Hg
Drift standard:	^{238}U	-
Dwell time:	30 ms/Isotope	

matogram was smoothed with an appropriate Gaussian filter. The used conditions provide a full separation of the analyzed species. As expected, no inorganic mercury (Hg^{2+}) was detected. In the bottom of the figure results obtained by complementary detection techniques are compared. A good agreement between MIP/OES and ICP/MS results is obvious. Moreover, all results are within the confidence limit of the certified content of $MeHg^{+}$. These results indicate that both sample preparation as well as the new MIP/OES system are suitable for mercury speciation analysis of fish.

6.3.2. Tin Speciation Analysis

For validation of tin speciation analysis with the MIP/OES system, the standard reference material BCR-646 was used. Samples were prepared in triplicate according to the method described under 6.1.7. The main components (MBT, DBT, TBT) were calibrated from 350 to 4200 ng (absolute, calculated as Sn) and the minor components were calibrated in a range from 8 ng to 300 ng (absolute, calculated as Sn).

A chromatogram of a calibration standard, collected with the MIP/OES detector, containing circa 1500 ng of the main species and circa 100 ng of the minor species is shown in top of figure 6.6. As no peaks for the minor components appear in the chromatogram, the corresponding species contents are below the detection limit for tin. Moreover, peak tailing of the main components is observed, which would cause quantification problems of the minor components. Therefore, just butyltin species were quantified in the reference material using tripropy-

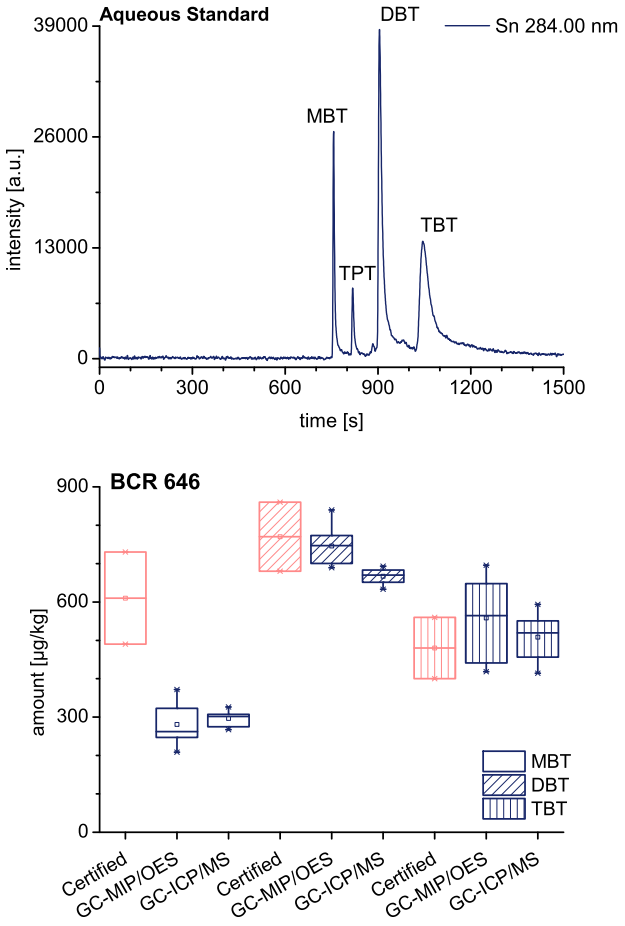

Figure 6.6.: *Top: MIP/OES chromatogram of an aqueous standard, smoothed with a Gaussian filter. Bottom: Results of the reference material BCR 646.*

Table 6.7.: *Results of the certified reference material BCR-646.*

	MBT [µg/kg]	**DBT** [µg/kg]	**TBT** [µg/kg]
Certified	610 ± 120	770 ± 90	480 ± 80
MIP/OES	281 ± 56	746 ± 55	558 ± 104
ICP/MS	297 ± 20	667 ± 18	509 ± 62
Recovery			
MIP/OES	46.1%	96.8%	116.3%
ICP/MS	48.7%	86.6%	106.0%

ltin (TPT) as internal standard. GC-ICP/MS hyphenated via a spray chamber was applied as reference method as with direct hyphenation no tin peaks were detectable. The reasons are not jet understood, particularly since Wahlen and Wolff-Briche reported detection limits of their used instrument that should be sufficient for real samples [175]. Relevant GC, MIP/OES and ICP/MS parameters are listed in table 6.8 and table 6.9. Calculated concentrations and certified values of MBT, DBT and TBT are depicted in figure 6.6.

Remarkable is the good agreement of the observed values and the certified content for DBT and TBT with recoveries about 100%. For MBT a poor recovery rate was observed. As MIP/OES data show high accordance with ICP/MS data, instrumental problems could be excluded. The high conformity of DBT and TBT results, excludes general problems

Table 6.8.: *Gaschromatographic parameters used for speciation analysis of tin in sediments.*

Injector		
	PTV	**Split/Splitless**
	Splitless: 0.5 min	0.5 min
	Inj. Vol.: 10 µL	1 µL
	Temp.: 40 °C (0.05 min)	250 °C
	12 °C/s	
	- 275 °C (2 min)	
	12 °C/s	
	- 300 °C (15 min)	
GC		
	Column:	HP-1 30 m; 0.25 mm; 0.25 µm
	p(front):	157 kPa (const.)
	Temp.:	40 °C (3 min)
		10 °C/min - 210 °C (3 min)
		40 °C/min - 290 °C (1 min)
Transferline		
	Temp.:	270 °C
Solvent vent		
	SCS	**ICP/MS**
	Cut: 0.0 min (off)	-
	1.0 min (on)	-
	5.0 min (off)	-

Table 6.9.: *Detection parameters used for tin analysis.*

MIP	
Plasma	
Power:	65 W
He flow:	300.7 mL/min
H_2 flow:	9.3 mL/min
Detection	
Integration:	50 ms
Averaging:	3
Wavelength:	270.65 nm
	284.00 nm

ICP/MS	
Plasma	**wet**
RF-Power:	1200 W
Sample depth:	5 mm
Coolant gas:	14.0 L/min
Carrier gas:	0.95 L/min
Makeup gas:	0.30 L/min
Mass spectrometer	
Isotopes:	^{118}Sn
	^{120}Sn
Drift standard:	^{115}In
Dwell time:	30 ms/Isotope

during sample preparation. Additionally the derivatization efficiency for MBT is expected to be higher compared to DBT and TBT as the lower sterical hindrance should facilitate the derivatization reaction. Otherwise, adsorption of monoalkylated tin species (MBT, MPT) on glass surfaces has been reported by Ceulemans *et al.* [122]. As glass vessels have been silanized to avoid this effect, it is implausible in the actual case. Another possible explanation is the high adsorption of MBT at the sediment matrix leading to incomplete extraction. As reasons are not yet totally understood, further investigations are required.

6.4. Interlaboratory study

A further validation of the new detection system has been carried out within an interlaboratory study. Due to the fact that only one MIP/OES detector was available, common range of interlaboratory studies with circa 10 participating laboratories was not feasible. Thus, the system was tested at two locations. This procedure was also intended to demonstrate the robustness of the developed instrument with regard to transport and dis- and re-assembling.

For the study the optimized GC-MIP/OES system was first sent to the Federal Institute for Materials Research and Testing (*BAM*), Berlin. After performance tests with standards, mercury and tin samples prepared in two independent experiments by different staff were analyzed. Subsequently, the system was uninstalled and reinstalled at the *University of Münster*. The interlaboratory study was finished by preparation and

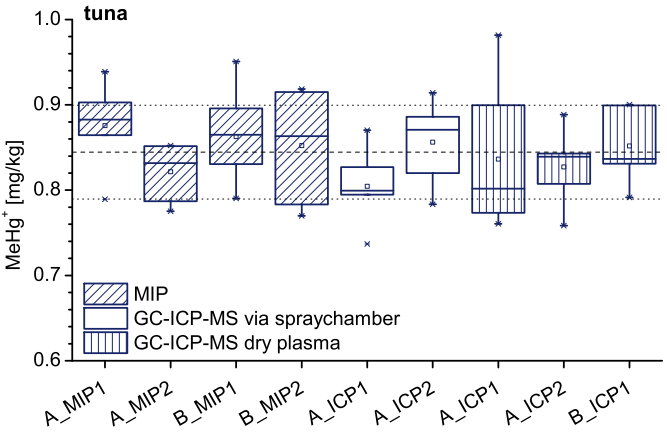

Figure 6.7.: *Results gained for the tuna material.*

analysis of the same sample materials used at the *BAM*, again by different staff in two independent sample treatments. Accordingly, laboratory and staff dependency of the found results could be evaluated.

6.4.1. Mercury

In addition to the reference material BCR-464 with high $MeHg^+$ content a naturally contaminated provisional reference material for tuna was analyzed during the interlaboratory study. According to literature, for naturally contaminated tuna 0.77 mg/kg of $MeHg^+$ in the dry mass should be expected [176]. Therefore, absolute amounts of circa 230 ng are resulting in the reaction vessel, when using a sample amount about

Table 6.10.: *Comparison of the calculated amounts of $MeHg^+$ in the tuna sample analyzed within the interlaboratory study. A and B are referring to the laboratories, while the number defines the staff member.*

Method	**$MeHg^+$** [mg/kg]
A-MIP1	0.876 ± 0.056
A-MIP2	0.822 ± 0.034
B-MIP1	0.863 ± 0.051
B-MIP2	0.852 ± 0.068
A-ICP1 spray	0.805 ± 0.044
A-ICP2 spray	0.856 ± 0.048
A-ICP1 dry	0.836 ± 0.100
A-ICP2 dry	0.827 ± 0.048
B-ICP1	0.852 ± 0.047

300 mg. In consequence, $MeHg^+$ was calibrated in a range from 150 to 400 ng. Samples and standards were prepared according to the procedure described in section 6.1.6. In both laboratories GC-ICP/MS was used as reference method. The instrumental parameters used for GC-MIP/OES and GC-ICP/MS are listed in table 6.5 and table 6.6. The results are summarized in figure 6.7 and table 6.10.

A high accordance of all results was found. Therefore it could be assumed that the used analytical methods are robust as data from both laboratories and different staff are in good agreement. Gener-

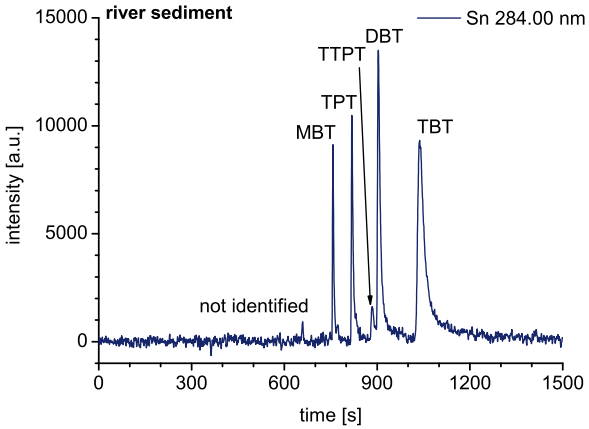

Figure 6.8.: *MIP/OES chromatogram of the tin contaminated river sediment. The chromatogram has been smoothed with a Gaussian filter.*

ally, ICP/MS and MIP/OES data are correlating well. That demonstrates that the new MIP/OES detection system provides high accuracy. Moreover, with the good agreement of MIP data from both laboratories, simplicity and robustness of the developed detection system was demonstrated.

6.4.2. Tin

To show easy and accurate tin speciation analysis using the new detection system, a river sediment from the "Elbe" river was analyzed

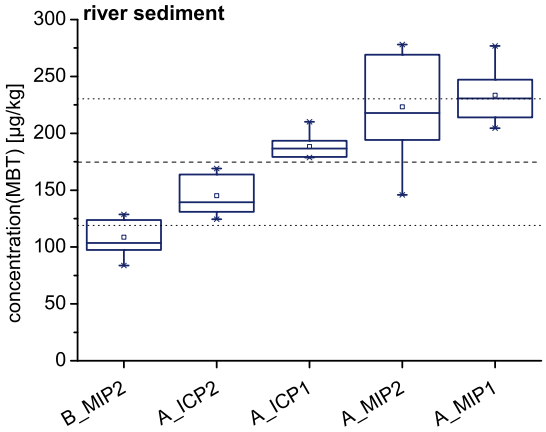

Figure 6.9.: *Amounts of MBT found in th river sediment analyzed in the interlaboratory study. A and B are referring to the laboratories and the number refer to the staff member.*

within the interlaboratory study. As shown in the chromatogram of the sediment collected with the MIP/OES system, the materials main components are MBT, DBT and TBT. Concentrations of the minor components are lower than the detection limit of the system. With a sample amount of 3 g, the same calibration strategy already used for the certified reference material was used here as well. Absolute species masses were calibrated in the range from 350 to 4200 ng.

Results from GC-MIP/OES and GC-ICP/MS measurements from all species are compared in figure 6.9, figure 6.10 and table 6.11. Applied instrumental parameters are summarized in table 6.8 and table 6.9. Vari-

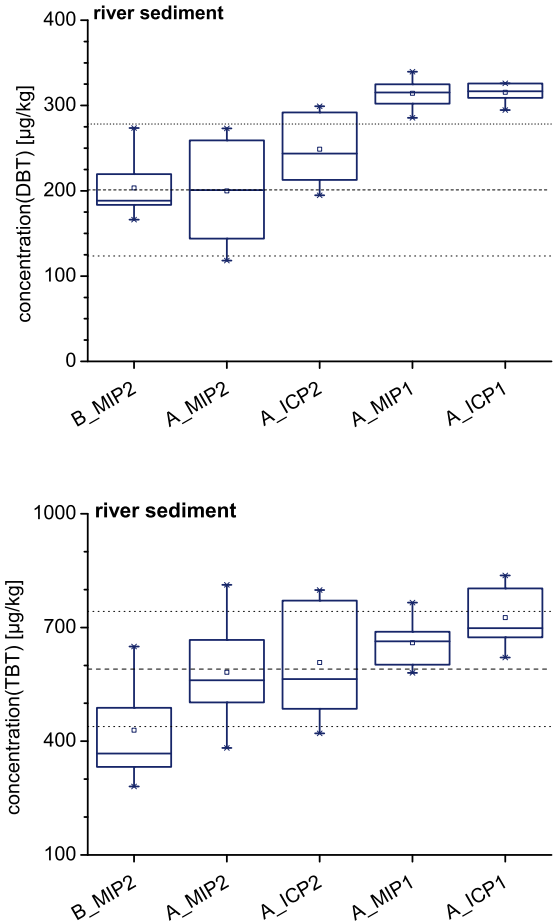

Figure 6.10.: *Amounts of DBT and TBT of the sediment, obtained within the interlaboratory study for laboratory A and B.*

Table 6.11.: *Summarized results of MBT, DBT and TBT in a river sediment analyzed within the interlaboratory study.*

Method	**MBT** [µg/kg]	**DBT** [µg/kg]	**TBT** [µg/kg]
B-MIP2	109 ± 15	203 ± 36	429 ± 119
A-ICP1	188 ± 11	315 ± 11	726 ± 78
A-ICP2	145 ± 18	249 ± 42	607 ± 153
A-MIP2	223 ± 48	200 ± 62	582 ± 138
A-MIP1	233 ± 23	314 ± 17	660 ± 64

ations in ICP/MS and MIP/OES data from MBT are significant, and thus again illustrate difficulties in MBT quantification. Possible reasons are manifold.

Apart from the observed TBT value from laboratory B, the results obtained for DBT and TBT are in good agreement. In this context a slight staff dependency was observed for DBT and TBT. Nevertheless, ICP and MIP data show high accordance as the variance of the results are statistically insignificant in context of variations over the complete method.

7. Conclusion and Future Perspectives

7.1. Conclusion

The present thesis deals with the development of a novel and cost efficient microwave induced plasma source with optical emission detection. The system was constructed as element selective detector for gas chromatography. Based on the small dimensions of the excitation source and microwave transfer via a coaxial cable, a high level of flexibility was achieved. In turn, only low microwave power (< 100 W) can be applied. Nonetheless, a robust plasma discharge is sustained with the ability of applying different plasma gases like helium and argon. Special attention was paid to a simple instrumental setup to provide simple maintenance and low production costs. By utilization of a high temperature resistant discharge tube made of Al_2O_3 additional cooling fluids were avoided. A complete automation was implemented in the new system assuring efficient controlling via the developed software. Detection was achieved by a CCD spectrometer so that a full multielement capability in the wave-

length range from 200 to 400 nm is provided. Therefore, the system is suitable for detection of organometallic compounds with emission lines in this spectral range.

Plasma characteristics like electron density and plasma temperature have been analyzed in cooperation with the *INP Greifswald*. The found electron number density of $2.1 \cdot 10^{21}$ m^{-3} is in the range of other, more complicate MIP systems described in literature working under comparable instrumental conditions. The determined gas temperature between 1500 - 2100 K are also similar to formerly presented MIPs [67, 69, 72, 74, 152].

System parameters have been systematically optimized to achieve highest sensitivity for detection of mercury and tin. In this context, a comparison of the new developed small plasma excitation source with a formerly in our group developed plasma, showed similar detection limits for mercury in the range of 0.3 pg mercury absolute, using the same optical system and data acquisition software. The fact that detection limits for mercury published in literature are 3 times higher compared to the new system [168] indicates that main improvements are related to advanced data processing and background correction. The developed background correction method applied to different mercury and tin emission wavelengths efficiently reduces noise from plasma fluctuation and other sources. For mercury an LOD of only 0.8 pg absolute were observed. The obtained LOD of $\sim$98 pg for tin is in the same range as the best reported literature values. A linear correlation between injected element amount and emission intensity was proven for the tested

elements starting at the quantification limit ranging over more than four decades. Therefore, quantification in a wide concentration range could be assured.

Accurate analytical performance of the MIP-OES detector was validated by means of measuring certified reference materials, containing different mercury (BCR-464) or tin (BCR-646) species, respectively. Good agreement of results gained with the new system was found in direct comparison with established alternative detection techniques. Moreover, the certified concentration for all mercury and tin species except MBT could be reproduced. As MIP-OES data and ICP-MS data were in good agreement, lower MBT recoveries have been related to high adsorption of this species to matrix components, and thus an inefficient extraction during sample pretreatment.

Robustness of the system was demonstrated in an interlaboratory study. Analytical quality and its laboratory and staff independency could be proven by comparison of the results gained for natural contaminated tuna (mercury) and river sediment (tin) samples. All results were in very good agreement. Thus, suitability of the developed detector for routine analysis could be shown successfully.

7.2. Future Perspectives

The new plasma detector is a strong tool for gas chromatography. So far it has been developed only for the detection of mercury, tin and carbon but the helium MIP offers further useful analytical opportuni-

ties. These should be investigated in the near future. Extension of the application range with respect to accessible elements, detectable with the new plasma source is one of the future perspectives. First experiments have been carried out to enable the detection of organolead components. For this purpose, different detection wavelengths with corresponding online background correction have been implemented in the software. Nevertheless, the main advantages of microwave induced plasma sources have often been considered to be the ability of simple helium discharge operation, offering high sensitive detection for nonmetals. Therefore, establishing the new detection systems in routine analysis would require the opportunity to perform nonmetal detection. Particularly the halogens are of great interest and it is well known that a helium MIP is a good detector for these elements including fluorine. Therefore, further work should also include the selection of most sensitive detection wavelengths and the development of efficient background correction methods.

Further room for future research is related to the detection of tin. Within this work detection limits for tin have been found to be higher compared to data published in literature. As plasma and detection conditions are similar, except for the discharge tube material, first experiments with fused quartz discharge tubes have been carried out to exclude adverse interactions of tin with the discharge tube walls. Within these experiments, helium and argon were tested as plasma gas and resulting detection limits for different mercury and tin species were calculated from the chromatograms. Obtained detection limits of tin have been found

to be five times lower using an argon plasma sustained in a fused quartz glass discharge tube. Thus, in future further experiments should be performed to evaluate the influence of the discharge tube material and the plasma gas on the sensitivity for tin detection. The inner diameter of the applied ceramic (Al_2O_3) and fused quartz discharge tubes was different (1.6 mm and 1.2 mm respectively) in these experiments. Thus the influence of the discharge tube's inner diameter is of further interest. In this context, mercury detection limits have not changed between helium and argon plasma operation, leading to the question, whether helium application is advantageous for high performance mercury detection. As argon is quite cheaper compared to helium, operational costs of the detector are reduced for operation with argon, allowing more economic detection of organometalls species.

As high solvent load of the plasma leads to reduced discharge tube durability, in this work a GC column switching system was used for solvent venting purpose. To simplify application of the system and reduce complexity of the technical setup, in future a solvent venting system should be integrated. Another opportunity to overcome the low solvent tolerance is the development of a tandem plasma source, sustaining two plasmas as described by Borer *et al.* and Duan *et al.* [177, 178]. With this setup, a high power plasma can be used for atomization of the introduced components, so that power of the second plasma is completely available for excitation. Therefore, lower matrix susceptibility and reduced spectral background can be expected, and increasing the detection limits.

According to the high robustness and simplicity of the developed detection system, application in routine analysis is conceivable. Especially the low costs for acquisition and application may support usage in small and medium-sized laboratories.

Bibliography

[1] J. J. Berzas Nevado, R. C. R. Martin-Doimeadios, E. Krupp, F. J. G. Bernardo, F. Rodriguez Farinas, M. J. Moreno, D. Wallace, and M. J. P. Ropero. Comparison of gas chromatographic hyphenated techniques for mercury speciation analysis. *J. Chromatogr. A*, 1218:4545–4551, 2011.

[2] D. Das, U. Gupta, and A. K. Das. Recent developments in solid phase extraction in elemental speciation of environmental samples with special reference to aqueous solutions. *Trends Anal. Chem.*, 38:163–171, 2012.

[3] V. L. Dressler, C. M. M. Santos, F. Goldschmidt Antes, F. R. S. Bentlin, D. Pozebon, and E. M. M. Flores. Total mercury, inorganic mercury and methyl mercury determination in red wine. *Food Anal. Meth.*, 5(3):505–511, 2012.

[4] W. Y. Feng, M. Wang, M. Guan, Y. Hui, J. W. Shi, B. Wang, M. Zhu, O. Y. Hong, Y. L. Zhao, and Z. F. Chai. Mercury speciation and mercury-binding protein study by HPLC-ICP-MS

on the estimation of mercury toxicity between maternal and infant rats. *J. Anal. At. Spectrom.*, 26(1):156–164, 2011.

[5] M. Vahcic, R. Milacic, and J. Scancar. Development of analytical procedure for the determination of methyltin, butyltin, phenyltin and octyltin compounds in landfill leachates by gas chromatography–inductively coupled plasma mass spectrometry. *Anal. Chim. Acta*, 694:21–30, 2011.

[6] M. Zabaljauregui, A. Delgado, A. Usobiaga, O. Zuloaga, A. de Diego, and J. M. Madariaga. Fast method for routine simultaneous analysis of methylmercury and butyltins in seafood. *J. Chromatogr. A*, 1148:78–85, 2007.

[7] G. A. Zachariadis and E. Rosenberg. Speciation analysis of triethyl-lead and tributyl-tin compounds in human urine by liquid–liquid extraction and gas chromatography microwave-induced plasma atomic emission detection. *J. Sep. Sci.*, 35(9):1132–1137, 2012.

[8] M. Hoch. Organotin compounds in the environment - an overview. *Appl. Geochem.*, 16(6):719–743, 2001.

[9] R. P. Mason and J. M. Benoit. Organomercury Compounds in the Environment. P. J. Craig, editor, *Organometallic Compounds in the Environment, Second Edition*. John Wiley & Sons Ltd, Chichester, 2003, pages 57–99.

[10] F. Cima, P. J. Craig, and C. F. Harrington. Organotin Compounds in the Environment. P. J. Craig, editor, *Organometallic Compounds in the Environment, Second Edition*. John Wiley & Sons Ltd, Chichester, 2003, pages 101–149.

[11] J. S. Thayer. *Organometallic compounds and living organisms*. ACADEMIC PRESS, NEW YORK, NY (USA), 1984.

[12] B. R. Ramaswamy, H. Tao, and M. Hojo. Contamination and biomethylation of organotin compounds in pearl/fish culture areas in Japan. *Anal. Sci.*, 20(1):45–55, 2004.

[13] R. C. Rodriguez Martin-Doimeadios, E. Tessier, D. Amouroux, R. Guyoneaud, R. Duran, P. Caumette, and O. F. X. Donard. Mercury methylation/demethylation and volatilization pathways in estuarine sediment slurries using species-specific enriched stable isotopes. *Mar. Chem.*, 90(1-4):107–123, 2004.

[14] J. S. Thayer. Biological methylation of less-studied elements. *Appl. Organomet. Chem.*, 16(12):677–671, 2002.

[15] C. Alzieu. Impact of tributyltin on marine invertebrates. *Ecotoxicol.*, 9(1-2):71–76, 2000.

[16] H. Iwata, S. Tanabe, T. Mizuno, and R. Tatsukawa. Bioaccumulation of butyltin compounds in marine mammals: The specific tissue distribution and composition. *Appl. Organomet. Chem.*, 11(4):257–264, 1997.

[17] K. Kannan, S. Tanabe, and R. Tatsukawa. Occurence of butyltin residues in certain foodstuffs. *Bull. Environ. Contam. Toxicol.*, 55(4):510–516, 1995.

[18] R. J. Maguire. Environmental aspects of tributyltin. *Appl. Organomet. Chem.*, 1(6):475–498, 1987.

[19] N. Folsvik, J. A. Berge, E. M. Brevik, and M. Walday. Quantification of organotin compounds and determination of imposex in populations of dogwhelks (nucella lapallus) from norway. *Chemosphere*, 38(3):681–691, 1999.

[20] J. German Rodriguez, A. Borja, J. Franco, J. Ignacia Garcia Alonso, J. M. Garmendia, I. Muxika, C. Sariego, and V. Valencia. Imposex and butyltin body burden in nassarius nitidus (Jeffreys, 1867), in coastal waters within the basque country (northern Spain). *Sci. Total Environ.*, 407(14):4333–4339, 2009.

[21] WHO. *Methylmercury (Environmental Health Criteria No. 101)*. World Health Organization (WHO) Geneva, 1990.

[22] H. Vrijhof. Organotin compounds and international treaties on the pollution of water by dangerous substances: Black or grey list substances? *Sci. Total Environ.*, 43(3):221–231, 1985.

[23] A. Gonzálvez, M. L. Cervera, S. Armenta, and M. de la Guardia. A review of non-chromatographic methods for speciation analysis. *Anal. Chim. Acta*, 636(2):129–157, 2009.

[24] M. A. Vieira, P. Grinberg, C. R. R. Bobeda, M. N. M. Reyes, and R. C. Campos. Non-chromatographic atomic spectrometric methods in speciation analysis: A review. *Spectrochim. Acta Part B*, 64(6):459–476, 2009.

[25] D. M. Templeton, F. Ariese, R. Cornelis, L. Danielsson, H. Mantau, H. P. Van Leeuwen, and R. Lobinski. Guidelines for terms related to chemical speciation and fractionation of elements. Definitions, structural aspects, and methodological approaches. *Pure Appl. Chem.*, 72(8):1453–1470, 2000.

[26] S. W. Chung and B. T. Chan. A reliable method to determine methylmercury and ethylmercury simultaneously in foods by gas chromatography with inductively coupled plasma mass spectrometry after enzymatic and acid digestion. *J. Chromatogr. A*, 1218:1260–1265, 2011.

[27] W. C. Davis, S. S. V. Pol, M. M. Schantz, S. E. Long, R. D. Day, and S. J. Christopher. An accurate and sensitive method for the determination of methylmercury in biological specimens using GC-ICP-MS with solid phase microextraction. *J. Anal. At. Spectrom.*, 19(12):1546–1551, 2004.

[28] P. Krystek and R. Ritsema. Determination of methylmercury and inorganic mercury in shark fillets. *Appl. Organomet. Chem.*, 18(12):640–645, 2004.

[29] M. Monperrus, E. Tessier, S. Veschambre, D. Amouroux, and O. Donard. Simultaneous speciation of mercury and butyltin

compounds in natural waters and snow by propylation and species-specific isotope dilution mass spectrometry analysis. *Anal. Bioanal. Chem.*, 381(4):854–862, 2005.

[30] J. L. Rodrigues, C. Rodriguez Alvarez, F. Rodriguez Farinas, J. J. Berzas Nevado, F. Barbosa/Jr, and R. C. Rodriguez Martín-Doimeadios. Mercury speciation in whole blood by gas chromatography coupled to ICP-MS with a fast microwave-assisted sample preparation procedure. *J. Anal. At. Spectrom.*, 26(2):436–442, 2011.

[31] P. Rodríguez-González, J. Ignacio García Alonso, and A. Sanz-Medel. Development of a triple spike methodology for validation of butyltin compounds speciation analysis by isotope dilution mass spectrometry part 2. Study of different extraction procedures for the determination of butyltin compounds in mussel tissue CRM 477. *J. Anal. At. Spectrom.*, 19(6):767–772, 2004.

[32] R. Wahlen and T. Catterick. Simultaneous co-extraction of organometallic species of different elements by accelerated solvent extraction and analysis by inductively coupled plasma mass spectrometry coupled to liquid and gas chromatography. *Rapid Commun. Mass Spectrom.*, 18(2):211–217, 2004.

[33] A. V. Hirner. Speciation of alkylated metals and metalloids in the environment. *Anal. Bioanal. Chem.*, 385(3):555–567, 2006.

[34] H. Hintelmann and H. T. Nguyen. Extraction of methylmercury

from tissue and plant samples by acid leaching. *Anal. Bioanal. Chem.*, 381(2):360–365, 2005.

[35] J. H. Huang. Artifact formation of methyl- and ethyl-mercury compounds from inorganic mercury during derivatization using sodium tetra(n-propyl)borate. *Anal. Chim. Acta*, 532(2):113–120, 2005.

[36] M. Monperrus, E. Krupp, D. Amouroux, O. F. X. Donard, and R. C. Rodríguez Martín-Doimeadios. Potential and limits of speciated isotope-dilution analysis for metrology and assessing environmental reactivity. *Trends Anal. Chem.*, 23(3):261–272, 2004.

[37] L. Perna, A. LaCroix-Fralish, and S. Stürup. Determination of inorganic mercury and methylmercury in zooplankton and fish samples by speciated isotopic dilution GC-ICP-MS after alkaline digestion. *J. Anal. At. Spectrom.*, 20(3):236–238, 2005.

[38] Y. Cai. Derivatization and vapor generation methods for trace element analysis and speciaton. Z. Mester and R. Sturgeon, editors, *Comprehensive Analytical Chemistry XLI*. Elsevier Science B.V., Amsterdam, 2003, pages 575–590.

[39] P. Rodríguez-González, J. R. Encinar, J. Ignacio García Alonso, and A. Sanz-Medel. Monitoring the degradation and solubilisation of butyltin compounds during in vitro gastrointestinal digestion using "triple spike" isotope dilution GC-ICP-MS. *Anal. Bioanal. Chem.*, 381(2):380–387, 2005.

[40] P. Rodríguez-González, J. R. Encinar, J. Ignacio García Alonso, and A. Sanz-Medel. Development of a triple spike methodology for validation of butyltin compounds speciation analysis by isotope dilution mass spectrometry part 1. Synthesis of the spike, characterisation and development of the mathematical equations. *J. Anal. At. Spectrom.*, 19(5):685–691, 2004.

[41] N. Campillo, N. Aguinaga, P. Vi nas, I. López-García, and M. Hernández-Córdoba. Speciation of organotin compounds in waters and marine sediments using purge-and-trap capillary gas chromatography with atomic emission detection. *Anal. Chim. Acta*, 525(2):273–280, 2004.

[42] B. Rosenkranz, J. Bettmer, W. Buscher, C. B. Breer, and K. Camman. The behaviour of different organometallic compounds in the presence of inorganic mercury(II): Transalkylation of mercury species and their analysis by the GC-MIP-AED. *Appl. Organomet. Chem.*, 11(9):721–725, 1997.

[43] I. Rodriguez Pereiro and A. C. Díaz. Speciation of mercury, tin, and lead compounds by gas chromatography with microwave-induced plasma and atomic-emission detection (GC-MIP-AED). *Anal. Bioanal. Chem.*, 372(1):74–90, 2002.

[44] A. A. Ansari, I. B. Singh, and H. J. Tobschall. Organotin compounds in surface and pore water of Ganga Plain in the Kanpur-Unnao industrial region, India. *Sci. Total Environ.*, 223(2):157–166, 1998.

[45] J. Bettmer, M. Bradter, W. Buscher, D. Erber, D. Rieping, and K. Camman. GC-MIP-PED as an element-specific system for the determination of organomercury compounds. *Appl. Organomet. Chem.*, 9(7):541–545, 1995.

[46] J. C. Botana, R. R. Rodríguez, A. C. Díaz, R. A. L. Ferreira, R. C. Torrijos, and I. Rodriguez Pereiro. Fast and simultaneous determination of tin and mercury species using SPME, multicapillary gas chromatography and MIP-AES detection. *J. Anal. At. Spectrom.*, 17(8):904–907, 2002.

[47] T. Kuballa, E. Leonhardt, K. Schoeberl, and D. W. Lachenmeier. Determination of methylmercury in fish and seafood using optimized digestion and derivatization followed by gas chromatography with atomic emission detection. *Eur. Food Res. Tech.*, 228(3):425–431, 2009.

[48] J. S. Landaluze, A. De Diego, J. C. Paposo, and J. M. Madariaga. Methylmercury determination in sediments and fish tissues from the Nerbioi-Ibaizabal estuary (Basque country, Spain). *Anal. Chim. Acta*, 508:107–117, 2004.

[49] B. F. Scott, Y. K. Chau, and A. Rais-Firouz. Determination of butyltin species by GC/atomic emission spectroscopy. *Appl. Organomet. Chem.*, 5(3):151–157, 1991.

[50] S. Tutschku, M. M. Schantz, and S. A. Wise. Determination of methylmercury and butyltin compounds in marine biota and sed-

iments using microwave-assisted acid extraction, solid-phase microextraction, and gas chromatography with microwave-induced plasma atomic emission spectrometric detection. *Anal. Chem.*, 74(18):4694–4701, 2002.

[51] G. A. Zachariadis and E. Rosenberg. Speciation of organotin compounds in urine by GC-MIP-AED and GC-MS after ethylation and liquid-liquid extraction. *J. Chromatogr. B*, 877(11):1140–1144, 2009.

[52] J. J. Sullivan and B. D. Quimby. Characterization of a computerized photodiode array spectrometer for gas chromatography-atomic emission spectrometry. *Anal. Chem.*, 62(10):1034–1043, 1990.

[53] I. Langmuir. Oscillations in ionized gases. *Proc. Natl. Acad. Sci. USA*, 14(8):627–637, 1929.

[54] W. R. McLean, D. L. Stanton, and G. E. Penketh. A quantitative tunable element-selective detector for gas chromatography. *Analyst*, 98(1167):432–442, 1973.

[55] M. Huang. Comparison between ICPs and MIPs in terms of excitation mechanism and deviation from LTE. *Microchem. J.*, 53(1):79–87, 1996.

[56] K. J. Jankowski and E. Reszke. *Microwave Induced Plasma Analytical Spectrometry*. RSC Publishing, Cambridge, 2011.

[57] C. I. M. Beenakker. Evaluation of a microwave-induced plasma in helium at atmospheric pressure as an element-selective detector for gas chromatography. *Spectrochim. Acta Part B*, 32(3-4):173–187, 1977.

[58] H. S. W. Massey, E. H. S. Burhop, and H. B. Gilbody. *Electronic and Ionic Impact Phenomena*, volume IV. Clarendon Press, Oxford, 1974.

[59] T. U. Wu. *Kinetic Equations on Gases and Plasmas*. Addison-Wesley, Reading, 1966.

[60] S. Murayama. Effect of sodium on the intensity distribution of rare-earth elements in a 2469 MHz discharge. *Spectrochim. Acta Part B*, 25(4):191–200, 1970.

[61] J. Alandari, A. M. Diamy, J. M. Guillerme, J. C. Legrand, and J. I. Ben-Aim. Rotational temperature in helium, argon, and oxygen microwave-induced plasmas: Comparison with translational and solid surface temperatures. *Appl. Spec.*, 43(4):681687, 1989.

[62] M. Huang, D. S. Hanselman, Q. Jin, and G. M. Hieftje. Non-thermal features of atmospheric-pressure argon and helium microwave-induced plasmas observed by laser-light Thomson scattering and Rayleigh scattering. *Spectrochim. Acta Part B*, 45(12):1339–1352, 1990.

[63] M. H. Abdallah and J. M. Mermet. Comparison of temperature

measurements in ICP and MIP with Ar and He as plasma gas. *Spectrochim. Acta Part B*, 37(5):391–397, 1982.

[64] D.-C. Fang and R. K. Marcus. Use of a cylindrical Langmuir probe for the characterization of charged particle populations in a planar, diode glow discharge device. *Spectrochim. Acta Part B*, 45(9):1053–1074, 1990.

[65] M. Huang and G. M. Hieftje. Simultaneous measurement of spatially resolved electron temperatures, electron number densities and gas temperatures by laser light scattering from the ICP. *Spectrochim. Acta Part B*, 44(8):739–749, 1989.

[66] B. Rosenkranz. *Development and Evaluation of the Automated Speciation Analyser (ASA)*. Doctorial Dissertation, Universität Münster, Münster (Germany), 1999.

[67] A. Rodero, M. C. Quintero, A. Sola, and A. Gamero. Preliminary spectroscopic experiments with helium microwave induced plasmas produced in air by use of a new structure: the axial injection torch. *Spectrochim. Acta Part B*, 51(5):467–479, 1996.

[68] A. Besner, M. Moisan, and J. Hubert. Fundamental properties of radiofrequency and microwave surface-wave induced plasmas. *J. Anal. At. Spectrom.*, 3(6):863–866, 1988.

[69] J. Cotrino, M. Saez, M. C. Quintero, A. Menendez, J. E. Sánchez-Uría, and A. Sanz-Medel. Spectroscopic determination of fundamental parameters in an argon microwave-induced plasma (sur-

fatron) at atmospheric pressure. *Spectrochim. Acta Part B*, 47(3):425–435, 1992.

[70] A. Geiger, S. Kirschner, B. Ramacher, and U. Telgheder. Characterisation of a microwave-induced plasma atomic emission spectrometry system using a modified plasma torch coupled with pneumatic and hydraulic high-pressure nebulization. *J. Anal. At. Spectrom.*, 12(9):1087–1090, 1997.

[71] J. Mierzwa, R. Brandt, J. A. C. Broekaert, P. Tschöpel, and G. Tölg. Performance of a microwave induced plasma (MIP) operated in a liquid-cooled discharge tube for atomic emission spectrometry. *Spectrochim. Acta Part B*, 51(1):117–126, 1996.

[72] M. Wlodarczyk and W. Zyrnicki. Spectroscopic characterization of low power argon microwaveinduced plasma with gaseous species produced from ethanol– water solutions in continuous hydride generation process. *Spectrochim. Acta Part B*, 58(3):511–522, 2003.

[73] K. Jankowski and M. Dreger. Study of an effect of easily ionizable elements on the excitation of 35 elements in an Ar-MIP system coupled with solution nebulization. *J. Anal. At. Spectrom.*, 15(3):269–276, 2000.

[74] E. A. H. Timmermans, J. Jonkers, I. A. J. Thomas, A. Rodero, M. C. Quintero, A. Sola, A. Gamero, and J. A. M. van der Mullen. The bahavior of molecules in microwave-induced plasmas studied

by optical emission spectroscopy. 1. Plasma at atmospheric pressure. *Spectrochim. Acta Part B*, 53(11):1553–1566, 1998.

[75] Q. Jin, Y. Duan, and J. A. Olivares. Development and investigation of microwave plasma techniques in analytical atomic spectrometry. *Spectrochim. Acta Part B*, 52(2):131–161, 1997.

[76] K. Fallgatter, V. Svoboda, and J. D. Winefordner. Physical and analytical aspects of a microwave excited plasma. *Appl. Spec.*, 25(3):347–352, 1971.

[77] T. K. Starn, N. N. Sesi, Horner J. A., and G. M. Hieftje. A LabVIEW® program for determining electron number density from stark broadening measurements of the hydrogen-beta line. *Spectrochim. Acta Part B*, 50(9):1147–1158, 1995.

[78] J. D. Cobine and D. A. Wilbur. The electronic torch and related high frequency phenomena. *J. Appl. Phys.*, 22(6):835–841, 1951.

[79] T. H. Risby and Y. Talmi. Microwave induced electrical discharge detectors for gas chromatography. *Crit. Rev. Anal. Chem.*, 14(3):231–265, 1983.

[80] B. Rosenkranz and J. Bettmer. Microwave-induced plasma-optical emission spectrometry - fundamental aspects and applications in metal speciation analysis. *Trends Anal. Chem.*, 19(2-3):138–156, 2000.

[81] H. P. Broida and J. W. Moyer. Spectroscopic analysis of deuterium in hydrogen-deuterium mixtures. *J. Opt. Soc. Am.*, 42(1):37–41, 1952.

[82] C. I. M. Beenakker. A cavity for microwave-induced plasmas operated in helium and argon at atmospheric pressure. *Spectrochim. Acta Part B*, 31(8-9):483–486, 1976.

[83] B. D. Quimby, P. C. Uden, and R. M. Barnes. Atmospheric pressure helium microwave detection system for gas chromatography. *Anal. Chem.*, 50(14):2112–2118, 1978.

[84] M. Moisan. A small microwave plasma source for long column production without magnetic field. *IEEE Trans. Plasma Sci.*, 3(2):55–59, 1975.

[85] J. Hubert, M. Moisan, and A. Ricard. A new microwave plasma at atmospheric pressure. *Spectrochim. Acta Part B*, 33(1):1–10, 1979.

[86] E. Bulska, J. A. C. Broekaert, P. Tschöpel, and G. Tölg. Comparative study of argon and helium plasmas in a TM010 cavity and a surfatron and their use for hydride generation microwave-induced plasma atomic emission spectrometry. *Anal. Chim. Acta*, 276(2):377–384, 1993.

[87] L. J. Galante, M. Selby, and G. M. Hieftje. A low-power surfatron source for the atomic-emission-spectrometric detection of nonmetals in aqueous solution. *Appl. Spec.*, 42(4):559–567, 1988.

[88] M. Selby and G. M. Hieftje. Taming the surfatron. *Spectrochim. Acta Part B*, 42(1-2):285–298, 1987.

[89] D. R. Luffer, L. J. Galante, P. A. David, M. Novotny, and G. M. Hieftje. Evaluation of a supercritical fluid chromatograph coupled to a surface-wave-sustained microwave- induced plasma detector. *Anal. Chem.*, 60(14):1365–1369, 1988.

[90] P. S. Moussounda, P. Ranson, and J. M. Mermet. Spatially resolved spectroscopic diagnostics of an argon MIP produced by surface wave propagation (surfatron). *Spectrochim. Acta Part B*, 40(4):641–651, 1985.

[91] M. Selby, R. Rezaaiyaan, and G. M. Hieftje. Spatial emission properties of a surface-wave-sustained plasma (surfatron) in helium. *Appl. Spec.*, 41:749–761, 1987.

[92] M. E. Birch. Solvent venting technique for gas chromatography with microwave-induced plasma atomic emission spectroscopy. *Anal. Chim. Acta*, 282(2):451–548, 1993.

[93] K. M. L. Holden, K. D. Bartle, and S. R. Hall. The importance of solvent venting to reduce memory effects with on-line LC-GC-AED. *J. High Resol. Chromatogr.*, 22(3):159–163, 1999.

[94] B. D. Quimby and J. J. Sullivan. Evaluation of a microwave cavity, discharge tube, and gas flow system for combined gas chromatography-atomic emission detection. *Anal. Chem.*, 62(10):1027–1034, 1990.

[95] L. Zhang, J. W. Carnahan, R. E. Winans, and P. H. Neill. Solvent venting interface for capillary gas chromatography and a microwave-induced plasma. *Anal. Chim. Acta*, 233:149–154, 1990.

[96] Q. Jin, C. Zhu, M. W. Borer, and G. M. Hieftje. A microwave plasma torch assembly for atomic emission spectrometry. *Spectrochim. Acta Part B*, 46(3):417–430, 1991.

[97] H. Matusiewicz. A novel microwave plasma cavity for atomic emission spectrometry. *Spectrochim. Acta Part B*, 47(10):1221–1227, 1992.

[98] R. M. Barnes and E. E. Reszke. Design concepts for strip-line microwave spectrochemical sources. *Anal. Chem.*, 62(23):2650–2654, 1990.

[99] K. A. Forbes, E. E. Reszke, P. C. Uden, and R. M. Barnes. Comparison of microwave-induced plasma sources. *J. Anal. At. Spectrom.*, 6(1):57–71, 1991.

[100] S. A. Estes, P. C. Uden, and R. M. Barnes. Microwave-excited atmospheric pressure helium plasma emission detection characteristics in fused silica capillary gas chromatography. *Anal. Chem.*, 53(12):1829–1837, 1981.

[101] K. G. Michlewicz, J. J. Urh, and J. W. Carnahan. A microwave induced plasma system for the maintenance of moderate power

plasmas of helium, argon, nitrogen and air. *Spectrochim. Acta Part B*, 40(3):493–499, 1985.

[102] Y. Okamoto. Annular-shaped microwave-induced nitrogen plasma at atmospheric pressure for emission spectrometry of solutions. *Anal. Sci.*, 7(2):283–288, 1991.

[103] A. T. Zander and G. M. Hieftje. Determination of trace metals by microwave plasma spectrometry with an atmospheric pressure helium discharge. *Anal. Chem.*, 50(9):1257–1260, 1978.

[104] M. M. Abdillahi and R. D. Snook. Determination of bromide using a helium microwave induced plasma with bromine generation and electrothermal vaporisation for sample introduction. *Analyst*, 111(3):265–267, 1986.

[105] P. G. Brown, T. M. Davidson, and J. A. Caruso. Application of helium microwave-induced plasma mass spectrometry to the detection of high Ionisation potential gas phase species. *J. Anal. At. Spectrom.*, 3(6):763–769, 1988.

[106] D. M. Chambers, J. W. Carnahan, Q Jin, and G. M. Hieftje. Fundamental studies of the sampling process in an inductively coupled of the inductively plasma-mass spectrometer Part IV .- Replacement coupled plasma with a helium microwave-induced plasma. *Spectrochim. Acta Part B*, 46(13):1745–1765, 1991.

[107] J. T. Creed, A. H. Mohamad, T. M. Davidson, G. Ataman, and J. A. Caruso. Helium source microwave-induced plasma mass

spectrometric detection in the anaiysis of gas-chromato graphic eluates. *J. Anal. At. Spectrom.*, 3(6):923–926, 1988.

[108] D. J. Douglas and J. B. French. Elemental analysis with a microwave-induced plasma/quadrupole mass spectrometer system. *Anal. Chem.*, 53(1):37–41, 1981.

[109] L. K. Olson and J. A. Caruso. The helium microwave-induced plasma: an alternative ion source for plasma mass spectrometry. *Spectrochim. Acta Part B*, 49(1):7–30, 1994.

[110] Y. Duan, X. Kong, H. Zhang, J. Liu, and Q Jin. Evaluation of a low-powered argon microwave plasma discharge as an atomizer for the determination of mercury by atomic fluorescence spectrometry. *J. Anal. At. Spectrom.*, 7(1):7–10, 1992.

[111] V. Rigin. Simultaneous atomic fluorescence spectrometric determination of traces of iron, cobalt and nickel after conversion to their carbonyls and gas-phase atomization by microwave-induced plasma. *Anal. Chim. Acta*, 283(2):895–901, 1993.

[112] Y. Duan, X. Li, and Q. Jin. Electrothermal vaporization for sample introduction in microwave-induced plasma atomic absorption spectrometry. *J. Anal. At. Spectrom.*, 8(8):1091–1096, 1993.

[113] C. Schnürer-Patschan and K. Niemax. Element selective detection of chlorine in capillary gas chromatography by wavelength modulation diode laser atomic absorption spectrometry in a microwave induced plasma. *Spectrochim. Acta Part B*, 50(9):963–969, 1995.

[114] F. E. Lichte and R. K. Skogerboe. Analysis of solution samples by microwave induced plasma excitation. *Anal. Chem.*, 45(2):399–401, 1973.

[115] D. A. Skoog and J. J. Leary. *Principles of Instrumental Analysis*. Saunders College Publishing, Fort Worth TX, 4th edition, 1992.

[116] K. Jankowski. Evaluation of analytical performance of low-power MIP-AES with direct solution nebulization for environmental analysis. *J. Anal. At. Spectrom.*, 14(9):1419–1423, 1999.

[117] R. K. Winge, V. J. Peterson, and V. A. Fassel. Inductively coupled plasma-atomic emission spectroscopy: Prominent lines. *Appl. Spec.*, 33(3):206–219, 1979.

[118] K. Cammann and H. Müller. Reduzierter Kalibrieraufwand in der Gaschromatographie durch Einsatz eines elementselektiven Plasma-Emissions-Detektors. *Fres. Z. Anal. Chem.*, 331(3-5):336–341, 1988.

[119] B. Rosenkranz, C. B. Breer, W. Buscher, J. Bettmer, and K. Camman. The plasma emission detector-a suitable detector for speciation and sum parameter analysis. *J. Anal. At. Spectrom.*, 12(9):993–996, 1997.

[120] K. J. Mulligan, M. Zerezhgi, and J. A. Caruso. Development of a rapid scanning spectrometer for gas chromatography with microwave induced plasma emission detection. *Spectrochim. Acta Part B*, 38(1-2):369–375, 1983.

[121] K. W. Busch and L. D. Benton. Multiplex methods in atomic spectroscopy. *Anal. Chem.*, 55(3):445A–460A, 1983.

[122] M. Ceulemans, R. Lobinski, W. M. R. Dirkx, and F. C. Adams. Rapid sensitive speciation analysis of butyl- and phenyltin compounds in water by capillary gas chromatography atomic emission spectrometry (GC-AES) after in-situ ethylation and in-line preconcentration. *Fres. J. Anal. Chem.*, 347(6-7):256–262, 1993.

[123] Y. K. Chau, F. Yang, and M. Brown. Evaluation of derivatization techniques for the analysis of organotin compounds in biological tissue. *Anal. Chim. Acta*, 338(1-2):51–55, 1997.

[124] A. Sadiki and D. T. Williams. Speciation of organotin and organolead compounds in drinking water by gas chromatography - atomic emission spectrometry. *Chemosphere*, 32(10):1983–1992, 1996.

[125] J. T. Andersson. Some unique properties of gas chromatography coupled with atomic-emission detection. *Anal. Bioanal. Chem.*, 373(6):344–355, 2002.

[126] L. Ebdon, S. Hill, and R. W. Ward. Directly coupled chromatography - atomic spectroscopy Part 1. Directly coupled gas chromatography - atomic spectroscopy a review. *Analyst*, 111(10):1113–1138, 1986.

[127] L. L. P. Van Stee and U. A. T. Brinkman. Gas chromatography

with atomic emission detection: a powerful technique. *Trends Anal. Chem.*, 21(9-10):618–626, 2002.

[128] O. F. X. Donard and F. M. Martin. Hyphenated techniques applied to environmental speciation studies. *Trends Anal. Chem.*, 11(1):17–26, 1992.

[129] B. Bouyssiere, J. Szpunar, and R. Lobinski. Gas chromatography with inductively coupled plasma mass spectrometry detection in speciation analysis. *Spectrochim. Acta Part B*, 57(5):805–828, 2002.

[130] P. C. Uden. Element-selective chromatographic detection by plasma atomic emission spectroscopy. *Trends Anal. Chem.*, 6(9):238–246, 1987.

[131] A. L. P. Valente and P. C. Uden. Memory effects in gas chromatographic detection with a microwave-induced plasma. *J. High Resol. Chromatogr.*, 16(5):275–278, 1993.

[132] T. De Smaele, P. Verrept, L. Moens, and R. Dams. A flexible interface for the coupling of capillary gas chromatography with inductively coupled plasma mass spectrometry. *Spectrochim. Acta Part B*, 50(11):1409–1416, 1995.

[133] E. Segovia Garcia, J. I. Garcia Alonso, and A. Sanz-Medel. Determination of butyltin compounds in sediments by means of hydride generation/cold trapping gas chromatography coupled to

inductively coupled plasma mass spectrometric detection. *J. Mass Spectrom.*, 32(5):542–549, 1997.

[134] I. A. Leal-Ganadillo, J. I. Garcia Alonso, and A. Sanz-Medel. Determination of the speciation of organolead compounds in airborne particulate matter by gas chromatography–inductively coupled plasma mass spectrometry. *Anal. Chim. Acta*, 423(1):21–29, 2000.

[135] M. Montes Bayón, M. G. Camblor, J. I. Garcia Alonso, and A. Sanz-Medel. An alternative GC-ICP-MS interface design for trace element speciation. *J. Anal. At. Spectrom.*, 14(9):1317–1322, 1999.

[136] W. G. Pretorius, L. Ebdon, and S. J. Rowland. Development of a high-temperature gas chromatography-inductively coupled plasma mass spectrometry interface for the determination of metalloporphyrins. *J. Chromatogr.*, 646(2):369–375, 1993.

[137] J. P. Snell, I. I. Stewart, R. E. Sturgeon, and W. Frech. Species specific isotope dilution calibration for determination of mercury species by gas chromatography coupled to inductively coupled plasma- or furnace atomisation plasma ionisation-mass spectrometry. *J. Anal. At. Spectrom.*, 15(12):1540–1545, 2000.

[138] Y. Cai and W. Zhang. Metals and Organometallics: Gas Chromatography for Speciation and Analysis. J. Cazes, editor, *Encyclop. Chromatogr.* Marcel Dekker, Inc., Marcel Dekker, 2002, pages 1–4.

[139] I. Rodriguez, S. Mounicou, R. Lobinski, V. Sidelnikov, Y. Patrushev, and M. Yamanaka. Species-selective analysis by microcolumn multicapillary gas chromatography with inductively coupled plasma mass spectrometric detection. *Anal. Chem.*, 71(20):4534–4543, 1999.

[140] P. Jitaru, H. Goenaga Infante, and F. C. Adams. Simultaneous multi-elemental speciation analysis of organometallic compounds by solid-phase microextraction and multicapillary gas chromatography hyphenated to inductively coupled plasma-time-of-flight-mass spectrometry. *J. Anal. At. Spectrom.*, 19(7):867–875, 2004.

[141] H. Tao, T. Murakami, M. Tominaga, and A. Miyazaki. Mercury speciation in natural gas condensate by gas chromatography-inductively coupled plasma mass spectrometry. *J. Anal. At. Spectrom.*, 13(10):1085–1093, 1998.

[142] R. Thomas. A beginners's guide to ICP-MS. Part V: The ion focusing system. *Spectroscopy*, 16(9):38–44, 2001.

[143] M. A. Vaughan and G. Horlick. Ion trajectories through the input ion optics of an inductively coupled plasma-mass spectrometer. *Spectrochim. Acta Part B*, 45(12):1301–1311, 1990.

[144] E. Krupp, C. Pécheyran, H. Pinaly, M. Motelica-Heino, D. Koller, S. M. M. Young, I. B. Brenner, and O. F. X. Donard. Isotopic precision for a lead species ($PbEt_4$) using capillary gas chromatography coupled to inductively coupled plasma-multicollector mass spectrometry. *Spectrochim. Acta Part B*, 56(7):1233–1240, 2001.

[145] G. R. Peters and D. Beauchemin. Versatile interface for gas chromatographic detection or solution nebulization analysis by inductively coupled plasma mass spectrometry: Preliminary results. *J. Anal. At. Spectrom.*, 7(6):965–969, 1992.

[146] T. Prohaska, M. Pfeffer, M. Tulipan, G. Stingeder, A. Mentler, and W. W. Wenzel. Speciation of arsenic of liquid and gaseous emissions from soil in a microcosmos experiment by liquid and gas chromatography with inductively coupled plasmamass spectrometer (ICP-MS) detection. *Fres. J. Anal. Chem.*, 364(5):467–470, 1999.

[147] J. Feldmann, R. Grümping, and A. V. Hirner. Determination of volatile metal and metalloid compounds in gases from domestic waste deposits with GC/ICP-MS. *Fres. J. Anal. Chem.*, 350:228–234, 1994.

[148] J. E. Sansonetti and W. C. Martin. Handbook of basic atomic spectroscopic data. *J. Phys. Chem. Ref. Data*, 34(4):1559–2259, 2005.

[149] R. Lobinski, W. M. R. Dirkx, M. Ceulemans, and F. C. Adams. Optimization of comprehensive speciation of organotin compounds in environmental samples by capillary gas chromatography helium microwave-induced plasma emission spectrometry. *Anal. Chem.*, 64(2):159–165, 1992.

[150] C. Lauzon, K. Chi Tran, and J. Hubert. Multi-wavelength detection in gas chromatography with microwave-induced plasma

atomic emission fourier transform spectrometry. *J. Anal. At. Spectrom.*, 3(6):901–905, 1988.

[151] K. Cammann, L. Lendero, H. Feuerbacher, and K. Ballschmitter. Power-modulated microwave-induced plasma with enhanced sensitivity and practicability as an element-specific GC-detector. *Fres. Z. Anal. Chem.*, 316(2):194–200, 1983.

[152] A. Besner and J. Hubert. Effects of dopants on tin emission in a helium microwave-induced plasma. *J. Anal. At. Spectrom.*, 3(2):381–385, 1988.

[153] P. W. J. M. Boumans. Measuring detection limits in inductively coupled plasma emission spectrometry using the "SBR-RSDB approach"-1. A tutorial discussion of the theory. *Spectrochimica Acta Part B*, 46(3):431–445, 1991.

[154] P. W. J. M. Boumans. Atomic emission detection limits more than incidental analytical figures of merit! -A tutorial discussion of the differences and links between two complementary approaches. *Spectrochimica Acta Part B*, 46(6-7):917–939, 1991.

[155] K. R. Betty and G. Horlick. Autocorrelation analysis of noisy periodic signals utilizing a serial analog memory. *Anal. Chem.*, 48(13):1899–1904, 1976.

[156] G. M. Hieftje. Application of correlation analysis for signal-to-noise enhancement in flame spectrometry use of correlation in

determination of rhodium by atomic fluorescence. *Anal. Chem.*, 45(2):253–258, 1973.

[157] R. B. Lam and T. L. Isenhour. Equivaltent width criterion for determining frequency domain cutoffs in fourier transform smoothing. *Anal. Chem.*, 53(8):1179–1182, 1981.

[158] R. B. Lam, D. T. Sparks, and T. L. Isenhour. Cross-correlation signal/noise enhancement with applications to quantitative gas chromatography/fourier transform infrared spectrometry. *Anal. Chem.*, 54(12):1927–1931, 1982.

[159] S. Prikler, D. Pick, and J. W. Einax. Comparing different means of signal treatment for improving the detection power in HPLC-ICP-MS. *Anal. Bioanal. Chem.*, 403(4):1109–1116, 2012.

[160] K. Tanabe, K. Chiba, H. Haraguchi, and K. Fuwa. Determination of mercury at the ultratrace level by atmospheric pressure helium microwave-induced plasma emission spectrometry. *Anal. Chem.*, 53(9):1450–1453, 1981.

[161] K. Tanabe, H. Haraguchi, and K. Fuwa. Application of an atmospheric pressure helium microwave-induced plasma as an element-selective detector for gas chromatography. *Spectrochimica Acta Part B*, 36(7):633–639, 1981.

[162] W. R. L. Masamba and J. D. Winefordner. Analytical characteristics of a helium/hydrogen capacitively coupled microwave plasma. *Spectrochimica Acta Part B*, 48(4):521–529, 1993.

[163] K. Jankowski and A. Jackowska. Continuous powder introduction as a solid sampling technique for microwave induced plasma optical emission spectrometry. *Trends Appl. Spectrosc.*, 6:17–25, 2007.

[164] B. Welz and M. Sperling. *Atomic Absorption Spectrometry*. Wiley-VCH, 1999.

[165] C. R. Vidal, J. Cooper, and E. W. Smith. Hydrogen Stark-broadening tables. *Astrophys. J. Suppl. Ser.*, 25:37–136, 1973.

[166] M. Baeva, A. Bösel, J. Ehlbeck, and D. Loffhagen. Modeling of microwave-induced plasma in argon at atmospheric pressure. *Phys. Rev. E*, 85:056404 1–9, 2012.

[167] M. Baeva, A. Bösel, J. Ehlbeck, W. Buscher, and R. Janzen. Microwave induced plasma source for analytical applications: Experimental and simulation study. *J. Chem. Chem. Eng.*, 5:502–513, 2011.

[168] S. Pedersen-Bjergaard. Gas Chromatography with Atomic Emission Detection in Environmental Analysis. R. A. Meyers, editor, *Encyclopedia of Analytical Chemistry*. John Wiley & Sons Ltd, Chichester, 2000, pages 1–15.

[169] Y. Liu, V. Lopez-Avila, M. Alcaraz, and W. F. Beckert. Determination of organotin compounds in environmental samples by supercritical fluid extraction and gas chromatography with atomic

emission detection. *J. High Resol. Chromatogr.*, 16(2):106–112, 1993.

[170] J. Van Loco, M. Elskens, C. Croux, and H. Beernaert. Linearity of calibration curves: use and misuse of the correlation coefficient. *Accred. Qual. Assur.*, 7(7):281–285, 2002.

[171] Sommerfeld, T. *Bestimmung von Methylquecksilber in Fischmehl mittels GC/AED*. BAM, 2007.

[172] A. W. Kim, M. E. Foulkes, L. Ebdon, S. J. Hill, R. L. Patience, A. G. Barwise, and S. J. Rowland. Construction of a capillary gas chromatography inductively coupled plasma mass spectrometry transfer line and application of the technique to the analysis of alkyllead species in fuel. *J. Anal. At. Spectrom.*, 7(7):1147–1149, 1992.

[173] E. Bulska, D. C. Baxter, and W. Frech. Capillary column gas chromatography for mercury speciation. *Anal. Chim. Acta*, 249(2):545–554, 1991.

[174] N. G. Orellana-Velado, R. Pereiro, and A. Sanz-Medel. Glow discharge atomic emission spectrometry as a detector in gas chromatography for mercury speciation. *J. Anal. At. Spectrom.*, 13(9):905–909, 1998.

[175] R. Wahlen and C. Wolff-Briche. Comparison of GC–ICP–MS and HPLC–ICP–MS for species-specific isotope dilution analysis of

tributyltin in sediment after accelerated solvent extraction. *Anal. Bioanal. Chem.*, 377(1):140–148, 2003.

[176] R. Kruse and E. Bartelt. *Exposition mit Methylquecksilber durch Fischverzehr*. Bundesministerium für Umwelt, Naturschutz und Reaktorsicherheit (BMU), 1st edition, 2008.

[177] M. W. Borer and G. M. Hieftje. Inductively coupled plasma-microwave induced plasma tandem source for atomic emission spectrometry. *J. Anal. At. Spectrom.*, 8(2):339–348, 1993.

[178] Y. Duan, Y Su, and Z. Jin. A new, simple, compact GD-MIP tandem ion source for elemental time-of-flight mass spectrometry. *J. Anal. At. Spectrom.*, 15(10):1289–1291, 2000.

A. Abbreviations

Table A.1.: *Abbreviations used in this work.*

AAS	Atomic Absorption Spectroscopy
AED	Atomic Emission Detection
AFS	Atom Fluorescence Spectroscopy
AOM	Acousto-Optic Modulated
ASA	Automated Speciation Analyzer
$BuHg^+$	Monobutylmercury
BuHgCl	Butylmercurychloride
CCD	Charged Coupled Device
CIS	Cold Injection System
CMP	Capacitively Coupled Plasma
CRM	Certified Reference Material
DBT	Dibutyltin
DBTCl	Dibutyltindichloride
DC	Direct Current
DL	Detection Limit
DOT	Dioctyltin

DOTCl	Dioctyltindichloride
DPhT	Diphenyltin
DPhTCl	Diphenyltindichloride
ECD	Electron Capture Detector
$EtHg^+$	Monoethylmercury
EtHgCl	Monoethylmercurychloride
FID	Flame Ionization Detector
FWHM	Full Width Half Maximum
GC	Gaschromatograph
GUI	Graphical User Interface
HCl	Hydrochloric Acid
HMDS	Hexamethyldisilazane
ICCD	Image Charge Coupled Device
ICP	Inductively Coupled Plasma
ID	Isotope Dilution
LAAS	Laser Absorption Spectroscopy
LDR	Linear Dynamic Range
LOD	Limit of Detection
LTE	Local Thermal Equilibrium
MBT	Monobutyltin
MBTCl	Monobutyltintrichloride
$MeHg^+$	Monomethylmercury
MeHgCl	Methylmercurychloride
MeOH	Methanol
MIP	Microwave Induced Plasma

MOT	Monooctyltin
MOTCl	Monooctyltintrichloride
MPCM	Microwave Plasma Cavity/Magnetron
MPhT	Monophenyltin
MPhTCl	Monophenyltintrichloride
MPS	Multi Purpose Sampler
MPT	Microwave Plasma Torch
MS	Mass-Spectrometry
MWP	Microwave Plasma
OES	Optical Emission Spectroscopy
PMP	Polymethylpentene
PMT	Photomultiplier Tube
PTFE	Polytetrafluoroethylene
PTV	Programmed Temperature Vaporization
SCS	Single Column Switching
SD	Standard Deviation
SSID	Species Specific Isotope Dilution
STEB	Sodiumtetraethylborate
STPhB	Sodiumtetraphenylborate
TBT	Tributyltin
TBTCl	Tributyltinchloride
TCD	Thermal Conductivity Detector
T_e	Electron Temperature
$T_{exc.}$	Excitation Temperature
$T_{gas.}$	Gas Temperature

THF	Tetrahydrofurane
$T_{ion.}$	Ionization Temperature
TPhT	Triphenyltin
TPhTCl	Triphenyltinchloride
TPT	Tripropyltin
TPTCl	Tripropyltinchloride
$T_{rot.}$	Rotational Temperature
TTBT	Tetrabutlytin
TTET	Tetraethyltin
TTMT	Tetramethyltin
TTPT	Tetrapropyltin

B. Chemicals

Table B.1.: *Chemicals used in this work.*

Chemical	Purity	CAS-Nr.
Acetic Acid	>99.8%	64-19-7 [I]
Argon	4.8	7440-37-1 [II]
Butylmercurychloride	not spec.	543-63-5 [I]
Butyltintrichloride	95%	1118-46-3 [I]
Copper Powder	p.a.	7440-50-8 [III]
Decane	≥99%	124-18-5 [I]
Dibutylmercury	not spec.	629-35-6 [IV]
Dibutyltindichlorid	96%	683-18-1 [I]
Dichlormethan	99.99%	75-09-02 [V]
Dimethylmercury	98%	593-74-8 [VI]

[I] Sigma-Aldrich, Steinhagen (Germany)
[II] Westfalen AG, Münster (Germany)
[III] Merck, Darmstadt (Germany)
[IV] Haihang IndustJinan City (China)
[V] Acros-Organics, New Jersey (USA)
[VI] ABCR, Karlsruhe (Germany)

Table B.1.: *Chemicals used in this work.*

Chemical	Purity	CAS-Nr.
Dioctyltindichloride	95%	3542-36-7 [VI]
Diphenyltindichloride	96%	1135-99-5 [I]
Ethylmercurychloride	not spec.	107-27-7 [VI]
Florisil®	not spec.	1343-88-0 [I]
Helium	4.9	7440-59-7 [II]
Hexamethyldisilazane	98%	999-97-3a [VI]
Hexane	97%	110-54-3 [VII]
Hydranal® Composite 5		[III]
Hydrochloric Acid	37%	7647-01-0 [VII]
Hydrogen	4.8	1333-74-0 [II]
IRMM-BCR-464		[I]
IRMM-BCR-646		[I]
iso-Propanol	$\geq$99.9%	67-63-0 [I]
Mercury(II)chloride	not spec.	7487-94-7 [VI]
Mercury(0)	not spec.	7439-97-6 [I]
Methanol	$\geq$99.9%	67-56-1 [VII]
Methylmercurychloride	not spec.	115-09-3 [VI]
Nitrogen	4.8	7727-37-9 [II]
Octyltintrichloride	95%	3091-25-6 [VI]
Oxygen	5.1	7784-44-7 [II]
Phenyltintrichlorid	98%	1124-19-2 [I]

[VII] VWR, Radnor (USA)

Table B.1.: *Chemicals used in this work.*

Chemical	Purity	CAS-Nr.
Sodium Acetate	>99%	6131-90-4 [V]
Sodiumtetraethylborate	97%	15523-24-7 [V]
Sodiumtetraphenylborate	99.5%	143-66-8 [VI]
Sodiumhydroxide	p.a.	1310-73-2 [III]
Sodiumsulfate	98%	7757-82-6 [VIII]
Tetrahydrofurane	>99.9%	109-99-9 [III]
Tetrabutyltin	99%	1461-25-2 [VI]
Tetraethyltin	98%	597-64-8 [VI]
Tetramethyltin	98%	594-27-4 [VI]
Tetrapropyltin	97%	2176-98-9 [VI]
Tributyltinchloride	96%	1461-22-9 [I]
Triphenyltinchloride	>97%	639-58-7 [I]
Tripropyltinchloride	not spec.	2279-76-7 [VI]
Xenon	5.1	7440-63-3 [II]

[VIII] Grüssing, Filsum (Germany)

C. Instrumentation

Table C.1.: *Instruments used in this work.*

Device	**Identification**	**Manufacturer**
Autosampler	MPS 2	GERSTEL [I]
Circulator	VFU 1045	Valvo [II]
Coaxial Cable		Telegärtner [III]
Column	HP-1	Agilent [IV]
Glass Connector		Supelco [V]
Spraychamber	Cyclon with baffle	AHF [VI]
Discharge Tube	Al_2O_3	Mainz Schleifwerkzeuge [VII]

[I] Mülheim (Germany)
[II] Hamburg (Germany)
[III] Steinenbronn (Germany)
[IV] Santa Clara (USA)
[V] Bellefonte (USA)
[VI] Tübingen (Germany)
[VII] Mainz (Germany)

Table C.1.: *Instruments used in this work.*

Device	Identification	Manufacturer
Monochromator 500 mm	SpectraPro-500i	Acton Research Corporation [VIII]
Monochromator 750 mm	Acton Sp 2750	Princeton-Instruments [IX]
Digital-Massflow-Controller	F-201CV-020-AGD-33-V	Bronkhorst MÄTTIG [X]
Drying Oven	ED 115	Binder [XI]
Fiber Optics	FPC-0400-22-02SMA	Mightex-Systems [XII]
Gaschromatograph	HP-6890	Agilent [IV]
Gaschromatograph	6890N	Agilent [IV]
High-Voltage-Module	G50R	HiVolt [XIII]
ICCD Camera	PI-MAX 3 1024i	Princeton-Instruments [IX]
ICP/MS	7500ce	Agilent [IV]
Karl Fischer Unit	841 Titrando	Metrohm [XIV]

[VIII] Acton (USA)
[IX] Trenton (USA)
[X] Kamen (Germany)
[XI] Tuttlingen (Germany)
[XII] Toronto (Canada)
[XIII] Hamburg (Germany)
[XIV] Filderstadt (Germany)

Table C.1.: *Instruments used in this work.*

Device	Identification	Manufacturer
	803 Ti-Stand	Metrohm [XIV]
	800 Dosino	Metrohm [XIV]
Labor Centrifuge	5416	Eppendorf [XV]
Labor Scale	TE214S	Sartorius [XVI]
Lens	Fused quartz glass	OptoSigma [XVII]
Line Scan Camera	TCE-1304-UW	Mightex-Systems [XII]
Liquid Sampler	7683B	Agilent [IV]
Micro controller	LabJack U12	Meilhaus [XVIII]
Microwave oven	MarsX	CEM [XIX]
Nebulizer	PFA MicroFlow	AHF [VI]
Pipette	Reference® variabel	Eppendorf [XV]
Pipette	Microman	Gilson [XX]
Pipette	Transferpette	Brand [XXI]
Plasmasource	ASA	GERSTEL [I]

[XV] Wesseling-Berzdorf (Germany)
[XVI] Göttingen (Germany)
[XVII] Santa Ana (USA)
[XVIII] Puchheim (Germany)
[XIX] Matthews (USA)
[XX] Middleton (USA)
[XXI] Wertheim (Germany)

Table C.1.: *Instruments used in this work.*

Device	Identification	Manufacturer
Plasmasource	MiniMIP	INP/ Neoplas [XXII]
GC Injector	CIS 4	GERSTEL [I]
Column Switching	SCS	GERSTEL[I]
Software	ChemStation	Agilent [IV]
Software	LabVIEW 2009	National Instruments[XXIII]
Software	Maestro	GERSTEL [I]
Software	MATLAB 2011	MathWorks [XXIV]
CCD Spectrometer	USB 2.0 Spectrometer	Mightex-Systems [XII]
Ultrasonic Bath	Sonorex RK100H	Bandelin [XXV]
Water purification	Aquatron water still A4000D	Stuart [XXVI]
Laboratory scale	TE214S	Sartorius [XXVII]

[XXII] Greifswald (Germany)
[XXIII] München (Germany)
[XXIV] Ismaning (Germany)
[XXV] Berlin (Germany)
[XXVI] Staffordshire (UK)
[XXVII] Göttingen (Germany)

D. Danksagung

E. Publications

Publications in Peer-Reviewed Journals

Pfeifer T.; Janzen R.; Steingrobe T.; Sperling M.; Franze, B.; Engelhard, C.; Buscher, B. "Development of a novel low-flow ion source/sampling cone geometry for inductively coupled plasma mass spectrometry and application in hyphenated techniques" *Spectrochim. Acta B*, 76 48–55 (2012).

Baeva, M.; Bösel, A.; Ehlbeck, J.; Buscher, W.; Janzen, R. "Microwave Induced Plasma Source for Analytical Applications: Experimental and Simulation Study" *J. Chem. Chem. Eng.*, 5/6 502–513 (2011).

Janzen R.; Schwarzer M.; Sperling M.; Vogel M.; Schwerdtle T.; Karst U. "Adduct formation of Thimerosal with human and rat hemoglobin: a study using liquid chromatography coupled to electrospray time-of-flight mass spectrometry (LC/ESI-TOF-MS)" *Metallomics*, 3/8 847–852 (2011).

Wilken A.; Janzen R.; Holtkamp M.; Nowak S.; Sperling M.; Vogel M.; Karst U. "Investigation of the interaction of Mer-

curochrome constituents with proteins using liquid chromatography/mass spectrometry" *Anal. Bioanal. Chem.*, 397 3525-3532 (2010).

Other Publications

Janzen, R.; Bösel, A.; Buscher, W.; Ehlbeck, J.; Lischka, S.; Piechotta, C.; Sperling, M. "Spezies-Analyse von Quecksilber-, Zinn- und Bleiverbindungen", *GIT Labor-Fachzeitschrift*, 1 22-27 (2011).

Oral Presentations

Janzen, R.; Buscher, W. "A small dimension microwave induced plasma source as element selective detector in gas chromatography" *Interdisziplinäres Doktoranden-Seminar des DASp und des A.M.S.El. 2012*, Mainz (Germany), July 2012.

Janzen, R.; Sperling, M.; Karst, U.; Buscher, W. "Entwicklung eines Plasma Emissionsdetektors für die Bestimmung von Schwermetallspezies" *Project Meeting*, Münster (Germany), June 2012.

Janzen, R.; Sperling, M.; Karst, U.; Buscher, W. "Entwicklung und Validierung eines neuen Detektors für die GC" *Project Meeting*, Berlin (Germany), November 2011.

Janzen, R.; Buscher, W. "Speziesanalyse von Hg, Sn und Pb" *Project Meeting*, Greifswald (Germany), November 2010.

Janzen, R.; Sperling, M.; Karst, U.; Buscher, W. "Probenvorbereitung und Untersuchung mit einem GC-MIP-OES System" *Project Meeting*, Berlin (Germany), February 2010.

Poster Presentations

Janzen, R.; Bösel, A.; Lischka, S.; Sperling, M.; Ehlbeck, J.; Piechotta, C.; Buscher, W. "A small microwave induced plasma as element selective detector in gas chromatography", *6th Nordic Conference on Plasma Spectrochemistry*, Loen (Norway), June 2012.

Janzen, R.; Bösel, A.; Lischka, S.; Sperling, M.; Ehlbeck, J.; Piechotta, C.; Buscher, W. "Speciation analysis of mercury with a new microwave induced plasma coupled to gas chromatography", *GDCh-Wissenschaftsforum 2011*, Bremen (Germany), September 2011.

Janzen, R.; Bösel, A.; Lischka, S.; Sperling, M.; Ehlbeck, J.; Piechotta, C.; Buscher, W. "Speciation analysis of mercury with a new microwave induced plasma coupled to gas chromatography", *Trace Elements in Food 4*, Abberdeen (Schottland), June 2011.

Janzen, R.; Bösel, A.; Lischka, S.; Sperling, M.; Ehlbeck, J.; Piechotta, C.; Buscher, W. "Speciation analysis of mercury with a new microwave induced plasma coupled to gas chromatography", *3rd International Symposium on Metallomics*, Münster (Germany), June 2011.

Janzen, R.; Bösel, A.; Lischka, S.; Sperling, M.; Ehlbeck, J.; Piechotta, C.; Buscher, W. "A new microwave induced plasma source for speciation analysis of heavy metals", *European Winter Conference on Plasma Spectrochemistry*, Zaragoza (Spain), January 2011.

Janzen, R.; Schwarzer, M.; Sperling, M.; Karst, U. "Wechselwirkung von Thimerosal mit Hämoglobin", *26. Jahrestag der Gesellschaft für Mineralstoffe und Spurenelemente*, Leipzig (Germany), October 2010.

Janzen, R.; Bösel, A.; Sperling, M.; Ehlbeck, J.; Buscher, W. "Characteristics of a microwave induced plasma source coupled with gas chromatography", *5th Nordic Conference on Plasma Spectrochemistry*, Loen (Norway), June 2010.

F. Curriculum Vitae

Index

E

F

G

H

I

L

M

O

P

R

S

T

W